

**ELECTRON MAGNETOHYDRODYNAMIC  
(EMHD) STUDIES ON ELECTRON TRANSPORT  
IN AN INHOMOGENEOUS PLASMA MEDIUM**

By

**SHARAD KUMAR YADAV**

**INSTITUTE FOR PLASMA RESEARCH, BHAT, GANDHINAGAR,  
GUJARAT, INDIA**

A thesis submitted to the  
Board of Studies in Physical Sciences

In partial fulfillment of the requirements

For the Degree of

**DOCTOR OF PHILOSOPHY**

*of*

**HOMI BHABHA NATIONAL INSTITUTE**



March 2011



# Homi Bhabha National Institute

Programme: Ph.D.

Board of Studies in .....Physical.....Sciences

**1. Name of the Constituent Institution:**

Institute For Plasma Research, Bhat, Gandhinagar-382428 INDIA

**2. Name of the Student:** Mr. Sharad Kumar Yadav

**3. Enrolment Number:** PHYS06200704005

**4. Date of Enrolment in HBNI:** Sept. 03, 2007

**5. Date of Submission of Thesis:** March 12, 2011

**6. Title of the Thesis:** Electron Magnetohydrodynamics (EMHD) studies on Electron Transport in an Inhomogeneous Plasma Medium.

**7. Composition of the Doctoral Committee:**

Sr No	Composition	Designation in HBNI	Name
a.	Chairman	Sr. Prof	P. K. Kaw
b.	Convener (Guide)	Asst. Prof	Amita Das
c.	Co-Guide, if any		NA
d.	Member	Asst. Prof	Sudip Sengupta
e.	Member	Sr. Prof	R. Singh, (in his absence he was replaced by A. Sen )
f.	The Technology Adviser, if any	Invitee	

**8. Number of Doctoral Committee Meetings held with respective dates:**

- (i) 10/10/2007
- (ii) 06/10/2008
- (iii) 10/02/2010
- (iv) 30/08/2010

**9. Name and Organization of the Examiner 1:** Dr. Kartik Patel

Laser and Plasma Technology Division, Bhabha Atomic Research Center, Trombay, Mumbai, INDIA

**Recommendations of the Examiner 1 (Thesis Evaluation)** (i)  accepted, (ii) accepted after revisions, or (iii) rejected:

**10. Name and Organization of the Examiner 2:** Prof. Kazuo A. Tanaka

Institute of Laser Engineering, Osaka University, Suita, Osaka Japan

**Recommendations of the Examiner 2 (Thesis Evaluation)** (i)  accepted, (ii) accepted after revisions, or (iii) rejected:

Name & Signature of Dean-Academic, CI:

Dr. Subroto Mukherje  
Associate Dean - Academic Affairs  
Institute For Plasma Research

## Recommendations of the Viva Voce Board

1. Date of Viva Voce Examination: 19 August 2011
2. Recommendations for the award of the Ph.D. degree: **Recommended / Not Recommended**  
(If Recommended, give summary of main findings and overall quality of thesis)  
(If Not Recommended, give reasons for not recommending and guidelines to be communicated by Convener of the Doctoral committee to the student for further work)

The viva voce examination of the candidate, Shri Sharad Kumar Yadav was held at IPR in the presence of the Doctoral Committee, external examiner, and the Chairman, Academic Committee as well as invited faculty.

He described the work done in the thesis. The presentation was competent and complete. The results of the work were presented and the new findings of the work explained.

The quality of the thesis has been judged to be excellent. The committee questioned the candidate on the work and these questions were answered satisfactorily.

It is recommended that the degree of Ph.D. be awarded to Shri Sharad Kumar Yadav.

In case Not Recommended, another date will be fixed by the Dean-Academic, CI, which shall not be earlier than a month after and not later than six months from the date of first viva.

Date: 19 August 2011

Name and Signature of the Viva Voce Board (Doctoral Committee and External Examiner):

External Examiner: Dr. K. Patel, BAEC.   
Chairman, Doctoral Committee: Prof. P. K. Kary   
Thesis Supervisor: Dr. Amrita Das.   
Member 1: Dr. Sudip Sengupta.   
Member 2: Prof. A. Sen.   
Chairman, Academic Committee; Prof. S. Mukherjee: 

# Homi Bhabha National Institute

## Recommendations of the Viva Voce Board

As members of Viva Voce Board, we certify that we have read the dissertation prepared by **Mr. Sharad Kumar Yadav** entitled "**Electron Magnetohydrodynamics (EMHD) studies on Electron Transport in an Inhomogeneous Plasma Medium**" and recommend that it may be accepted as fulfilling the dissertation requirement for the Degree of Doctor of Philosophy.

Date: 19/8/2011

.....  
External Examiner- Dr. Kartik Patel  
Bhabha Atomic Research Center,  
Trombay, Mumbai, India

Date: 19/8/11

.....  
Chairman – Prof. P. K. Kaw  
Institute For Plasma Research  
Bhat, Gandhinagar-382428, India

Date: 19-08-2011

.....  
Guide: Prof. Amita Das  
Institute For Plasma Research  
Bhat, Gandhinagar-382428, India

Date: 19/8/2011

.....  
Member 1 – Dr. Sudip Sengupta  
Institute For Plasma Research  
Bhat, Gandhinagar-382428, India

Date: 19/8/2011

.....  
Member 2 -Prof. A. Sen  
Institute For Plasma Research  
Bhat, Gandhinagar-382428, India

.....  
Dean Academic – Dr. Subroto Mukhrje  
Associate Dean – Academic Affairs  
Institute For Plasma Research  
Bhat, Gandhinagar-382428, India

19/8/2011

I hereby certify that I have read this dissertation prepared under my direction and recommend that it may be accepted as fulfilling the dissertation requirement.

.....  
Guide : Prof. Amita Das  
Date : 19-08-2011

Place : Gandhinagar



# Homi Bhabha National Institute

## Ph.D. Thesis Evaluation Report

- |   |   |
|---|---|
| 1. Name of the Constituent Institution: | Institute For Plasma Research   |
| 2. Name of the Student:                 | Bhat, Gandhinagar-382428 INDIA<br>Mr. Sharad Kumar Yadav  |
| 3. Enrolment No.:                       | PHYS06200704005   |
| 4. Title of the Thesis:                 | Electron Magnetohydrodynamics (EMHD) studies on<br>Electron Transport in an Inhomogeneous Plasma Medium . |
| 5. Name of the Board of Studies:        | Physical Sciences   |

### Recommendations

Tick one of the following:

1. The thesis in its present form is commended for the award of the Ph.D. Degree.
2. The thesis is commended for the award of the Ph.D. degree. However, my suggestions for improving the thesis may be considered at the time of the viva voce examination and if the viva voce board deems it appropriate, the same may be incorporated in the thesis based on the discussions during the viva voce examination. The revised thesis need not be sent to me.
3. The thesis should be revised as per the suggestions enclosed. I would like to see the revised thesis incorporating my suggestions before I give further recommendations.
4. The thesis is not acceptable for the award of the Ph.D. degree.

(Signature):

Name of Examiner: Prof. Kazuo A. Tanaka

Date:

June 13 2011

Please give your detailed report in the attached sheet. You may use additional sheets, if required.

1. Name of the Student: Sharad Kumar Yadav

2. Title of the Thesis: Electron Magnetohydrodynamics (EMHD) studies on Electron Transport in an Inhomogeneous Plasma Medium.

### DETAILED REPORT

June 13 2011

To whom it may concern,

I am writing the following comments after I scrutinized the thesis draft submitted by Mr. Sharad K. Yadav

This thesis reports the behaviours of magnetic dipole around the electron current in inhomogeneous plasmas, especially at a steep rise density ramp. The behaviours are extremely relevant to understand the energy transport of fast relativistic electrons in the fast ignition scheme.

This thesis introduces a unique new mechanism of electron dipole transmitting through a sharp density ramp by forming a shock followed by the destabilization. The concept could be extendable to the case similar to the highly relativistic electron stopping in very high density plasmas. In a near future a complicated integral experiment of fast ignition scheme is about to be performed.

They have used EMHD calculation to show the electron dipole current ending up as a strong shock formation. The resultant energy dissipation is basically a fraction of shock length divided by density scale length. They claim that hot electrons as high as 10 MeV could be stopped and those energy can be dissipated in the plasmas. The proposal is fully consistent with the experimental results obtained at Osaka University published in New Journal of Physics in 09.

When properly shaped density plasma is prepared, the dipole current is shown to follow the arranged curved path. The proposal is consistent with the early experimental study published in Nature in 02.

The text is well written and should be approved by the PhD thesis committee.

I have following questions if he can discuss at the summary and found a minor misprint.

Comments:-

- (1) He should define the word "destabilization". How is the different from instability for example ?
- (2) The dipole behaviour has its limit to simulate a large relativistic fast electron current. What are the possible events not counted in this thesis compared to the ones in the real situation ?

Misprint.

- (3) "in this thesis " appears twice within the sentences . This should be corrected.

Name of Examiner: Prof. Kazuo A. Tanaka

  
Signature and Date:

June 13 2011



# Homi Bhabha National Institute

## Ph.D. Thesis Evaluation Report

1. Name of the Constituent Institution: IPR, Bhat, Gandhinagar.
2. Name of the Student: SHARAD KUMAR YADAV
3. Enrolment No. : PHYS 06200 704005
4. Title of the Thesis: Electron Magneto hydrodynamic (EMHD) Studies on Electron Transport in an Inhomogeneous Plasma Medium
5. Board of Studies: PHYSICAL SCIENCES

### Recommendations

Tick one of the following:

1. The thesis in its present form is commended for the award of the Ph.D. Degree.
2. The thesis is commended for the award of the Ph.D. degree. However, my suggestions for improving the thesis may be considered at the time of the viva voce examination and if the viva voce board deems it appropriate, the same may be incorporated in the thesis based on the discussions during the viva voce examination. The revised thesis need not be sent to me.
3. The thesis should be revised as per the suggestions enclosed. I would like to see the revised thesis incorporating my suggestions before I give further recommendations.
4. The thesis is not acceptable for the award of the Ph.D. degree.

(Signature):

*Kartik Patel*

Name of Examiner:

KARTIK PATEL

Date: 20 MAY 2011

भौतिकी अधिकारी  
लेसर एवं प्लाज्मा प्रौद्योगिकी प्रभाग  
भारत सरकार  
भामा परमाणु अनुसंधान केन्द्र  
मुंबई-४०० ०८५.

Please give your detailed report in the attached sheet. You may use additional sheets, if required.

Name of the Student: Sharad Kumar Yadav  
Enrolment no: (not specified in thesis) *PHYS 062 0070 4005*  
Title of the Thesis: Electron Magnetohydrodynamic (EMHD) Studies on Electron Transport in an Inhomogeneous Plasma Medium  
Board of Studies: Physical Sciences

## DETAILED REPORT

A fundamental issue in the interaction of high energy electrons with a plasma is the manner of energy exchange under different conditions. The understanding of this has significant implications in many problem areas such as fusion, particle accelerators, ion sources, etc. A lot of work and considerable effort has been invested in a number of institutions worldwide to investigate beam-plasma systems and the various phenomena that occur in them.

This thesis investigates electron transport within a plasma and associated interactions in two different areas, which have some aspects in common. The first is in the context of Inertial Confinement Fusion, where it has been observed that in the process of Fast Ignition (FI) the deposition of electron energy is greatest in those regions where the density variation is maximum. The second is related to the guidance of energetic electrons in a plasma near regions of steep variations in density. In both these areas, the role played by spatial variation of density is significant, and its effect on electron motion needs to be understood.

The Electron Magnetohydrodynamic (EMHD) model has been employed in investigating the systems being studied. This is appropriate for the short time scales and small lengths in which the phenomena typically occur. The approach used is computer simulation in two-dimensions by generalizing the model to include an inhomogeneous plasma.

The thesis describes the procedure of generalization of the EMHD model, and the numerical method used to solve it in two dimensions. A computer code based on this has been developed. It is stated that this code reproduces known results in the limit of uniform density. The validation of the code for non-uniform density is done by matching the inverse of the operator matrices with analytical cases.

The code has been used to investigate the propagation of monopolar and dipolar electron current pulses through various types of plasma inhomogeneities. The behaviour of these pulses as they propagate through the density variation has been characterized by varying different parameters. A criterion for trapping and transmission of the current pulses have been obtained in terms of the scale lengths involved.

It is shown that the trapping of the current pulses in regions of high density results in significant energy dissipation in those regions locally. The thesis studies the mechanism of energy dissipation and the formation of magnetic shocks during the propagation of the current pulse through the inhomogeneities, and its application to Fast Ignition.

The thesis presents simulations of the destabilization of the electron current via a Kelvin-Helmholtz like instability introduced due to elongated density inhomogeneities, as well as the guiding of electron currents by a high density plasma channel.

The thesis addresses its subject area competently and in a coherent manner. It is reasonably complete and the work has been published in reputed peer-reviewed international journals. The award of the degree of PhD is recommended to the thesis.

During the viva-voce examination, the candidate may be asked to clarify the following queries:

1. What is the order of error in the numerical scheme employed for the solution of the GEMHD equations?

2. Examples of the verification that the inverse of the operator matrices matches with known analytical cases (while validating the code for non-uniform density) may be presented.
3. In studying the motion of an electron current pulse through an inhomogeneous plasma, the solution assumed at time  $t=0$  is that of a pulse existing in a homogeneous plasma system. This is then tracked through the inhomogeneity. However, the self-consistency of a solution to Maxwell's equations also demands that the electron current in the presence of an inhomogeneity will be different at time  $t=0$  itself. In what way is the assumed initial solution expected to change when this is taken into account?
4. How would one experimentally generate the monopolar and dipolar current pulses used in the simulations presented in chapter 4 of the thesis?
5. The inhomogeneous plasma density profile is assumed to be unperturbed by the passage of the current pulse in the simulations presented in chapter 4. Justify this.
6. Assuming that the current pulse perturbs the inhomogeneity, how will the criteria for transmission versus trapping be affected?
7. It is observed that the energy dissipation, during the shock formed while a dipolar current pulse traverses an inhomogeneity, is essentially independent of grid resolution, resistivity and viscosity. What could be the possible physical causes for energy exchange between the current pulse and the plasma?
8. If a dipolar current pulse is trapped in an inhomogeneity, will all the energy get eventually dissipated? If so, what would be the effect on the current pulse and the inhomogeneity?
9. What is the variation in total energy in the simulations of the Kelvin-Helmholtz destabilization of electron current presented in chapter 6?
10. With relation to question 9 above, what is the cause of the energy change, if any?
11. What is the variation in total energy during the restoration of the Isichenko form of the dipole in fig. 6.2? Does it increase or decrease, and why?
12. Is the arbitrary dipole of fig. 6.2 a physically valid configuration, in the sense of satisfying Maxwell's equations at  $t=0$ ?
13. In fig. 6.2, if the Isichenko form of the dipole had been assumed at  $t=0$  itself, would it imply that there would be no change in the current pulse and hence no energy change?
14. In a number of places, it has been pointed out that the results of simulations presented using the GEMHD model have also been observed in simulations done elsewhere using the PIC model. Since the motion of ions is explicitly included PIC simulations, and explicitly excluded in GEMHD, justify why the results should be similar.

Name of Examiner: Kartik Patel  
L & PTD, BARC,  
Mumbai, 400085

Signature:  
Date:

*Kartik Patel*

20 MAY 2011

वैज्ञानिक अधिकारी  
लेसर एवं प्लाज्मा प्रौद्योगिकी प्रभाग  
भारत सरकार  
भाभा परमाणु अनुसंधान केन्द्र  
दुर्गे, मुंबई-४०० ०८५.

## CERTIFICATION FROM GUIDE

This is to certify that viva voce of **Mr. Sharad Kumar Yadav** took place on 19<sup>th</sup> August 2011 in the Institute for Plasma Research, Bhat, Gandhinagar, Gujarat in the presence of all the following doctoral committee and the external referee **Dr. Kartik Patel**.

Prof. P. K. Kaw (Chairman)

*P. Kaw*

Prof. Amita Das (Guide)

*Amita Das.*

Dr. Sudip Sengupta (Member)

*Sudip Sengupta*

Prof. A. Sen (Member)

*A. Sen*

The correction as indicated in the thesis evaluation report of both the referees, have been incorporated in this copy of the thesis.

Date: *19-08-2011*

*Amita Das.*

(Prof. Amita Das)  
Guide

## STATEMENT BY AUTHOR

This dissertation has been submitted in partial fulfillment of requirements for an advanced degree at Homi Bhabha National Institute (HBNI) and is deposited in the Library to be made available to borrowers under rules of the HBNI.

Brief quotations from this dissertation are allowable without special permission, provided that accurate acknowledgement of source is made. Requests for permission for extended quotation from or reproduction of this manuscript in whole or in part may be granted by the Competent Authority of HBNI when in his or her judgement the proposed use of the material is in the interests of scholarship. In all other instances, however, permission must be obtained from the author.

*Sharad K. Yadav*

Sharad Kumar Yadav

## DECLARATION

I, hereby declare that the investigation presented in the thesis has been carried out by me. The work is original and has not been submitted earlier as a whole or in part for a degree / diploma at this or any other Institution / University.

*Sharad K. Yadav.*

Sharad Kumar Yadav

## ACKNOWLEDGEMENTS

It is not possible for me to list by name all who have made useful suggestions in the completion of this thesis. I am grateful for these. In the text, I attempt to give specific attribution for this thesis. I apologize in advance for any omissions.

I feel honoured to express my thanks to my supervisor Prof. Amita Das for spending her precious time in discussion with me. During the early days of my Ph.D., she taught me the computational tools and technique related to fluid simulation. She has also helped me in many ways. It is hard for me to count those. As much I know her, probably she know the potential of student then she guides him/her accordingly. Special acknowledgment is due to the chairman of doctoral committee Prof. P. K. Kaw, who influenced many of things in this thesis. I also thank the other members of my doctoral committee, Dr. Sudip Sengupta and Prof. Raghvendra Singh for all their support and encouragement in my annual reviews.

When I joined IPR (Institute for Plasma Research ) I did not know much about plasma physics. So I am thankful to faculty members who taught me theoretical, experimental and computational aspects of plasma physics during my course work. I especially would like to acknowledge the chairman of academic committee Dr. R. Ganesh, who was also my mentor during the project work. During this project I have learned a lot of computational skills from him.

Some colleagues have been particularly generous in providing me comments and suggestions for correcting the thesis. I especially want to thank Sita, Gurudatt, Sanat, Vikrant, Sunita and Aditya.

I am also thankful to my seniors and friends Jyotirmoy, Neeraj, Pintu, Ritu, Shyama, Manash, Rajneesh, Suraj, Anand, Santosh, Bhaskar, Maya, Kishor, Anurag, Subhash, Surendra, Jugal, Shekar, Satyanand, Puraram, Vikram Sagar, Ujjwal, Ashwin, Deepak, Prabal, Kshitish, Tayyab, Linthish, Sushil, Rameshwar, Pravesh, Nishant, Partha, Sayak, Manjeet, Ilyas, Soumen, Vikram, Vikash, Ravi for providing a pleasant working environment. I would also like to acknowledge Sarveshwar Sharma and Avadhesh Maurya who helped me in the installation of operating system and computational softwares in my computer whenever required.

My thanks and gratitude are extended to those who have helped me other way: ( Library Staff ) Ms. Pragnya Pathak, Shravan Kumar, Smita, Shilpa and

Vaibhavi; (Computer Center Staff) Ms. Sutapa Ranjan, Hemant Joshi, Shailendra Trivedi and Arvind; (Administrative Staff) Ms. Shirin, Mr. Khanduri and Mr. Chamunde.

I would greatly acknowledge the moral support that I continuously received from my parents.

*Sharad K. Yadav.*

Sharad Kumar Yadav

## LIST OF PUBLICATIONS

### Publications in Journals:

- [1] **“Propagation of Electron Magnetohydrodynamic Structures in a Two-Dimensional Inhomogeneous Plasma”**,  
Sharad Kumar Yadav, Amita Das, and Predhiman Kaw  
*Phys. Plasmas* **15**, 062308 (2008)
- [2] **“Near-Complete Absorption of Intense, Ultrashort Laser Light by Sub- $\lambda$  Gratings”**,  
S. Kahaly, S. K. Yadav, W. M. Wang, S. Sengupta, Z. M. Sheng, A. Das, P. K. Kaw, and G. Ravindra Kumar  
*Phys. Rev. Lett.* **101**, 145001 (2008)
- [3] **“Anomalous Energy Dissipation of Electron Current Pulses Propagating through an Inhomogeneous Collisionless Plasma Medium”**,  
Sharad Kumar Yadav, Amita Das, Predhiman Kaw, and Sudip Sengupta  
*Phys. Plasmas* **16**, 040701 (2009)
- [4] **“Role of Natural Length and Time Scales on Shear Driven Two Dimensional Electron Magnetohydrodynamic Instability”**,  
G. Gaur, S. Sundar, S. K. Yadav, A. Das, P. Kaw, and S. Sharma  
*Phys. Plasmas* **16**, 072310 (2009)
- [5] **“Nonlinear Studies of Fast Electron Current Pulse Propagation in a Two Dimensional Inhomogeneous Plasma”**,  
Sharad Kumar Yadav, and Amita Das  
*Phys. Plasmas* **17**, 052306 (2010)
- [6] **“Guiding and Collimation of Fast Electron Current Pulse in a Plasma”**,  
*under preparation*

## Publication in Conference:

- [1] “**Hot Electron Generation by Highly Efficient Absorption of High Intensity Femtosecond Laser Light in Plasma Generated on Sub- $\lambda$  Gratings**”,

S. Kahaly, G. R. Kumar, S. K. Yadav, S. Sengupta, A. Das, and P. K. Kaw  
*Journal of Physics: Conference Series* **112** , 022102 (2008)

## SYNOPSIS

The main theme of this thesis is to understand the propagation of electron current in an inhomogeneous plasma medium. A proper understanding of the transport of electron current in plasma is of importance in a variety of frontline research activities. For instance in the area of inertial confinement fusion studies [1] a recent fast ignition technique [2] which separates the task of target compression from the creation of ignition spark, holds a lot of promise. In this technique electrons have the key role of absorbing energy from laser at the critical layer of the precompressed target and transporting it to the overdense regime and depositing it for the creation of hot spark. Another area of frontline research is related to particle acceleration. The conventional high energy accelerators [3] are becoming too huge and expensive to build. Plasma based accelerators proposed by Dawson [4,5] on the other hand is set to revolutionize and offer an alternative which reduces the accelerator length by a factor of almost 1000. In these accelerators, it is the electron species again whose dynamical response in the plasma defines the acceleration parameters.

For these reasons the study of electron transport takes a prominent stage in research activities worldwide. The experiments [6,7] concerning the physics associated with the electron response in plasma medium have focused on issues pertaining to the coupling of laser energy to the plasma in which electrons act as conduit. The measurements in these experiments involved time resolved reflectivity, X - ray emission and magnetic field data which provide information of electrons. For instance, the time evolution of the magnetic field profile has provided good insights on electron dynamics in plasma medium. The decay of magnetic field suggests the presence of anomalous dissipation in the propagation of electrons through plasma. There have also been PIC simulations studies [8-11] in the context of fast ignition which aim at the understanding of the creation of hot spark by fast energetic electrons. Another area where interest lies is associated with the possibility of guiding and collimating electron currents in plasma medium in a desirable fashion. In this context experiments [12] as well as theoretical studies [13] on the design of novel structured targets have been done.

In some of these applications , e.g. Fast Ignition (FI) [2] experiments the electrons are required to propagate through an inhomogeneous plasma medium. Keeping this in view we seek to understand the influence of plasma density inho-

mogeneity on electron propagation in this thesis. For this purpose we adopt the framework of Electron Magnetohydrodynamic (EMHD) [14-16] fluid description. This model represents the physics in the domain of fast electron time scale at which the ions in plasma remain unresponsive. The EMHD model has been frequently used for the purpose of understanding a host of physical phenomena pertaining to astrophysical plasmas, earth's magnetosphere, and even laboratory plasma. The EMHD model has been invoked for the basic understanding of the phenomena of collisionless magnetic field line reconnection [17-23], generation of large scale magnetic field, and rapid dissipation of magnetic field energy in the context of astrophysical plasmas [24, 25] The description of earth's plasma sheet and magnetotail region are other areas where the EMHD has been applied [26, 27]. With the availability of high power short pulse lasers and fast diagnostic tools, much of the experimental observations on laser plasma [28] and laser solid interaction studies [29] has been understood with EMHD description . However, in all these studies EMHD model has been used in the context of homogeneous plasma density. Some authors have incorporated the non uniformity of plasma density within the purview of EMHD model [30, 31]. However, their equations are fairly approximate in terms of the choice of plasma inhomogeneity and/or neglect of electron inertia.

As stated earlier our objective here is to study the transport of electrons through inhomogeneous plasma medium. We have, therefore, generalized the EMHD model in its full glory to incorporate effects arising due to any arbitrary plasma density inhomogeneity. The new model is termed as the Generalized Electronmagnetohydrodynamics ( G-EMHD ) [32]. A comprehensive derivation of the G-EMHD model both in 3D as well as 2D has been presented in the thesis. The salient aspects (Integral invariants associated with this model ) of the G-EMHD equations are also discussed. Furthermore, various limiting forms of the G-EMHD model equations in reduced spatial dimension and simplified electron flow configuration are also presented in the thesis. The equations of the G-EMHD model are then employed for the purpose of studying electron current propagation. The G-EMHD evolution equations being nonlinear, a numerical code has been developed to solve the evolution equations in 2-D. The flux corrected scheme of Boris *et al.* [33] has been adopted for this purpose. A detailed description of the numerical procedure has been provided in the thesis.

The numerical study helps in identifying the role of density inhomogeneity

on the propagation of electron current pulses. For this purpose we chose exact nonlinear solutions [34] for a homogeneous plasma in the form of EMHD monopoles and dipoles. The monopoles are non-propagating rotating current structures in a homogeneous plasma whereas the dipoles are known to propagate along their axis with uniform velocity. Our numerical studies show that (i) these current pulse structures acquire an additional drift velocity,  $\vec{v}_d = b\hat{z} \times \nabla n/n^2$  (Here  $b$  is the magnetic field along the symmetry direction  $\hat{z}$ , associated with the electron current and  $n$  denotes plasma density) in the presence of density inhomogeneity. The drift is transverse to the magnetic field ( $b\hat{z}$ ) and the density gradient ( $\nabla n$ ). (ii) The dipole can readily penetrate inside a high density plasma region but finds it hard and is often unable to come out from there. It thus often gets trapped within a high plasma density region. (iii) The dipole acquires the size of the skin depth associated with the local plasma density.

The phenomena of trapping has been investigated in detail to formulate a threshold criteria (the ratio of the density inhomogeneity scale length and the distance traversed by the structure) for trapping vs. transmission of the structures [35]. The trapping of the dipole current pulse structure in high density region indicates the violation of time reversal invariance and is suggestive of a dissipative mechanism at work. We indeed observe that as the dipolar current pulse structure passes through the density inhomogeneity to penetrate the high density region, it forms magnetic shocks and/or sharp current layers [36]. A strong energy dissipation at the location of magnetic shock region occurs when the dipole structure enters the high density region. Our numerical studies show that the total energy dissipation is independent of the magnitude and the character of the dissipative processes present in the system. This explains the irreversible propagation of the electron current pulse and also provides us with the possibility of a collision - less scheme of electron energy dissipation in a plasma. It can be used as a method for efficient localized heating of plasma by energetic electrons. The electrons can be easily accelerated to high energies and hence are readily available as good source of energy. Furthermore, electrons can be used to heat overdense plasma region as well, where lasers are unable to penetrate. The only drawback for using electrons for the purpose of plasma heating so far has been due to the fact that higher the energy of electrons more difficult it becomes to stop them, as their Rutherford collision cross section falls off drastically with increasing energy. Against this backdrop the possibility of

collision - less energy dissipation through shock formation at the inhomogeneous layer observed and proposed by us is very attractive.

A semi - analytic approximate estimate for the total energy dissipation has also been made which confirms the numerical observation of the independence of the total dissipated energy to the magnitude and character (resistivity and/or viscosity) of the dissipative processes at work. Furthermore the calculation show that the energy dissipation depends on the ratio of the traversed distance by the structure and the inhomogeneity scale length. This parameter is identical to what defines the threshold for trapping vs. transmission in our numerical studies. This clearly shows that the energy dissipation occurring at the shock layer is behind the irreversible propagation of the structures.

We apply our shock induced anomalous energy dissipation scheme to the problem of Fast Ignition (FI) [2] which relies on the stopping of energetic electrons for the creation of hot spot . A recent experimental work by Yabuuchi *et al.* [37] provides conclusive experimental evidence of the proposed dissipation scheme at work in fast ignition related experiments. Furthermore, a number of PIC simulations [8-11] carried out through worldwide in the context of fast ignition using distinct codes show very clearly plasma heating at the location of the target inhomogeneity. This provides another conclusive evidence for our mechanism at work.

We also propose a new simpler scheme to collimate and guide the path of energetic electrons using a tailored plasma density inhomogeneity profile. We show that the electrons path can be guided through plasma density inhomogeneity just as optical fibers guide the path of photons. The schemes suggested by other authors on electron guiding adopt a complicated procedure of specially prepared structured targets of different materials [12, 13]. Such targets would neither be easy to prepare nor can they be employed with ease in each and every experiment. We offer the possibility of achieving this objective through a properly tailored plasma density profile. This has been illustrated in the thesis with numerical simulations. The experiment [38] at Institute for Laser Engineering ( ILE ), Osaka, Japan shows that the energetic electrons generated at the critical density layer gets guided along the direction defined by the orientation of a solid carbon wire. We feel that inhomogeneous plasma density spontaneously created by the ionization of the wire by the energetic electrons provides the requisite inhomogeneous plasma profile for the guiding of the wire in this ILE experiment.

In addition a number of fundamental observations, e.g. illustration of the (Kelvin - Helmholtz) KH destabilization [39] of the sharp current pulses in the presence of plasma density inhomogeneity and the formation of a novel coherent nonlinear state in the form of vortex beads aligned along the density inhomogeneity have also been made and form a part of the thesis.

- 
- [1] J. D. Lindl, *Inertial Confinement Fusion: The Quest for Ignition and Energy Gain Using Indirect Drive*, Springer-Verlag, New York (1998).
  - [2] M. Tabak, J. Hammer, M. E. Glinsky, W. L. Kruer, S. C. Wilks, J. Woodworth, E. M. Campbell, M. D. Perry and R. J. Mason, *Phys. Plasmas* **1**, 1626 (1994).
  - [3] M. S. Livingston and J. Blewett, *Particle Accelerators*, New York: McGraw-Hill, (1962).
  - [4] J. M. Dawson, *Scientific American* **260**, 54 (1989).
  - [5] T. Tajima and J. M. Dawson, *Phys. Rev. Lett.* **43**, 267 (1979).
  - [6] S. Kahaly, S. Mondal, G. R. Kumar, S. Sengupta, A. Das and P. K. Kaw, *Phys. Plasmas*, **16**, 043114 (2009).
  - [7] S. Sengupta, A. S. Sandhu, G. R. Kumar, A. Das and P. K. Kaw, *Nucl. Fusion* **45**, 1377 (2005).
  - [8] R. B. Campbell, R. Kodama, T. A. Melhorn, K. A. Tanka and D. R. Welch, *Phys. Rev. Lett.* **94**, 055001 (2005).
  - [9] M. Honda, J. Meyer-ter-Vehn and A. Pukhov, *Phys. Rev. Lett.* **85**, 2128 (2000).
  - [10] M. Honda, J. Meyer-ter-Vehn and A. Pukhov, *Phys. Plasmas* **7**, 1302 (2000).
  - [11] J. J. Honorubia and J. Meyer-ter-Vehn, *Nucl. Fusion* **46**, L25 (2006).
  - [12] S. Kar, A. P. L. Robinson, D. C. Carroll, O. Lundh, K. Markey, P. Mckenna, P. Norreys and M. Zepf, *Phys. Rev. Lett.* **102**, 055001 (2009).

- [13] A. P. L. Robinson and M. Sherlock, *Phys. Plasmas* **14**, 083105 (2007).
- [14] A. S. Kingsep, K. V. Chukbar and V. V. Yankov, *Reviews of Plasma Physics* (Consultant Bureau, New York), vol. 16, 1990.
- [15] A. Das and P. H. Diamond, *Phys. Plasmas* **7**, 170 (2000).
- [16] F. Califano, R. Prandi, F. Pegoraro and S. V. Bulanov, *Phys. Plasmas* **6**, 2332 (1999).
- [17] S. V. Bulanov, F. Pegoraro and A. S. Sakharov, *Phys. Fluids B* **4**, 2499 (1992).
- [18] D. Biskamp, E. Schwarz, A. Zeiler, A. Celani and J. F. Drake, *Phys. Plasmas* **6**, 751 (1999).
- [19] N. Attico, F. Califano and F. Pegoraro, *Phys. Plasmas* **7**, 2381 (2000).
- [20] N. Attico, F. Califano and F. Pegoraro, *Phys. Plasmas* **9**, 458 (2002).
- [21] F. Califano, N. Attico, F. Pegoraro, G. Bertin and S. V. Bulanov, *Phys. Rev. Lett.* **86**, 5293 (2001).
- [22] J. C. Dorelli and J. Brin, *Phys. Plasmas* **8**, 4010 (2001).
- [23] L. Chacon, A. N. Simakov and A. Zocco, *Phys. Rev. Lett.* **99**, 235001 (2007).
- [24] S. I. Vainshtein, S. M. Chitre and A. V. Olinto, *Phys. Rev. E* **61**, 4422 (2000).
- [25] M. Rheinhardt and U. Geppert, *Phys. Rev. Lett.* **88**, 101103 (2002).
- [26] A. Teste and G. K. Parks, *Phys. Rev. Lett.* **102**, 075003 (2009).
- [27] N. Jain and S. Sharma, *Phys. Plasmas* **16**, 050704 (2009).
- [28] W. L. Kruer, *Physics of laser Plasma interaction*, Addison-Wesley, 1988.
- [29] A. S. Sandhu, A. K. Dharmadhikari, P.P. Rajeev, G. R. Kumar, S. Sengupta, A. Das and P. K. Kaw, *Phys. Rev. Lett.* **89**, 225002 (2002).

- [30] B. N. Kuvshinov, J. Rem, T. J. Schep and E. Westerhof, *Phys. Plasmas* **8**, 3232 (2001).
- [31] B. N. Kuvshinov, E. Westerhof, T. J. Schep and M. Berning, *Phys. Letts. A* **241**, 287 (1998).
- [32] S. K. Yadav, A. Das and P. Kaw, *Phys. Plasmas* **15**, 062308 (2008).
- [33] J. P. Boris, *Flux Corrected Transport Modules for Generalized Continuity Equations*, (NRL Memorandum Report 3237, Naval Research Laboratory, Washington DC ), 1976.
- [34] M. B. Isichenko and A. M. Marnachev, *Sov. Phys. JETP* **66**, 702 (1987).
- [35] S. K. Yadav and A. Das, *Phys. Plasmas* **17**, 052306 (2010).
- [36] S. K. Yadav, A. Das, P. Kaw and S. Sengupta, *Phys. Plasmas* **16**, 040456 (2009).
- [37] T. Yabuuchi, A. Das, G. R. Kumar, H. Habara, P. K. Kaw, R. Kodama, K. Mima, P. A. Norreys, S. Sengupta and K. A. Tanaka, *New Journal of Physics* **11**, 093031 (2009).
- [38] R. Kodama, Y. Sentoku, Z. L. Chen, G. R. Kumar, S. P. Hatchett, Y. Toyama, T. E. Cowan, R. R. Freeman, J. Fuchs, Y. Izawa, M. H. Key, Y. Kitagawa, K. Kondo, T. Matsuoka, H. Nakamura, M. Nakatsutsumi, P. A. Norreys, T. Norimatsu, R. A. Snavely, R. B. Stephens, M. Tampo, K. A. Tanaka and T. Yabuuchi, *Nature* **432**, 1005 (2004).
- [39] A. Das and P. Kaw, *Phys. Plasmas* **8**, 4518 (2001).

# Contents

List of Figures . . . . .	iii
List of Tables . . . . .	viii
<b>1 Introduction</b>	<b>1</b>
1.1 Motivation . . . . .	1
1.2 Models for Description . . . . .	2
1.3 Previous Work on Electron Species Related Phenomena in Plasmas	4
1.3.1 Generation . . . . .	4
1.3.2 Propagation, Stopping and Heat Deposition . . . . .	5
1.3.3 Fundamental Issues . . . . .	8
1.4 Earlier Studies on EMHD Phenomena with Inhomogeneous Plasma Density . . . . .	9
1.5 Scope of the Thesis . . . . .	10
<b>2 The Generalized Electron Magnetohydrodynamic ( G-EMHD ) Model</b>	<b>13</b>
2.1 Introduction . . . . .	13
2.2 Derivation of G-EMHD Model Equations . . . . .	14
2.2.1 G-EMHD Model Equations . . . . .	15
2.2.2 G-EMHD Model in 2-D . . . . .	16
2.3 Square Integral Invariants Supported by G-EMHD Model Equations	17
2.4 G-EMHD Model in Various Limits . . . . .	18
2.5 Summary . . . . .	19
<b>3 Description of Numerical Scheme for the Evolution of 2-D G- EMHD Model Equations</b>	<b>20</b>
3.1 Introduction . . . . .	20

3.2	Numerical Scheme for Nonlinear 2-D G-EMHD Model . . . . .	21
3.3	Validation and Benchmarking of the Code . . . . .	30
3.4	Summary . . . . .	30
<b>4</b>	<b>G-EMHD Simulation: Fundamental Results on Current Pulse Propagation through Inhomogeneity</b>	<b>32</b>
4.1	Preliminary Description . . . . .	33
4.1.1	Choice of Initial Conditions . . . . .	33
4.1.2	Choice of Density Inhomogeneity Profile . . . . .	35
4.2	Inhomogeneity Induced Drift Velocity . . . . .	40
4.3	Dipole Penetration in High Density Region . . . . .	43
4.4	Trapping vs. Transmission through High Density Region . . . . .	50
4.5	Summary . . . . .	53
<b>5</b>	<b>Collision - less Energy Dissipation of Electron Current Pulse: Application to Fast Ignition</b>	<b>55</b>
5.1	Introduction . . . . .	56
5.2	Shock Formation: Current Pulse Propagation through Inhomogeneity . . . . .	58
5.3	Evolution of Total Energy Associated with Current Pulse . . . . .	61
5.4	Energy Dissipation through Shock Formation . . . . .	62
5.5	Oblique Incidence of Current Pulse on Plasma Density Inhomogeneity	65
5.6	Application : Fast Ignition . . . . .	67
5.7	Summary . . . . .	69
<b>6</b>	<b>Kelvin Helmholtz Destabilization of Short Current Pulse in an Inhomogeneous Plasma</b>	<b>71</b>
6.1	Introduction . . . . .	72
6.2	Destabilization of Current Layers . . . . .	73
6.3	Formation of Stationary Vortex Beads . . . . .	78
6.4	Summary . . . . .	78
<b>7</b>	<b>Guiding and Collimation of Fast Electron Current Pulse in a Plasma</b>	<b>80</b>
7.1	Introduction . . . . .	80

7.2	Guiding of Monopoles . . . . .	81
7.3	Collimation of the Current Pulse . . . . .	82
7.4	Guiding Behavior of the Current Pulse . . . . .	84
7.5	Bifurcation of the Current Pulse Structure . . . . .	85
7.6	Summary . . . . .	86
<b>8</b>	<b>Conclusion and Scope for Further Research</b>	<b>87</b>
8.1	Summary and Conclusions . . . . .	87
8.2	Future Directions for Research . . . . .	92
<b>A</b>	<b>Derivation of the G-EMHD Model Equations</b>	<b>94</b>
<b>B</b>	<b>Solution of the Nonlinear EMHD Equation</b>	<b>99</b>
<b>C</b>	<b>Solution of the Inertialess G-EMHD Model</b>	<b>102</b>
	Bibliography . . . . .	107

# List of Figures

3.1	This is the simulation space in $x - y$ plane. The circle represents the grid points where the equilibrium value for the variables is to be assigned in the simulation. The derivative of the fields $(b, \psi)$ inside of the boundary, for example at $(i, j)$ are calculated by the neighbouring points using the central differencing scheme. As in the simulation the periodic boundary condition is considered. So for the boundary points $(N_x, j)$ the derivative of the fields can be calculated by using the points $(1, j)$ as is shown in the figure. . . . .	23
3.2	This figure represents the reduction of the 2D grid space $(i, j)$ in one dimensional space $(l)$ . That is obtained by using the relation $l = (i-1)N_y + j$ where $i = 1, 2, \dots, N_x$ and $j = 1, 2, \dots, N_y$ . The index $l$ is running along the $y$ direction as is shown in the figure. Thus in this new representation the consecutive two grid points along the $x$ -direction is displaced by the $N_y$ no. of grid points while along the $y$ direction they are separated only by a single grid point as is shown at the point $l$ . . . . .	25
4.1	This is the constant contour of the scalar field $(b)$ forming a monopole. The associated parameters of the monopole are $A = 5.5, x_0 = 0.0, y_0 = 3.0, \sigma_x = 1.0$ and $\sigma_y = 1.0$ . . . . .	34
4.2	This is the constant contour of scalar field $b$ forming a dipole within the spatial extant of $r_0 \approx 1$ and having the axial velocity $u = 0.1$ along the negative $y$ -direction. The left lobe of the dipole corresponds to positive value of amplitude while the right one corresponds to negative value of amplitude. . . . .	35

4.3	<b>STH</b> density profile ( $h_1 = 5.5, h_2 = 4.5, w = 2.0, y_0 = 0.0, \sigma_y = 1.0, \sigma = 0.5$ ) . . . . .	36
4.4	<b>STC</b> density profile ( $h_1 = 0.6, h_2 = -0.4, w = 2.0, y_0 = 0.0, \sigma_y = 1.0, \sigma = 0.5$ ) . . . . .	37
4.5	<b>SGH</b> density profile ( $h_1 = 1.0, h_2 = 9.0, y_0 = 0.0, \sigma^2 = 3.0$ ) . . . . .	37
4.6	<b>SGC</b> density profile ( $h_1 = 1.0, h_2 = -0.9, y_0 = 0.0, \sigma^2 = 3.0$ ) . . . . .	38
4.7	<b>RTH</b> density profile ( $h_1 = 5.5, h_2 = 4.5, w = 2.0, x_0 = 0.0, y_0 = 0.0, \sigma_x = 1.0, \sigma_y = 1.0, \sigma = 0.5$ ) . . . . .	38
4.8	<b>RTC</b> density profile ( $h_1 = 0.6, h_2 = -0.4, w = 2.0, x_0 = 0.0, y_0 = 0.0, \sigma_x = 1.0, \sigma_y = 1.0, \sigma = 0.5$ ) . . . . .	39
4.9	<b>RGH</b> density profile ( $h_1 = 1.0, h_2 = 9.0, x_0 = 0.0, y_0 = 0.0, \sigma_x = \sqrt{3.0}, \sigma_y = \sqrt{3.0}$ ) . . . . .	39
4.10	<b>RGC</b> density profile ( $h_1 = 1.0, h_2 = -0.9, x_0 = 0.0, y_0 = 0.0, \sigma_x = \sqrt{3.0}, \sigma_y = \sqrt{3.0}$ ) . . . . .	40
4.11	The propagation of the monopolar structure (color contours) in an inhomogeneous plasma density is depicted by showing the location of the structure at various times in the different subplots of the figure. The thick black lines represent the plasma density contour. In this case the plasma density is chosen to be a function of $y$ only. The central $y$ region of width $w = \pm 2.0$ corresponds to a high density (10 times of the density at the edge region) . . . . .	41
4.12	Various stages of the propagation of a dipolar structure through an inhomogeneous density plasma has been shown. The inhomogeneity in plasma density is similar to that of Fig. (4.11) in this case. The figure clearly shows the penetration of the dipole through the plasma density inhomogeneity to enter the high density region. The lobes of the dipole structure are squeezed towards each other as they pass through the inhomogeneous region. However, once inside the high density homogeneous region they again acquire a balanced form. . . . .	43
4.13	In this figure the dipole is shown to approach a density cavity (lower density plasma region). It can be observed that the dipole is unable to penetrate the lower density plasma. The two lobes of the dipole get separated transverse to the density gradient direction and subsequently they evolve as separate monopolar structures. . . . .	46

4.14	The trapping of the dipolar structure in a high density plasma has been illustrated in this figure. A high density plasma with a circular profile in the $x-y$ plane represented by the thick black contour lines are depicted on the various subplots. A dipole structure can be seen to penetrate the high density region. However, once inside the high density region it continues to remain trapped in this region. . . . .	47
4.15	The propagation of the dipole through an inhomogeneous density profile when it form a cavity within the finite region of the space as is shown in the each subplot of the figure with the black thick contours. In this case the dipole structure do not get to penetrate inside the cavity. . . . .	48
4.16	This figure represents the collisional behavior of two dipoles in the presence of density inhomogeneity when the <b>RTH</b> density profile is considered in the simulation. . . . .	49
4.17	The four columns of the subplots represent four different cases of propagation of current pulse structure past the plasma density inhomogeneity. The detailed configuration of the density profile and the current pulse structure for each of the four cases has been mentioned in the text. The thick dark straight lines in the plot show the constant density contour at the location of maximum gradient. The cases corresponding to the (a) and (d) columns show trapping (lobes get separated upon reaching the other end ) and those for (c) and (d) columns show transmission. In each subplots, the red and blue lobe of the structure implies positive and negative amplitude of the magnetic field directed along the symmetry direction $\hat{z}$ , respectively. . . . .	51
5.1	This is the schematic diagram for current pulse associated with the 2-D nonlinear solutions of Electron Magnetohydrodynamics (EMHD) model equations. Subplots (a), (b) and (c) show the contour plot of the associated magnetic field, the profile of magnetic field and the electron flow at the mid $y = 0$ section of the structure respectively for the monopolar. Subplots (d), (e) and (f) corresponds to the same features for the dipolar structure. . . . .	57

5.2	The contour plots of the magnetic field $b$ in the $x$ - $y$ plane is shown in subplots [a,b] (inertialess case) [d,e] (full G-EMHD) at two different times. The numbers (-2,0,2) on the axis of these plots show length in units of electron skin depth (corresponding to the low density plasma). The magnetic field $b$ profile in $x$ at the mid plane of the structure in $y$ has been depicted at various times in subplot (c) and (f) for inertialess and the full G-EMHD simulations respectively. The subplot (g) and (h) show the inhomogeneous plasma density profile through which the dipolar structure evolves. The cross $\times$ and the arrow $\rightarrow$ mark on these subplots show the initial location of the dipole for inertialess (dipole has no axial velocity in this case) and full G-EMHD simulations. . . . .	59
5.3	Schematic diagram of the dynamics of the dipole when it encounters the density inhomogeneity (shown by a thick curved black line that is varying along the $y$ - direction having different region of inhomogeneity). . . . .	60
5.4	Evolution of the total energy of the structure for full G-EMHD simulations, as it propagates through the inhomogeneous plasma density (a) for various grid resolutions (b) for simulations with finite resistivity parameter $\eta$ and (c) with finite viscosity parameter $\mu$ in G-EMHD equations. A thick dashed vertical line shows the time when the dipole enters the inhomogeneous plasma density region. . . . .	61
5.5	The propagation of current pulse structure incident at angles of 30, 20, 10 and 5 degrees with respect to the density gradient direction have been shown in the plots of first, second, third and fourth columns respectively. . . . .	66
5.6	The evolution of the total energy has been shown when the current pulse is incident at (i) $5^\circ$ ( curve with blue stars), (ii) $10^\circ$ (curve with green + sign, (iii) $20^\circ$ (curve with magenta crosses) and (iv) $30^\circ$ (curve with red circles). . . . .	67

6.1	The various stages of evolution as the current pulse propagates towards an elongated sharp density profile. The thick black curve represents the outline of the density profile. The collimation of the current pulse structure as it enters the high density plasma region can be clearly seen. The KH destabilization is clearly evident from the plots at $t = 2820$ . . . . .	74
6.2	In this figure the robustness of the dipole solution is shown. Initially the dipole structure is taken elongated along the $y-$ axis. During the evolution it is observed that dipole ,finally ,form the Isichenko <i>et al.</i> solution [65] propagating along the negative $\hat{y}$ direction with some constant axial velocity. . . . .	76
7.1	In this figure the collimating behavior of the dipole has been demonstrated. The current pulse passes through a high density profile that has an elongated profile (shown in the figure by the closed black thick line) along the $y-$ direction. . . . .	83
7.2	This figure shows that a dipolar current pulse can be guided. The single black contour in each subplot represents the curved high density profile chosen in the simulation. The inside region of the closed black line is of the high density amplitude. The circular region attached at the left end of the half circular region is of high amplitude in comparison to the half circular region. . . . .	84
7.3	This figure show the bifurcation of the current pulse. The thick black lines show the plasma density profile that has been chosen for these simulation. . . . .	86

# List of Tables

4.1	Profile <b>SGH</b> . . . . .	52
4.2	Profile <b>STH</b> . . . . .	52

# Chapter 1

## Introduction

This thesis is devoted to the study of the propagation and transport features of electron current pulses through an inhomogeneous plasma medium. Interesting observations of both fundamental and applied nature are made. This has been done with the help of simulations of Electron - Magnetohydrodynamic model [1, 2, 3, 4] which has been generalized to treat an inhomogeneous plasma. A new collisionless scheme to extract energy from fast electrons at the plasma inhomogeneity layer for the purpose of plasma heating has been elucidated. This is specially useful for heating plasma in overdense regimes where lasers can not be employed. This scheme of plasma heating by electrons is maneuverable, as the heating efficiency, the specific location for energy dissipation in plasma etc., can be decided by properly tailoring the plasma density inhomogeneity profile. Another novel possibility of guiding the path of the electron current pulse with the help of appropriately tailored plasma inhomogeneity profile has also been demonstrated in these studies.

The direct relevance of both effects shown here, viz., (i) the possible guiding of the electron path in the plasma and (ii) the deposition of its energy to heat the plasma, to the problem of Fast Ignition (FI) [5] has also been outlined.

### 1.1 Motivation

In recent years there has been a phenomenal progress in the development of high power of peta-watt (PW) range, short pulse (sub-picoseconds) lasers. These high power lasers have led to the exploration of hitherto unknown regime of plasma re-

## Chapter 1: Introduction

sponse. Furthermore, the availability of fast diagnostic tools has helped in watching the response of the plasma at these fast time scales in considerable detail. This has opened up an entirely new area of research. At these fast time scales electrons are the main species which participate in dynamics and the heavier ion species have a dormant role of merely providing a static neutralizing background. Various plasma physics phenomena are now being explored from the fast electron time scale evolution perspective. For instance, the work carried out to investigate the physics of the fast magnetic field line reconnection events [6, 7, 8, 9, 10, 11], the fast Z pinches [12, 13], fast plasma switches [14, 15, 16, 17, 18, 19, 20], the generation of quasi - static intense magnetic fields in laboratory experiments [21, 22, 23, 24] etc., are explored on the basis of underlying electron dynamics. It thus appears that a proper theoretical understanding of electron transport through plasma is of considerable importance.

### 1.2 Models for Description

A variety of models and tools have been employed for the purpose of these studies. The use of electron fluid model along with the Maxwell set of equations for the description of the evolution of electromagnetic fields associated with electron motion is a commonly adopted approach towards the depiction of most phenomena in this particular regime [1, 2, 3, 4, 25, 26]. Both analytical and numerical studies have been carried out with this description. There are Particle - In - Cell (PIC) models [27, 28, 29, 30], which treat kinetic aspect of the plasma particles, and are used extensively numerically. A combination of fluid and particle description in various regimes have also been adopted in hybrid codes [31, 32, 33].

For fast electron propagation in a plasma, the current associated with the system can be very high. The electrons in the presence of self consistently generated magnetic field in such a situation behaves like a magnetized fluid. A simplified description treating the flow of magnetized electrons is the Electron Magnetohydrodynamic (EMHD) fluid model [1, 2, 3, 4]. The time scale associated with this model are fast so as to ignore ion dynamics, but it is slower than the electron plasma period of the system. The model, thus, rules out the space charge contribution. The electron density perturbations are therefore ignored in the context of

## Chapter 1: Introduction

EMHD model. The EMHD model has led to the understanding and prediction of a host of novel phenomena, e.g. the fast penetration of magnetic fields [34, 35], the phenomena of Electron Magnetohydrodynamic (EMH) resistance [1]etc. The simulations of this particular fluid model has also been carried out extensively, to understand the coherent as well as turbulent dynamics associated with electron fluids in a plasma [36, 37, 38, 39].

As mentioned earlier, the investigation of electron dynamics in plasmas can also be carried out with the help of Particle - in - Cell (PIC) computations [27, 28, 29, 30]. In these computations a large assembly of electrons are evolved as fat particles under the action of self consistent electromagnetic fields. These simulations do contain the space charge fluctuation associated with the fast electron plasma period. In this sense they are more complete than the simplified EMHD model. Furthermore, the kinetic effects associated with finite temperature are also present in this depiction. The PIC simulations, however, are often very computationally demanding. One therefore, typically, restricts to lower space dimensions and/or compromises with spatial resolution. These limitations exist even when the state of the art computational facilities are employed. For instance, even now the spatial grid in some PIC studies [32] barely resolve the electron skin depth, which is a crucial length scale associated with electron dynamics. This, in a sense, is tantamount to ignoring the physics of electron inertia. In contrast the simulations with EMHD fluid model resolve the electron skin depth scale, thereby retaining the contribution of electron inertial effects. Clearly, there are always pros and cons of any tool and model that one adopts. The approach should be to glean as much physics as possible from the judicious use of the available tools.

We have chosen to investigate the problem of electron transport with the help of a fluid model in the EMHD domain. The specific question associated with the transport of electrons in an inhomogeneous plasma constitutes the main focus of study in this thesis.

## 1.3 Previous Work on Electron Species Related Phenomena in Plasmas

We summarize here some earlier studies associated with electron species in the plasma which underline the relevance of the specific question that have been investigated in this thesis. The theoretical and experimental work on studies associated with the response of lighter electron species have primarily addressed issues concerning (i) the generation of fast electrons (by lasers etc.,) in plasma medium (ii) the propagation, stopping and energy deposition of the energetic electrons in plasmas and (iii) certain fundamental issues associated with electron transport (e.g. evolution of the associated magnetic fields, associated instabilities and nonlinear features in coherent and turbulent regimes etc.,).

### 1.3.1 Generation

The possibility to employ electrons as an energy source for heating plasma medium (specially in overdense regimes where lasers cannot penetrate) has led to the quest for efficient generation of energetic electrons. The resonant [40] and the vacuum heating mechanism proposed by Brunel [41] being some such schemes. The experimental study by Sandhu *et al.* [42] have provided experimental evidence of fast electron generation by the process of resonant absorption. They have shown that the wave breaking of nonlinear plasma wave leads to an efficient generation of energetic electrons.

Studies to enhance hot electron generation has led to various suggestions for improved laser coupling to plasma. In this regard introducing preplasma [43] has been fruitful. However, major improvements have resulted by structuring the target surface by nanoparticles [44], nanowires [45] and other deposits [46, 47, 48]. Periodic modulations such as grating structures have also been tried and have produced good enhancement on hot electron generation which has been attributed to the excitation of surface plasmons [46, 47, 49]. In a recent experimental study [50] with sub  $\lambda$  grating target almost 100% absorption was shown. Analytical and PIC studies were carried out for the experimental conditions to clearly demonstrate the role of surface plasmon in such an efficient absorption. These studies have thus

## Chapter 1: Introduction

demonstrated clearly the possibility of efficient generation of energetic electrons.

In order to use such energetic electrons for the purpose of plasma heating a study of their propagation characteristics through the plasma medium is important. The next subsection summarizes the attempts that have been made in this regard.

### 1.3.2 Propagation, Stopping and Heat Deposition

The energetic electrons typically carries very high currents along with it. The flow of electrons with huge currents is known to get inhibited by its own self generated magnetic fields. In fact it has been shown that there exists a limit known as the 'Alfven limit' on the magnitude of current, beyond which the current cannot propagate [51]. This is because the associated magnetic field becomes very high to curve the electron trajectories backwards. Inside a plasma, however, the current carried by the energetic electrons can often exceed the Alfven limit. This is so as the plasma provides for the return shielding current. The return current being in opposite direction it neutralizes the magnetic field and allows the forward current due to the energetic electrons to be of a magnitude higher than the Alfven limit. It is now well established by the 3-D PIC simulations of Sentoku *et al.* [29, 30] that the combination of the forward and return shielding currents get spatially separated by Weibel instability [52]. The Weibel separation of currents leads to the formation of alternating sheets of oppositely propagating currents. These sheets tear and form several cylindrical current filaments whose core carries the forward current and the outer cylindrical shell contains the return shielding current. These filaments then coalesce and form fewer cylindrical current carrying filaments. Each coalesced filaments have currents below the Alfven limit. Combination of such filaments carry the total current associated with the hot energetic electrons inside a plasma.

The electrons carrying the forward current in these channels are a good source of energy. They can be employed for the purpose of plasma heating if they can be stopped at a desired location, where they dissipate their energy into heating the background plasma. The collisional stopping of the energetic electrons involves Rutherford's cross section for electron ion collision. This cross section however, decreases with increasing electron energy and hence is not an efficient process to stop high energy electrons. On the other hand, efficient heating would require that the energy content of the electrons be high. In this regard the presence of

## Chapter 1: Introduction

anomalous stopping mechanism would be of great use. There are debates on the presence as well as the possible role of anomalous mechanisms for stopping. In fact a simulation by Sentoku *et al.* [29, 30] in a 3-D homogeneous plasma shows that after coalescence the channel shows bending and ultimately degenerates forming small scale turbulent structures. This generation of electromagnetic turbulence can explain the rapid electron energy dissipation in those simulations. The mechanism behind the generation of this electromagnetic turbulence was identified in the studies by Jain *et al.* [53, 54, 55] based on the Kelvin Helmholtz (KH) destabilization of the sheared electron flow [56] amidst the spatially separated forward and return shielding electron currents flowing in the channel.

The studies on electron stopping and the possibility of heating the plasma by it have primarily been motivated by the problem of Fast Ignition (FI) [5]. FI is a simple variant of the Inertial Confinement Fusion (ICF) [57, 58], in the sense that the two tasks of compression and the creation of hot spark in the plasma are separated. The compression is achieved by a slow nanosecond laser pulse throughout which the target remains cold. The appearance of Rayleigh Taylor (RT) like hydrodynamic instabilities [59] thus become inconsequential as there can be no mixing between the hot and cold fuels at this stage. This removes the stringent criteria of high uniformity of the drive pressure and on the spherical symmetry of the target. To create a hot spot in the target a separate sub - picoseconds ultra intense laser (UIL) pulse is sent. The target being compressed the UIL cannot penetrate it but generates energetic electrons at the critical density surface through the various mechanism outlined earlier. The expectation then is that these electrons would penetrate the high density core of the compressed target core and deposit their energy at some localized region. The calculations based on classical estimates even after taking into account effects due to correlated collisions, dense plasma effects etc., predict that the electrons will traverse past the core without depositing their energy. On the other hand the sub - ignition small experiments have shown the success of the FI scheme [60, 61]. This shows that the electrons do stop and deposit their energy in the target core despite contrary predictions provided by the classical collisional estimates. It, therefore, appears that for this system an anomalous collision - less mechanism exists.

In the FI scenario the electrons have to propagate from the low density plasma corona region of the critical layer ( $n = 10^{22}/cc$ ) towards the high density plasma

## Chapter 1: Introduction

core ( $n \sim 10^{26}/cc$ ). In this case thus the energetic electrons would need to propagate inhomogeneous plasma region. The studies on electron propagation through inhomogeneous plasma in the context of FI has been carried out by various groups primarily using PIC simulations. The PIC studies on electron propagation through inhomogeneous plasma medium have been carried out by various authors in 2-D [32, 33]. An interesting aspect of all these simulation studies, which employ different PIC codes and have been conducted by various groups is that the plasma gets heated at the location where the density gradient is maximum. This result have been reported in a number of publication, however, with no comments on the possible origin of this effect.

*One of the prime motivation of our studies in this thesis has been to understand and physically interpret this observation. For this purpose we study the propagation of electron current pulse structures through an inhomogeneous plasma medium. A simplified fluid description of EMHD is used for this purpose*

A possible maneuvering of the path of energetic electrons is another issue of interest. In this context novel structured targets having materials with different resistivity have been designed and experimented upon [62, 63]. Kar *et al.* [63] have experimentally shown the guiding of relativistic electron beams in solid targets by magnetic fields created at the interface of two metals of different electrical resistivity. This experiment provided a proof of the theoretical study done by Robinson & Sherlock [62] on the guiding of the fast electrons at the interface of two metals of the different resistivity. The design of such targets and employing it in any given experiment, however, would be a complex task.

A recent experiment by Kodama *et al.* [64] shows an interesting simple method to guide the electrons. They showed in their experiment that a metal wire attached on the tip of the cone (where the fast electron generation occurs by an ultra intense laser pulse) guides the path of the electrons. By tilting the angle of the wire they were able to show that the electrons followed the direction defined by the wire. It is believed that the wire gets ionized by the front of the energetic electron pulse and the plasma thus created guides the electrons along a desired path. The experiment clearly indicates that there exists a role of a sharp inhomogeneous plasma (transverse to the wire) in guiding the electron current pulse path.

*Another motivation for investigating the role of plasma density inhomogeneity on electron transport in this thesis is with the viewpoint of seeking a simplified*

*scheme to maneuver and guide the path of energetic electrons.*

### 1.3.3 Fundamental Issues

The electron time scale regime dynamics in plasma offers an interesting and simple nonlinear medium for exploring fundamental questions pertaining to the coherent and turbulent response of plasma medium. The EMHD model description have often been used by various authors to theoretically explore the coherent as well as the turbulent behavior of the plasma medium [65, 66, 67, 68, 69, 70, 71] in this regime. The presence of the inherent length scale viz., the electron skin depth scale and the whistler frequency (when external magnetic field is also present ) distinguishes this system from the neutral hydrodynamic scale free fluid system. The electron skin depth scale causes a change in the spectral scaling of decaying EMHD turbulence [38]. Furthermore, the magnetized character of the electron fluid also influences and produces novel features to hydrodynamic fluid phenomena. These studies have attracted attention recently. For instance, the well known fluid instabilities such as Kelvin - Helmholtz mode etc., in the context of EMHD has been shown to get suitably altered [55, 72] in terms of growth rate and range of unstable wavenumbers.

Recently, some experiments have also been conducted which shed light on various fundamental processes associated with the propagation of electrons in a plasma medium. A propagating electron current pulse has an associated magnetic field with it. Thus the generation, evolution and decay of magnetic field in the plasma often provides information on the characteristic features of the electron current. This has been employed in the papers by Sandhu *et al.* [21, 22] and Subhendu *et al.* [50] to infer the properties of the electron flow. The experiment a pump probe system of lasers to study the magnetic field evolution from Cotton Mouton effect. The rapid decay of the magnetic field observed in the experiment by Sandhu *et al.* [21] provided evidence for presence of anomalous dissipation and hence the presence of turbulence in flows.

It would be interesting to study how plasma inhomogeneity would alter the propagation behavior of the electron current pulse structure in the nonlinear regime. This is specially important for the FI experiment related studies where the electrons have to propagate through inhomogeneous plasma density and where anomalous

mechanisms for dissipation are being sought for.

*The nonlinear propagation of electron current pulses through an inhomogeneous plasma density by a generalized EMHD description in 2-D has been explored extensively in this thesis keeping the fundamental physics issues under consideration.*

### 1.4 Earlier Studies on EMHD Phenomena with Inhomogeneous Plasma Density

The thesis focuses on the study of electron transport through inhomogeneous plasma density for EMHD time scales. For these studies, therefore, a generalization of the EMHD model to include effects due to plasma inhomogeneity is essential. We briefly review here previous studies where EMHD studies have been carried out for an inhomogeneous plasma density.

Kingsep *et al.* [1] have ignored the electron inertia related terms and incorporated inhomogeneous density of a specific simplified form to arrive at a reduced Burger's equation for the magnetic field evolution. From this study it was inferred that the magnetic shocks can form at the inhomogeneous plasma density layer. Kingsep *et al.* [1] also derived an equation for magnetic field evolution with electron inertia, however, again a specific form viz., a linear weakly varying plasma density was assumed. This equation was later solved by Petvishvili in a moving frame using the ansatz of stationarity to obtain solitons in 1-D, and monopoles and dipoles in 2-D [73]. These solutions were later shown to be stable using the Zakharov-Kuznetsov method [74].

Fruchtman *et al.* [75] have also considered an inhomogeneous plasma, however they ignore electron inertia related terms in the EMHD equation. They have, however, considered the evolution of energy in conjunction with the EMHD equation. Thus it forms a coupled set of magnetic field and the energy evolution. This was used to study the penetration of magnetic field in Plasma Opening devices (POS).

Kuvshinov *et al.* [76] have considered again an inhomogeneous plasma for their studies. However, they have gone beyond the EMHD description by incorporating effects due to space charge fluctuation. Both, the space charge fluctuation ( $\tilde{n}/n_0$ ) and the equilibrium density variation ( $L_n = n_0/n'_0$ ) in comparison to relevant scale of the phenomena ( $k$ ) were considered to be very small and treated perturbatively.

## Chapter 1: Introduction

The exact solutions for this set were obtained by Kuvshinov *et al.* [77] and the evolution of such structures have also been investigated numerically [77].

We have obtained a generalization of Electron Magnetohydrodynamics (EMHD) equations in the presence of inertia related terms and have also made no approximation for any specific form of the density inhomogeneity. No approximation as regards to slow variation of the inhomogeneity has been made in the derivation of our equations. The complete set has then been numerically investigated for various forms of the plasma inhomogeneity profile as demonstrated in the subsequent Chapters.

### 1.5 Scope of the Thesis

As stated earlier the understanding of electron transport in an inhomogeneous plasma constitutes the main theme of this thesis. For this purpose we employ the fluid description in the EMHD domain. The EMHD model [1, 2, 3, 4] describes the evolution of magnetized electron fluid in a homogeneous plasma. We, therefore, first generalize the EMHD description to inhomogeneous plasma density. The new model is termed as the Generalized EMHD (G-EMHD) [78].

Chapter 2 of the thesis provides a detail derivation of the G-EMHD model [78]. The salient aspects of the G-EMHD equations are discussed in detail. Furthermore, various limits of G-EMHD equations in reduced spatial dimension and simplified electron flow configuration are also discussed in this chapter. In Chapter 3 we describe in detail the numerical procedure adopted for simulating the G-EMHD equations. The G-EMHD equations can be cast in the form of convective equation with appropriate source term. We use the flux corrected scheme [79] to evolve the G-EMHD equations in time. The main challenge appears when at each step of evolution one has to evaluate the magnetic field/convective velocity. This involves solving a Helmholtz kind of equation whose coefficient is a function of space.

In Chapter 4 we present our observations on 2-D G-EMHD simulations [78] for the simplified case where the electron current flow is confined in the 2-D symmetry plane. Our objective being to study the role of plasma density inhomogeneity on the electron current pulse propagation, we chose exact current pulse solutions of the homogeneous EMHD as initial condition and made them evolve through in-

## Chapter 1: Introduction

homogeneous plasma density. The nonlinear EMHD solutions are of two varieties [65]. One has monopolar magnetic field configuration and represents rotating electron currents. This is a stationary solution of EMHD. The EMHD also permits traveling solutions with dipolar magnetic fields. These dipoles move with constant axial speed and have a current configuration which mocks up a spatially separated forward electron current along the central axis and return shielding current at the edges. A variety of inhomogeneous plasma density profiles were chosen for studying the propagation of these current pulses. The numerical studies show (i) that the structures acquire an additional drift in the presence of density inhomogeneity which is transverse to the magnetic field and the density gradient (ii) The dipole can penetrate inside a high density plasma region but is unable to come out from there. It thus gets trapped within a high plasma density region. (iii) While the dipole structure passes through the density inhomogeneity to penetrate the high density region, it forms magnetic shocks and/or sharp current layers [80]. A threshold criteria is formulated for trapping vs. transmission of the structures [81]. The trapping of the dipole current pulse structure in high density region indicates the violation of time reversal invariance and is suggestive of a dissipative mechanism at work. Indeed it is shown in Chapter 5 that a strong energy dissipation is associated with the magnetic shock which form at the inhomogeneity layer when the dipole structure enters the high density region. It is shown that the energy dissipation is independent of the magnitude and the character of the dissipation present in the system. This provides a novel collision - less scheme for the energy dissipation of electron current pulse in plasma. The electrons are a good source of energy as they can be easily accelerated to high energies. A high energy electron whose classical Rutherford collision cross section is known to fall drastically with increasing energy. But with the help of this mechanism of energy dissipation we can still deposit its energy efficiently. Furthermore, the electrons can be used to heat overdense plasma region where lasers are unable to penetrate. This is precisely the situation in the context of Fast Ignition (FI) laser fusion [5]. This relevance of the density inhomogeneity based electron stopping mechanism to the frontline concept of fast ignition laser fusion experiment is also shown in detail in Chapter 5. In the limit of small and/or negligible electron - ion collisions the Kelvin - Helmholtz destabilization of the sharp current layers which form at the density inhomogeneity would produce anomalous viscosity and

## Chapter 1: Introduction

would be instrumental in energy dissipation. The generation of turbulence and anomalous viscosity have been shown earlier in the context of homogeneous 3-D EMHD simulations for sharp electron current layers [53]. In Chapter 6 we show the process of KH destabilization of sharp current layers in the presence of density inhomogeneity in 2-D. The 2-D case as expected the KH destabilization leads to the formation of coherent pattern in the case of G-EMHD as well, which can be traced to the existence of two integral square invariants supported by the system [81]. In Chapter 7 we discuss another application where the density inhomogeneity has an important role. Often one wants to collimate and guide the electron current inside a plasma. There have been many proposals of especially structured targets prepared of different materials of different resistivity [62, 63]. Such targets would neither be easy to prepare nor can they be employed with ease in each and every experiment. Again a proper tailoring of the plasma density offers an easier accessible scheme. We illustrate this by placing arbitrary shaped wire like density inhomogeneous structure along the path of the electron current pulse structure. It is observed that the current flows along the path defined by the inhomogeneous path. In an experiment [64] at ILE, Osaka, Japan the energetic electrons generated at the critical density layer were guided with the help of solid carbon wire. The experiment showed that the electrons moved along the wire, as the wire was tilted the path of the electrons changed accordingly. We feel that inhomogeneous plasma density spontaneously created by the ionization of the wire by the electrons is responsible for this.

We summarize our work in Chapter 8 and provide discussions for the future scope of the thesis.

# Chapter 2

## The Generalized Electron Magnetohydrodynamic ( G-EMHD ) Model

The propagation of fast electron current pulse structures through an inhomogeneous plasma medium is the prime concern of this thesis. For this purpose we seek a fluid description of the plasma under the framework of EMHD domain. The EMHD model [1, 2, 3, 4] describes the evolution of magnetized electron fluid in a *homogeneous* plasma. We, therefore, present in this chapter the generalization of the EMHD description to a plasma with inhomogeneous density. The new model is termed as the Generalized EMHD (G-EMHD) model [78]. The discussion of salient aspects of the G-EMHD model along with the integral conservations supported by the set of G-EMHD model equations is provided. The simplification of the G-EMHD model in reduced spatial dimensions as well as that of simple 2-D electron flow configurations are also presented.

### 2.1 Introduction

The well known single fluid model known as Electron - Magnetohydrodynamics (EMHD) provides a suitable description of the fast dynamical response of electron species in a homogeneous plasma. The EMHD model treats the positively charged ions as a static neutralizing background. The coupled set of electron fluid evolution

along with the Maxwell's equation define the EMHD model. The model ignores the displacement current contribution in the Ampere's law. This is valid when the space charge related effects can be considered to be negligible and/or the phase speed associated with the phenomena of interest is slower than that of the speed of light. The typical time scales are thus chosen to be slower than the electron plasma period making the continuity equation for the electron density fluctuation irrelevant. The Ampere's law then directly relates the current of the system to the curl of magnetic field. Since the ions are at rest, then the entire current in plasma is only due to the flow of electron species. Thus for a uniform plasma the current is directly proportional to the electron velocity. The combination of the electron fluid momentum and the Maxwell set of equations thus get simplified and the system can be represented entirely in terms of the magnetic field evolution equation.

In a real scenario the plasma can often be inhomogeneous. Thus the coefficient relating the curl of magnetic field with the electron velocity in the Ampere's Law becomes space dependent. This space dependent part alters the evolution equation significantly. This is the genesis of the G-EMHD model whose derivation is illustrated in the next section. The consequences of the density inhomogeneity terms will be explored in the subsequent chapters by simulating the G-EMHD model equations [78, 80, 81].

## 2.2 Derivation of G-EMHD Model Equations

The G-EMHD model is a generalization of the Electron Magnetohydrodynamics for the case when the background plasma density is inhomogeneous. The G-EMHD model, therefore, also represents the same range of length and time scales for which EMHD is typically applied. Even though the background plasma density is taken to be inhomogeneous, the density perturbations are ignored as in EMHD. Thus the displacement current as well as the electron continuity equations are ignored in this case too, under the approximation of

$$\omega \ll \omega_{pe}, \omega_{pe}^2/\omega_{ce}$$

Here  $\omega$  represents the typical time period of the phenomena under consideration. The electron plasma frequency and the gyrofrequency is represented by  $\omega_{pe} = 4\pi ne^2/m_e$  and  $\omega_{ce} = eB_0/m_e c$  respectively. Here  $B_0$  represents the magnitude of magnetic field and  $n$  is the background plasma density. When the background plasma density  $n$  is inhomogeneous, the plasma frequency is defined in a local sense.

### 2.2.1 G-EMHD Model Equations

The ions being static the equations associated with ion motion, viz., continuity and momentum are irrelevant. Furthermore, since charge density fluctuation are ignored within the EMHD domain of time scales, we consider the electron momentum equation alone for the evolution. A cold plasma has been considered in our derivation. Thus the pressure term is ignored in the electron momentum equation.

$$m_e \left[ \frac{\partial \vec{V}_e}{\partial t} + (\vec{V}_e \cdot \nabla) \vec{V}_e \right] = -e \left[ \vec{E} + \frac{\vec{V}_e \times \vec{B}}{c} \right] - m_e \nu \vec{V}_e \quad (2.1)$$

Here  $\nu$  denotes the electron - ion collision frequency. Expressing the electric field  $\vec{E}$  and the magnetic field vector  $\vec{B}$  in terms of scalar and vector potentials and then taking the curl of Eq. (2.1) one obtains the following equation :

$$\frac{\partial (\nabla \times \vec{P})}{\partial t} = \nabla \times (\vec{V}_e \times (\nabla \times \vec{P})) - \nu \nabla \times \vec{V}_e \quad (2.2)$$

Here  $\vec{P} = \vec{V}_e - e\vec{A}/m_e c$  is the generalized momentum containing both electron flow velocity  $V_e$  as well as the vector field  $\vec{A}$ . Thus Eq. (2.2) provides an evolution equation for  $\nabla \times \vec{P} = \nabla \times \vec{V}_e - e\vec{B}/m_e c$  : a combination of the curl of the electron velocity and the magnetic field. We seek another equation relating the vectors  $\vec{V}_e$  and  $\vec{B}$  from the approximate form (obtained after ignoring the displacement current) of the Ampere's law. Thus from  $\nabla \times \vec{B} = (4\pi/c)\vec{J}$  we have

$$\vec{V}_e = - \left( \frac{c}{4\pi n_e e} \right) \nabla \times \vec{B} \quad (2.3)$$

Upto this stage the derivation of G-EMHD equations are identical with those of the EMHD model. The difference arises now when the curl of the electron velocity given by Eq. (2.3) is taken for expressing  $\nabla \times \vec{P}$  entirely in terms of magnetic field  $\vec{B}$  vector. There is an extra term which arises due to the nonuniformity of the plasma density (and hence  $n_e$  as well) as plasma is quasineutral. Defining  $\vec{G} = (m_e c/e)\nabla \times \vec{P}$  we have

$$\vec{G} = \frac{d_{e0}^2}{n} \nabla^2 \vec{B} + \frac{d_{e0}^2}{n^2} \nabla n \times (\nabla \times \vec{B}) - \vec{B} \quad (2.4)$$

Here  $n = n_e/n_0$  (where  $n_0$  is a constant typical value chosen to normalize the density),  $d_{e0}^2 = c^2/\omega_{pe0}^2$  is the electron skin depth at  $n_0$ , (where  $\omega_{pe0}^2 = 4\pi n_0 e^2/m_e$  is the square of electron plasma frequency corresponding to the plasma density ( $n_0$ )). From Eq. (2.4) it is clear that in addition to the space dependent coefficient  $1/n$  of  $\nabla^2 \vec{B}$  we have an extra density gradient dependent term appearing in the expression of  $\vec{G}$ . The impact of this term on the evolution of fields would be seen in the subsequent Chapters.

We choose to normalize the magnetic field  $\vec{B}$  by a typical value  $B_0$ , time by the corresponding electron gyro period  $\omega_{ce}^{-1} = (eB_0/m_e c)^{-1}$ , length by  $d_{e0}$  ( defined above ) to obtain the following normalized evolution equation for the G-EMHD model [78]:

$$\begin{aligned} \frac{\partial \vec{g}}{\partial t} &= \nabla \times (\vec{V} \times \vec{g}) - \eta \left( \frac{\nabla^2 \vec{B}}{n} + \frac{1}{n^2} \nabla n \times \nabla \times \vec{B} \right) \\ \vec{g} &= \frac{1}{n} \nabla^2 \vec{B} + \frac{1}{n^2} \nabla n \times (\nabla \times \vec{B}) - \vec{B}; \quad \vec{V} = -\frac{\nabla \times \vec{B}}{n} \end{aligned} \quad (2.5)$$

Here,  $\vec{g}$  and  $\vec{V}$  are normalized fields  $\vec{G}$  and  $\vec{V}_e$  respectively. The field  $\vec{B}$  in Eq. (2.5) though having the same symbol as before is the normalized magnetic field and  $\eta = \nu/\omega_{ce}$  is normalized resistivity.

### 2.2.2 G-EMHD Model in 2-D

The G-EMHD model Eq. (2.5) gets simplified when the variation of the fields are assumed to be confined in a 2-D plane. We consider  $\hat{e}_p, \hat{e}_q$  and  $\hat{e}_s$  as the right handed triad of unit vectors and take the symmetry axis to be along  $\hat{e}_s$ .

The magnetic field being divergenceless can be expressed in terms of two scalar fields in 2-D as  $\vec{B} = b\hat{e}_s + \hat{e}_s \times \nabla\psi$ . The electron velocity can be written as  $\vec{V} = -(\nabla \times \vec{B})/n = (\hat{e}_s \times \nabla b)/n - \hat{e}_s \nabla^2 \psi/n$ ; the first term in the velocity expression corresponds to the electron flow in the 2-D plane (defined by  $\hat{e}_p$  and  $\hat{e}_q$  unit vectors) and the second is associated with the electron flow along the symmetry direction.

The G-EMHD model in this 2-D case reduces to the following two coupled set of evolution equation for  $b$  and  $\psi$ .

$$\begin{aligned} \frac{\partial}{\partial t} \left\{ b - \nabla \cdot \left( \frac{\nabla b}{n} \right) \right\} + \hat{e}_s \times \nabla b \cdot \nabla \left[ \frac{1}{n} \left\{ b - \nabla \cdot \left( \frac{\nabla b}{n} \right) \right\} \right] + \hat{e}_s \times \nabla \psi \cdot \nabla \left( \frac{\nabla^2 \psi}{n} \right) \\ = \eta \nabla \cdot \left( \frac{\nabla b}{n} \right) \end{aligned} \quad (2.6)$$

and

$$\frac{\partial}{\partial t} \left\{ \psi - \frac{\nabla^2 \psi}{n} \right\} + \frac{\hat{e}_s \times \nabla b}{n} \cdot \nabla \left\{ \psi - \frac{\nabla^2 \psi}{n} \right\} = \eta \frac{\nabla^2 \psi}{n} \quad (2.7)$$

A detailed derivation of Eqs. (2.6, 2.7) from the 3-D G-EMHD model (Eq. (2.5)) has been given in Appendix A. For a constant plasma density  $n$  the above equations reduces to the standard 2-D form of the EMHD model as expected. We will mainly concentrate on the study of the 2-D form provided by Eqs. (2.6, 2.7) of the G-EMHD model. A further simplification of the model results when the electron flow is confined in the 2-D plane. In this case magnetic field has only one component along the symmetry direction ( $\hat{e}_s$ ). Thus only  $b$  field is finite and  $\psi$  is zero for this specific case.

## 2.3 Square Integral Invariants Supported by G-EMHD Model Equations

We now seek conservation of integral quantities which are supported by the G-EMHD equations. These conservation law provide crucial information on evolution. They are also used to benchmark any numerical code that one adopts/develops for evolution studies.

The G-EMHD model conserves total energy of the system in the non - dissipa-

tive limit,  $\eta = 0$ . The total energy in this case is the sum of electron kinetic and the magnetic field energy. Thus

$$\frac{1}{2} \frac{d}{dt} \int \left\{ b^2 + \frac{(\nabla b)^2}{n} + (\nabla \psi)^2 + \frac{\nabla^2 \psi}{n} \right\} d^2 \vec{X} = \frac{dE}{dt} = 0 \quad (2.8)$$

Where

$$E = \frac{1}{2} \int \left\{ b^2 + \frac{(\nabla b)^2}{n} + (\nabla \psi)^2 + \frac{(\nabla^2 \psi)^2}{n} \right\} d^2 \vec{X} \quad (2.9)$$

Here  $[b^2 + (\nabla \psi)^2]$  represents the magnetic energy and the remaining terms  $(1/n)[(\nabla b)^2 + (\nabla^2 \psi)^2]$  are the kinetic energy associated with the electron motion of the G-EMHD fluid. The derivation for this conservation is given in Appendix A.

In the simplified limit when the electron flow is confined in the 2-D plane (the case of  $\psi = 0$  discussed in the previous section) an additional square integral quantity shown below is conserved (see detailed derivation in Appendix A).

$$\frac{1}{2} \frac{d}{dt} \int \frac{1}{n} \left( b - \nabla \cdot \left( \frac{\nabla b}{n} \right) \right)^2 d^2 \vec{X} = \frac{dH}{dt} = 0 \quad (2.10)$$

The invariant  $H$  is like the enstrophy invariant of the 2-D hydrodynamic flow. Here, however, it has contribution from the magnetic field as well.

## 2.4 G-EMHD Model in Various Limits

We have seen that our G-EMHD model equations reduce to the EMHD equations in the limit of uniform plasma density. When the electron flow is confined to the 2-D plane the model equations can be cast in terms of a single scalar field  $b$  corresponding to the magnetic field in the direction of symmetry and can be written as:

$$\frac{\partial}{\partial t} (b - \nabla^2 b) + \hat{e}_s \times \nabla b \cdot \nabla (b - \nabla^2 b) = 0 \quad (2.11)$$

In this limit of uniform plasma density, this equation has the same form as the Hasegawa - Mima (HM) equation [82] which is obtained for the description of low frequency plasma behavior.

The hydrodynamic 2-D fluid evolution equation results when the typical scale

lengths are shorter than the electron skin depth, i.e. when  $b < \nabla^2 b$ . In this limit the electron kinetic energy dominates over the magnetic field energy and the electron behaves like a neutral hydrodynamic fluid.

## 2.5 Summary

A generalized fluid model (G-EMHD) for the depiction of magnetized electron flow in a non - uniform plasma has been obtained. In 2-D the G-EMHD model has been shown to reduce to a coupled set of evolution equation amidst two scalar fields representing magnetic field and vector potential component along symmetry direction. For a simplified case when the electron flow is confined in 2-D plane the evolution equation of G-EMHD model reduces to a single equation of evolution of magnetic field component along symmetry direction. The G-EMHD equations conserve total energy of the system in the non-dissipative limit. An additional square integral invariant in 2-D (similar to enstrophy conservation in 2-D neutral hydrodynamic fluid) is also supported by G-EMHD for the special case when electron flow is confined in the 2-D plane.

# Chapter 3

## Description of Numerical Scheme for the Evolution of 2-D G-EMHD Model Equations

In this Chapter we describe in detail the numerical procedure adopted for simulating the 2-D G-EMHD equations [78, 80, 81]. The 2-D G-EMHD Eqs. (2.6) and (2.7) can be cast in the form of convective equation for those fields which are essentially obtained by the action of Helmholtz like operator (second order spatial derivative equation having space dependent coefficients) on  $b$  and  $\psi$  fields introduced in Chapter 2 of the thesis. These convective equations also have source terms. A flux corrected scheme has been used to evolve the G-EMHD equations in time. The main challenge appears when at each time step of evolution one has to invert the Helmholtz like operator (with space dependent coefficients) to evaluate the magnetic field and the corresponding convective velocity.

### 3.1 Introduction

The G-EMHD model in 2-D is a coupled set of equations between two scalar fields  $b$  and  $\psi$  which are the magnetic field and the vector potential component respectively, along the symmetry direction  $\hat{e}_s$ . The evolution equation for  $\Omega_b$  and  $\Omega_\psi$  given by

$$\Omega_b = \left\{ b - \nabla \cdot \left( \frac{\nabla b}{n} \right) \right\} = \| \mathcal{A} \| b \quad (3.1)$$

and

$$\Omega_\psi = \left\{ \psi - \frac{\nabla^2 \psi}{n} \right\} = \|\mathcal{B}\| \psi \quad (3.2)$$

respectively are of the form of convective equations.

$$\frac{\partial \Omega_b}{\partial t} + \nabla \cdot \left( \frac{\hat{e}_s \times \nabla b}{n} \Omega_b \right) = \nabla \cdot [(\hat{e}_s \times \nabla \psi) \Omega_\psi] \quad (3.3)$$

and,

$$\frac{\partial \Omega_\psi}{\partial t} + \frac{\hat{e}_s \times \nabla b}{n} \cdot \nabla \Omega_\psi = 0 \quad (3.4)$$

From Eqs. (3.3) and (3.4) it is clear that the quantities  $\Omega_b$  and  $\Omega_\psi$  get convected by the in - plane electron velocity of  $\vec{V}_\perp = (\hat{e}_s \times \nabla b)/n$ . The evolution of  $\Omega_b$  (which can be looked upon as the component of generalized vorticity along the symmetry direction) has a source term in the right hand side. Unlike 2-D hydrodynamic flow in this case the generalized vorticity has a source term in the presence of  $\psi$  and  $\nabla^2 \psi$ , i.e. in the presence of electron flow along  $\hat{e}_s$ . The generalized vortex stretching arises here from the curl of  $\vec{J} \times \vec{B}$  force. It should be noted that when the electron flow is confined in the 2-D symmetry plane,  $\psi$  is zero and there is no source in the  $\Omega_b$  evolution. Eq. (3.4) shows the evolution of the component (along the symmetry axis  $\hat{e}_s$ ) of conjugate momentum  $\Omega_\psi$  (having contribution both from field as well as the electron velocity part). It can be seen that  $\Omega_\psi$  is merely convected in the 2-D plane and has no source in its evolution. The symbols  $\|\mathcal{A}\|$  and  $\|\mathcal{B}\|$  are the short hand notations for the operators relating  $b$  with  $\Omega_b$  and  $\psi$  with  $\Omega_\psi$  in Eq. (3.1) and Eq. (3.2) respectively.

## 3.2 Numerical Scheme for Nonlinear 2-D G-EMHD Model

Eqs. (3.3) and (3.4) are evolved using the flux corrected scheme of Boris *et al.* [79]. A collection of FORTRAN subroutines LCPFCT (Laboratory for Computational Physics, Flux-Corrected Transport) implements "**Flux-Corrected Transport**" algorithm to solve one dimensional generalized convective transport equation in various geometries. We employ these suite of subroutines using **time splitting technique** to evolve the 2-D system of Eqs. (3.3) and (3.4). In some earlier studies

[54, 72] related to EMHD model system, this procedure has been successfully implemented. In the EMHD system  $n$  being uniform  $b$  and  $\psi$  can be obtained by inverting the Helmholtz operator  $\| \mathcal{O} \|$

$$\| \mathcal{O} \| b = b - \nabla^2 b = \Omega_b; \quad \| \mathcal{O} \| \psi = \psi - \nabla^2 \psi = \Omega_\psi$$

at each time step once  $\Omega_b$  and  $\Omega_\psi$  are from the evolution of Eqs. (3.3) and (3.4). Standard Helmholtz Solvers [83] are available and were used for this purpose in these earlier studies [54, 72]. Once  $b$  is known, the convective velocity is evaluated using relation  $\vec{V}_\perp = \hat{e}_s \times \nabla b$  to evaluate the value  $\Omega_b$  and  $\Omega_\psi$  at the next time step. Thus this completes the entire loop of evolution.

In our G-EMHD case [78], however, the operators ( $\| A \|$  &  $\| B \|$ ) relating  $b$  to  $\Omega_b$  and  $\psi$  to  $\Omega_\psi$  respectively, have a complicated form than that of a simple Helmholtz system [83]. The coefficients of  $b$  and  $\psi$  that form the operators ( $\| A \|$  &  $\| B \|$ ) are space dependent. This is so because we are considering density ( $n$ ) to be inhomogeneous. Therefore, the standard routines for solving Helmholtz equation can not be used for this particular case. We have implemented a direct procedure wherein the space dependent operator is expressed in the form of a matrix in the 2-D discretized space. The inversion of the operator matrix and its multiplication with the vector formed with the values of  $\Omega_b$  and  $\Omega_\psi$  at all the grid points gives us the solution for  $b$  and  $\psi$  from their respective equations. We provide a detailed description of the method below.

The 2-D space in the  $x-y$  plane (choosing  $\hat{z}$  as the symmetry axis) is discretized as shown in Fig. (3.1). The field variables  $b(x, y)$ ,  $\psi(x, y)$ ,  $n(x, y)$ ,  $\Omega_b(x, y)$  and  $\Omega_\psi(x, y)$  being functions of the  $x, y$  space are defined at the grid points at the center of each cell in Fig. (3.1). The  $x$  and  $y$  dimensions of the simulation box  $L_x$  and  $L_y$  are discretized in  $N_x$  and  $N_y$  grid points as shown in Fig. (3.1). Each grid point can be represented by the combination of running index  $i$  and  $j$ , which take values from 1 to  $N_x$  and 1 to  $N_y$  respectively. Thus the field variables at any location are represented by  $p(x, y) = p(i, j)$ . Where  $p$  stands for the field variables. The operators  $\| \mathcal{A} \|$  and  $\| \mathcal{B} \|$  corresponding to  $\Omega_b$  and  $\Omega_\psi$  respectively, have second order spatial derivatives. Using the centered difference scheme for the representation of the second order spatial derivative it can be shown that these operators connect the field variables at point  $(i, j)$  with those at 4 neighbouring

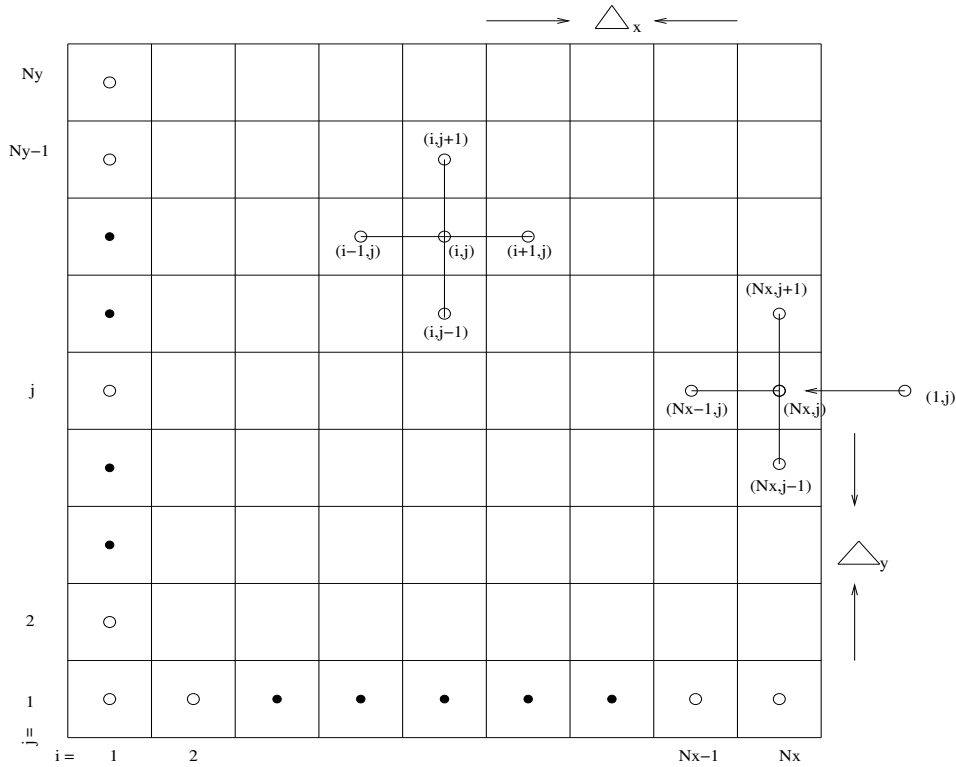


Figure 3.1: This is the simulation space in  $x - y$  plane. The circle represents the grid points where the equilibrium value for the variables is to be assigned in the simulation. The derivative of the fields  $(b, \psi)$  inside of the boundary, for example at  $(i, j)$  are calculated by the neighbouring points using the central differencing scheme. As in the simulation the periodic boundary condition is considered. So for the boundary points  $(N_x, j)$  the derivative of the fields can be calculated by using the points  $(1, j)$  as is shown in the figure.

points  $(i - 1, j)$ ,  $(i + 1, j)$  (for second order derivative along  $x$ ) and  $(i, j - 1)$  and  $(i, j + 1)$  (for second order derivative along  $y$ ) as shown in the Fig. (3.1). Thus equations  $\| \mathcal{A} \| b = \Omega_b$  and  $\| \mathcal{B} \| \psi = \Omega_\psi$  relates  $\Omega_b$  and  $\Omega_\psi$  at each of the spatial point  $(i, j)$  with 4 neighbouring distinct points of the field  $b$  and  $\psi$  respectively. Such a relationship can be expressed in terms of a matrix representation for the operators  $\| \mathcal{A} \|$  and  $\| \mathcal{B} \|$  where the fields  $b$  and  $\psi$  in the 2-D space are cast as vectors  $[b]$  and  $[\psi]$  having single distinct index  $l$  for each spatial point of the 2-D space as shown in Fig. (3.2). The index  $l$  thus varies from 1 to  $N_x \times N_y$ . The matrix corresponding to operators  $\| \mathcal{A} \|$  and  $\| \mathcal{B} \|$  has a dimension of  $N_x^2 \times N_y^2$ . We now illustrate how the two matrices are defined.

The equation  $\| \mathcal{A} \| b = \Omega_b$  in an expanded form can be written as

$$b - \frac{1}{n} \frac{\partial^2 b}{\partial x^2} - \frac{1}{n} \frac{\partial^2 b}{\partial y^2} + \frac{1}{n^2} \frac{\partial n}{\partial x} \frac{\partial b}{\partial x} + \frac{1}{n^2} \frac{\partial n}{\partial y} \frac{\partial b}{\partial y} = \Omega_b \quad (3.5)$$

In the discrete 2-D space the equation takes the form of

$$b_{(i,j)} - \left[ \frac{b_{(i+1,j)} - 2b_{(i,j)} + b_{(i-1,j)}}{n_{(i,j)} \Delta_x^2} \right] - \left[ \frac{b_{(i,j+1)} - 2b_{(i,j)} + b_{(i,j-1)}}{n_{(i,j)} \Delta_y^2} \right] + \frac{n'_{x(i,j)}}{n_{(i,j)}^2} \left[ \frac{b_{(i+1,j)} - b_{(i-1,j)}}{2\Delta_x} \right] + \frac{n'_{y(i,j)}}{n_{(i,j)}^2} \left[ \frac{b_{(i,j+1)} - b_{(i,j-1)}}{2\Delta_y} \right] = \Omega_{b_{(i,j)}}$$

Or equivalently

$$\begin{aligned} & (1/2n_{(i,j)}^2 \Delta_x^2) \left( -2n_{(i,j)} + n'_{x(i,j)} \Delta_x \right) b_{(i+1,j)} - (1/2n_{(i,j)}^2 \Delta_x^2) \left( 2n_{(i,j)} + n'_{x(i,j)} \Delta_x \right) b_{(i-1,j)} \\ & + (1/2n_{(i,j)}^2 \Delta_x^2 \Delta_y^2) \left( 2n_{(i,j)}^2 \Delta_x^2 \Delta_y^2 + 4n_{(i,j)} \Delta_y^2 + 4n_{(i,j)} \Delta_x^2 \right) b_{(i,j)} + (1/2n_{(i,j)}^2 \Delta_y^2) \\ & \left( 2n_{(i,j)} - n'_{y(i,j)} \Delta_y \right) b_{(i,j+1)} - (1/2n_{(i,j)}^2 \Delta_y^2) \left( 2n_{(i,j)} + n'_{y(i,j)} \Delta_y \right) b_{(i,j-1)} = \Omega_{b_{(i,j)}} \end{aligned} \quad (3.6)$$

The spatial index for the fields has been written as a suffix within small brackets and the suffix  $x$  and  $y$  denote the variable with respect to which differentiation has been taken. In the above expression  $\Delta_x$  &  $\Delta_y$  are grid size along  $x$  &  $y$  direction respectively. We now represent the field in 2-D space as a one dimensional vector. To achieve this we define a running index

$$l = N_y (i - 1) + j \quad \text{for } i = 1, 2, \dots, N_x ; j = 1, 2, \dots, N_y$$

The value of  $l$  corresponding to each grid point has been shown in Fig. (3.2). It is clear from the expanded discretized form of the Eq. (3.6) that the matrix representing operator  $\| \mathcal{A} \|$  will in general have finite main diagonal elements ( $\mathcal{A}(l, l)$  non zero), two diagonals in the immediate neighbourhood of the main diagonal as finite ( $\mathcal{A}(l, l \pm 1)$  non zero) and two more (displaced by  $\Delta l = \pm N_y$ , i.e.  $\mathcal{A}(l, l \pm N_y)$ ) as finite. Furthermore, the elements connecting the boundary points of the fields  $b$  need to be defined properly so as to be consistent with periodic boundary condition that has been adopted for all the simulations presented in this thesis work. The plasma density profile  $n(x, y)$  is known and chosen to have

### Chapter 3: Description of Numerical Scheme for the Evolution of 2D ....

different spatial profiles for various problems that have been investigated in the subsequent Chapters. The spatial profile of  $\Omega_b$  is known at each time step from the evolution equation and hence it is also a given function of space. Therefore, the field  $b$  is determined from

$$\mathcal{A}[b] = [\Omega_b] \implies [b] = \mathcal{A}^{-1}[\Omega_b] \quad (3.7)$$

The elements of the matrix  $\mathcal{A}$  are as follows:

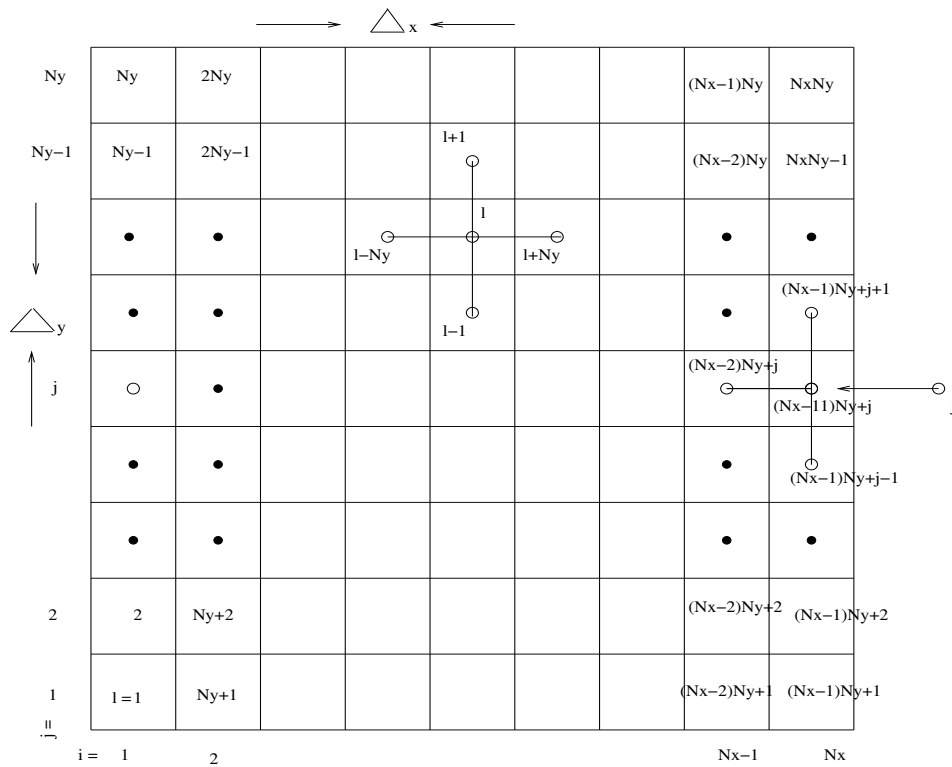


Figure 3.2: This figure represents the reduction of the 2D grid space  $(i, j)$  in one dimensional space  $l$ . That is obtained by using the relation  $l = (i-1)N_y + j$  where  $i = 1, 2, \dots, N_x$  and  $j = 1, 2, \dots, N_y$ . The index  $l$  is running along the  $y$  direction as is shown in the figure. Thus in this new representation the consecutive two grid points along the  $x$ -direction is displaced by the  $N_y$  no. of grid points while along the  $y$  direction they are separated only by a single grid point as is shown at the point  $l$ .

Main diagonal element  $\mathcal{A}(l, l)$

$$\mathcal{A}(l, l) = (1/2n_{(i,j)}^2 \Delta_x^2 \Delta_y^2) (2n_{(i,j)}^2 \Delta_x^2 \Delta_y^2 + 4n_{(i,j)} \Delta_y^2 + 4n_{(i,j)} \Delta_x^2)$$

$$i = 1, 2, 3, \dots, N_x; \quad j = 1, 2, 3, \dots, N_y$$

Upper diagonal elements  $\mathcal{A}(l, l + 1)$

$$\mathcal{A}(l, l + 1) = (1/2n_{(i,j)}^2 \Delta_y^2) (2n_{(i,j)} - n'_{y(i,j)} \Delta_y)$$

$$i = 2, 3, \dots, N_x - 1; \quad j = 2, 3, \dots, N_y - 1$$

$$\mathcal{A}(l, l + 1) = (1/2n_{(1,j)}^2 \Delta_y^2) (2n_{(1,j)} - n'_{y(1,j)} \Delta_y)$$

$$j = 2, 3, \dots, N_y - 1$$

$$\mathcal{A}(l, l + 1) = (1/2n_{(N_x,j)}^2 \Delta_y^2) (2n_{(N_x,j)} - n'_{y(N_x,j)} \Delta_y)$$

$$j = 2, 3, \dots, N_y - 1$$

$$\mathcal{A}(l, l + 1) = (1/2n_{(i,1)}^2 \Delta_y^2) (2n_{(i,1)} - n'_{y(i,1)} \Delta_y)$$

$$i = 1, 2, 3, \dots, N_x$$

$$\mathcal{A}(l, l - (N_y - 1)) = (1/2n_{(i,N_y)}^2 \Delta_y^2) (2n_{(i,N_y)} - n'_{y(i,N_y)} \Delta_y)$$

$$i = 1, 2, 3, \dots, N_x$$

Lower diagonal elements  $\mathcal{A}(l, l - 1)$

$$\mathcal{A}(l, l - 1) = - (1/2n_{(i,j)}^2 \Delta_y^2) (2n_{(i,j)} + n'_{y(i,j)} \Delta_y)$$

$$i = 2, 3, \dots, N_x - 1; \quad j = 2, 3, \dots, N_y - 1$$

$$\mathcal{A}(l, l - 1) = - (1/2n_{(1,j)}^2 \Delta_y^2) (2n_{(1,j)} + n'_{y(1,j)} \Delta_y)$$

$$j = 2, 3, \dots, N_y - 1$$

$$\mathcal{A}(l, l - 1) = - (1/2n_{(N_x,j)}^2 \Delta_y^2) (2n_{(N_x,j)} + n'_{y(N_x,j)} \Delta_y)$$

$$j = 2, 3, \dots, N_y - 1$$

$$\mathcal{A}(l, l + N_y - 1) = - (1/2n_{(i,1)}^2 \Delta_y^2) (2n_{(i,1)} + n'_{y(i,1)} \Delta_y)$$

$$i = 1, 2, 3, \dots, N_x$$

$$\mathcal{A}(l, l - 1) = - \left( 1/2n_{i,N_y}^2 \Delta_y^2 \right) \left( 2n_{(i,N_y)} + n'_{y(i,N_y)} \Delta_y \right)$$

$$i = 1, 2, 3, \dots, N_x$$

Displaced diagonal elements  $\mathcal{A}(l, l + N_y)$

$$\mathcal{A}(l, l + N_y) = \left( 1/2n_{(i,j)}^2 \Delta_x^2 \right) \left( -2n_{(i,j)} + n'_{x(i,j)} \Delta_x \right)$$

$$i = 2, 3, \dots, N_x - 1; \quad j = 2, 3, \dots, N_y - 1$$

$$\mathcal{A}(l, l + N_y) = \left( 1/2n_{(1,j)}^2 \Delta_x^2 \right) \left( -2n_{(1,j)} + n'_{x(1,j)} \Delta_x \right)$$

$$j = 1, 2, 3, \dots, N_y$$

$$\mathcal{A}(l, l - (N_x - 1)N_y) = \left( 1/2n_{(N_x,j)}^2 \Delta_x^2 \right) \left( -2n_{(N_x,j)} + n'_{x(N_x,j)} \Delta_x \right)$$

$$j = 1, 2, 3, \dots, N_y$$

$$\mathcal{A}(l, l + N_y) = \left( 1/2n_{(i,1)}^2 \Delta_x^2 \right) \left( -2n_{(i,1)} + n'_{x(i,1)} \Delta_x \right)$$

$$i = 2, 3, \dots, N_x - 1$$

$$\mathcal{A}(l, l + N_y) = \left( 1/2n_{(i,N_y)}^2 \Delta_x^2 \right) \left( -2n_{(i,N_y)} + n'_{x(i,N_y)} \Delta_x \right)$$

$$i = 2, 3, \dots, N_x - 1$$

Displaced diagonal elements  $\mathcal{A}(l, l - N_y)$

$$\mathcal{A}(l, l - N_y) = - \left( 1/2n_{(i,j)}^2 \Delta_x^2 \right) \left( 2n_{(i,j)} + n'_{x(i,j)} \Delta_x \right)$$

$$i = 2, 3, \dots, N_x - 1; \quad j = 2, 3, \dots, N_y - 1$$

$$\mathcal{A}(l, l + (N_x - 1)N_y) = - \left( 1/2n_{(1,j)}^2 \Delta_x^2 \right) \left( 2n_{(1,j)} + n'_{x(1,j)} \Delta_x \right)$$

$$j = 1, 2, 3, \dots, N_y$$

$$\mathcal{A}(l, l - N_y) = - \left( 1/2n_{(N_x,j)}^2 \Delta_x^2 \right) \left( 2n_{(N_x,j)} + n'_{x(N_x,j)} \Delta_x \right)$$

$$j = 1, 2, 3, \dots, N_y$$

$$\mathcal{A}(l, l - N_y) = - \left( 1/2n_{(i,1)}^2 \Delta_x^2 \right) \left( 2n_{(i,1)} + n'_{x(i,1)} \Delta_x \right)$$

$$i = 2, 3, \dots, N_x - 1$$

### Chapter 3: Description of Numerical Scheme for the Evolution of 2D ...

$$\mathcal{A}(l, l - N_y) = - \left( 1/2n_{(i, N_y)}^2 \Delta_x^2 \right) \left( 2n_{(i, N_y)} + n'_{x(i, N_y)} \Delta_x \right)$$

$$i = 2, 3, \dots, N_x - 1$$

The matrix  $\mathcal{B}$  relating  $\psi$  to  $\Omega_\psi$  is also similarly defined by representing the operator equation  $\|\mathcal{B}\| \psi = \Omega_\psi$  in discretized 2-D space. The elements of this matrix are :  
Main diagonal element  $\mathcal{B}(l, l)$

$$\mathcal{B}(l, l) = - \left( 1 + 2/n_{(i, j)} \Delta_x^2 + 2/n_{(i, j)} \Delta_y^2 \right)$$

$$i = 1, 2, 3, \dots, N_x; \quad j = 1, 2, 3, \dots, N_y$$

Upper diagonal elements  $\mathcal{B}(l, l + 1)$

$$\mathcal{B}(l, l + 1) = \left( -1/n_{(i, j)} \Delta_y^2 \right)$$

$$i = 2, 3, \dots, N_x - 1; \quad j = 2, 3, \dots, N_y - 1$$

$$\mathcal{B}(l, l + 1) = \left( -1/n_{(1, j)} \Delta_y^2 \right)$$

$$j = 2, 3, \dots, N_y - 1$$

$$\mathcal{B}(l, l + 1) = \left( -1/n_{(N_x, j)} \Delta_y^2 \right)$$

$$j = 2, 3, \dots, N_y - 1$$

$$\mathcal{B}(l, l + 1) = \left( -1/n_{(i, 1)} \Delta_y^2 \right)$$

$$i = 1, 2, 3, \dots, N_x$$

$$\mathcal{B}(l, l - (N_y - 1)) = \left( -1/n_{(i, N_y)} \Delta_y^2 \right)$$

$$i = 1, 2, 3, \dots, N_x$$

Lower diagonal elements  $\mathcal{B}(l, l - 1)$

$$\mathcal{B}(l, l - 1) = \left( -1/n_{(i, j)} \Delta_y^2 \right)$$

$$i = 2, 3, \dots, N_x - 1; \quad j = 2, 3, \dots, N_y - 1$$

$$\mathcal{B}(l, l - 1) = \left( -1/n_{(1, j)} \Delta_y^2 \right)$$

$$j = 2, 3, \dots, N_y - 1$$

$$\mathcal{B}(l, l - 1) = (-1/n_{(N_x, j)} \Delta_y^2)$$

$$j = 2, 3, \dots, N_y - 1$$

$$\mathcal{B}(l, l + N_y - 1) = (-1/n_{(i, 1)} \Delta_y^2)$$

$$i = 1, 2, 3, \dots, N_x$$

$$\mathcal{B}(l, l - 1) = (-1/n_{(i, N_y)} \Delta_y^2)$$

$$i = 1, 2, 3, \dots, N_x$$

Displaced diagonal elements  $\mathcal{B}(l, l + N_y)$

$$\mathcal{B}(l, l + N_y) = (-1/n_{(i, j)} \Delta_x^2)$$

$$i = 2, 3, \dots, N_x - 1; \quad j = 2, 3, \dots, N_y - 1$$

$$\mathcal{B}(l, l + N_y) = (-1/n_{(1, j)} \Delta_x^2)$$

$$j = 1, 2, 3, \dots, N_y$$

$$\mathcal{B}(l, l - (N_x - 1)N_y) = (-1/n_{(N_x, j)} \Delta_x^2)$$

$$j = 1, 2, 3, \dots, N_y$$

$$\mathcal{B}(l, l + N_y) = (-1/n_{(i, 1)} \Delta_x^2)$$

$$i = 2, 3, \dots, N_x - 1$$

$$\mathcal{B}(l, l + N_y) = (-1/n_{(i, N_y)} \Delta_x^2)$$

$$i = 2, 3, \dots, N_x - 1$$

Displaced diagonal elements  $\mathcal{B}(l, l - N_y)$

$$\mathcal{B}(l, l - N_y) = (-1/n_{(i, j)} \Delta_y^2)$$

$$i = 2, 3, \dots, N_x - 1; \quad j = 2, 3, \dots, N_y - 1$$

$$\mathcal{B}(l, l + (N_x - 1)N_y) = (-1/n_{(1, j)} \Delta_y^2)$$

$$j = 1, 2, 3, \dots, N_y$$

$$\mathcal{B}(l, l - N_y) = (-1/n_{(N_x, j)} \Delta_y^2)$$

$$\begin{aligned}
 j &= 1, 2, 3, \dots, N_y \\
 \mathcal{B}(l, l - N_y) &= (-1/n_{(i,1)}\Delta_y^2) \\
 i &= 2, 3, \dots, N_x - 1 \\
 \mathcal{B}(l, l - N_y) &= (-1/n_{(i,N_y)}\Delta_y^2) \\
 i &= 2, 3, \dots, N_x - 1
 \end{aligned}$$

This process of direct evaluation of the  $b$  and  $\psi$  fields by the inversion of the matrices  $\mathcal{A}$  and  $\mathcal{B}$  is very expensive in terms of memory as is evident from the size of the matrices which depends on the square of the total number of grid points (viz.  $N_x^2 \times N_y^2$ ). Thus at higher spatial resolutions and for the case of 3-D studies this method would be prohibitively memory extensive and it cannot be implemented. This is a major drawback of this particular scheme.

The development of an alternative scheme which uses the standard Helmholtz solver [83] iteratively to solve for the spatially dependent part of the operator needs to be developed. This is an important task and would be taken up as a future extension of the work presented in this thesis.

### 3.3 Validation and Benchmarking of the Code

Our code for the G-EMHD evolution has been benchmarked by reproducing the well known simulation results for the uniform density EMHD case. The simulation cases for the evolution of the various configuration of the current pulse structures in EMHD shown in the paper by Das *et al.* [36] by a pseudo spectral code has been reproduced by our simulation method. For non uniform density the definition of the two operator matrices and the evaluation of their inverse has been tested by checking out known analytic cases. Furthermore, the energy integral is tracked in time to ascertain the appropriate resolution necessary for the simulation.

### 3.4 Summary

A numerical scheme for solving the 2-D G-EMHD set of equations [78] has been presented. The flux corrected scheme of Boris *et al.* [79] has been implemented

for the time evolution of the 2-D G-EMHD set of equations. The 2-D G-EMHD model equations are a set of two coupled equations, representing the evolution of the generalized vorticity and generalized momentum along the symmetry direction. At the end of each time step (in the evolution of the 2-D G-EMHD equations) we obtain the values of the generalized vorticity and generalized momentum along the symmetry direction. The evaluation of magnetic field and the vector potential component(along the symmetry direction) from these at each step requires solving a second order differential equation in space with inhomogeneous coefficients. We have implemented a brute force scheme. Whereby this evaluation is done by inverting the matrix representing the operator corresponding to this differential equation. It should be noted that this procedure is prohibitively memory expensive and has indeed restraint our simulations to low spatial resolution. A development relaxation scheme in which the standard Helmholtz operator is used for the evaluation of second order derivatives and the contribution from the space dependent part is evaluated iteratively is desirable.

# Chapter 4

## G-EMHD Simulation: Fundamental Results on Current Pulse Propagation through Inhomogeneity

This chapter of the thesis is devoted towards exploring various fundamental aspects of the electron current transport through an inhomogeneous plasma medium. For this purpose we have employed the 2-D G-EMHD model [78] equations in the simulation. For simplicity the electron current flow is considered to be confined in the 2-D plane only. The objective being to understand the role of plasma density inhomogeneity on the electron current pulse propagation, exact current pulse solutions of the homogeneous EMHD plasma [36, 65] were chosen as initial conditions for study. Both varieties of nonlinear EMHD solutions (i) stationary rotating electron currents with monopolar magnetic field configuration and (ii) traveling solutions with dipolar magnetic fields were chosen as initial states. A variety of inhomogeneous plasma density profiles were chosen for studying the propagation of these current pulses. The studies have resulted in a wide variety of fundamental observations which have been briefly listed out here. These results are presented in detail in the various sections of this Chapter.

In short, our studies have shown that the current pulse structures acquire an additional drift in the presence of density inhomogeneity. This drift is transverse to both the magnetic field and the density gradient. Thus the stationary monopolar structures, in the presence of inhomogeneity, drift along the constant density

contours and are unable to move across the density gradient. The dipolar structure which have a constant axial speed in a homogeneous plasma, on the other hand can penetrate inside a high density plasma region but are unable to come out in a region with lower plasma density. They thus often get trapped within a high plasma density region. The criteria for trapping vs. transmission of the current pulses have been clearly identified from simulations.

## 4.1 Preliminary Description

We focus here on novel fundamental features associated with the transport of electron current pulse structure in an inhomogeneous plasma. For this purpose we simulate the simplified form (electron current flow is confined in the 2-D plane) of the 2-D G-EMHD model equations with specified plasma density inhomogeneity [78]. The initial current pulse configuration is chosen as exact solutions of the 2-D nonlinear EMHD equations for homogeneous plasma, so as to be able to clearly identify the role of density inhomogeneity during evolution.

### 4.1.1 Choice of Initial Conditions

There are two varieties of exact nonlinear solutions of EMHD equations [65] which are used as initial configuration. One of them corresponds to a stationary radially symmetric rotating electron current with monopolar magnetic field (the magnetic field essentially has the same sign, positive or negative depending on whether the electron current rotates clockwise or counterclockwise respectively). The other structure moves with an axial velocity and has a dipolar magnetic configuration.

#### Monopoles

The monopoles being radially symmetric solutions in the 2-D  $x - y$  plane (here  $\hat{z}$  has been chosen as the symmetry axis) we have chosen them to have the following form:

$$b(x, y, t = 0) = A \exp\left(-\frac{(x - x_0)^2}{\sigma_x^2} - \frac{(y - y_0)^2}{\sigma_y^2}\right) \quad (4.1)$$

where  $A, \sigma_x$  and  $\sigma_y$  are the constants deciding the strength as well as the spatial extent of the structure respectively. The values of  $x_0$  and  $y_0$  fix the location of the central point of monopole in the 2-D space.

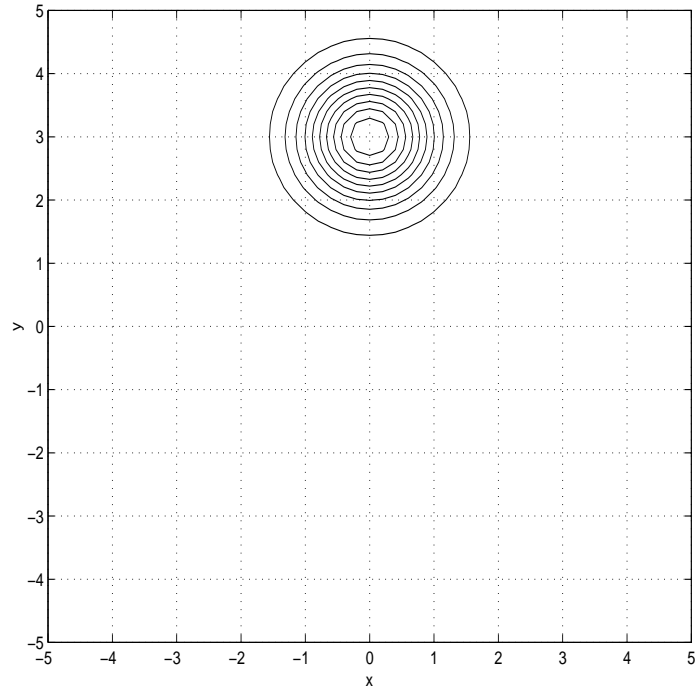


Figure 4.1: This is the constant contour of the scalar field ( $b$ ) forming a monopole. The associated parameters of the monopole are  $A = 5.5, x_0 = 0.0, y_0 = 3.0, \sigma_x = 1.0$  and  $\sigma_y = 1.0$ .

### Dipoles

The other solutions of 2-D EMHD equations are in the form of dipoles which are known to translate at a constant axial speed. These solutions have been obtained by Isichenko *et al.* [65] by seeking stationarity in a frame moving with a velocity  $u$  along some direction (say  $y$  for definiteness) . The EMHD equation in the moving frame can then be expressed in terms of a Poisson bracket  $[b - \nabla^2 b, b - ux] = 0$  whose solutions can be obtained by seeking  $b - \nabla^2 b = f(b - ux)$ . Here  $f$  can be any function of its argument. Isichenko *et al.* [65] sought localized solutions by choosing separate functional forms for  $f$  in two regions. For radii  $r = \sqrt{(x^2 + y^2)} \leq r_0$ ,  $f$  was chosen as a linear function and for  $r > r_0$ ,  $f = 0$ . This leads to the following form for the solution

$$b_i(r, \theta, t = 0) = [d_1 J_1(k_1 r) + d_2] \cos(\theta) \quad (4.2)$$

$$b_o(r, \theta, t = 0) = d_3 K_1(r) \cos(\theta) \quad (4.3)$$

The choice of  $r_0$  typically defines the spatial extent of the dipole structure. The

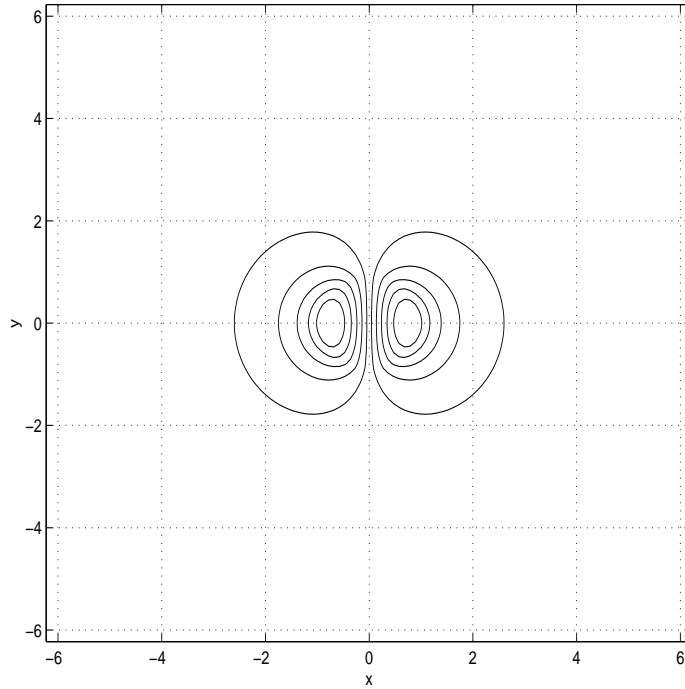


Figure 4.2: This is the constant contour of scalar field  $b$  forming a dipole within the spatial extent of  $r_0 \approx 1$  and having the axial velocity  $u = 0.1$  along the negative  $y$ -direction. The left lobe of the dipole corresponds to positive value of amplitude while the right one corresponds to negative value of amplitude.

coefficients  $d_1, d_2$  and  $d_3$  of the solution are obtained by matching the solution and its derivative at  $r = r_0$  as described in the Appendix B.

### 4.1.2 Choice of Density Inhomogeneity Profile

We have chosen various kinds of density inhomogeneities. We provide a list below of the density profiles that we have adopted in our studies. One of them are essentially slab configuration for which the constant density contours are straight lines along one axis. In this case the variation of density profile is considered to be a function of only one of the cartesian coordinates, e.g.  $y$  in our case. In the other variety we choose constant density contours in the shape of circles, i.e the density is radially symmetric. These two slab and radially symmetric density profiles are represented by the letter **S** and **R** respectively. The spatial variations for the slab

and circular profiles are chosen to have either tangent hyperbolic dependence or a gaussian form which are identified by letters **T** and **G** respectively. Furthermore, when this spatial density profile has a higher density compared to that of the background region in the simulation space it is called a density hump and denoted by the letter **H**, and when it has a lower density than the background region we call it a cavity **C**. Thus there are 8 possible combinations (**STH**, **STC**, **SGH**, **SGC**, **RTH**, **RTC**, **RGH**, **RGC**) that have typically been considered in our simulations. These profiles have been shown in the following Figures (4.3), (4.4), (4.5), (4.6), (4.7), (4.8), (4.9) and (4.10) respectively. The functional form of these density profiles have also been given.

---

**Profile : STH & STC**

$$n(x, y) = h_1 - h_2 \tanh \left\{ \frac{\sqrt{(y - y_0)^2 / \sigma_y^2 - w}}{\sigma} \right\} \quad (4.4)$$

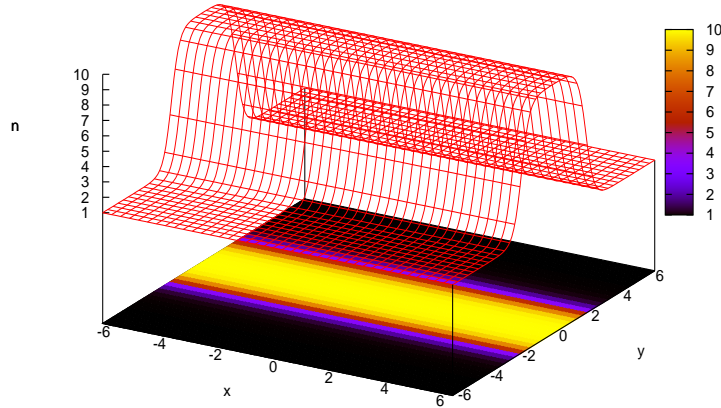


Figure 4.3: **STH** density profile ( $h_1 = 5.5, h_2 = 4.5, w = 2.0, y_0 = 0.0, \sigma_y = 1.0, \sigma = 0.5$ )

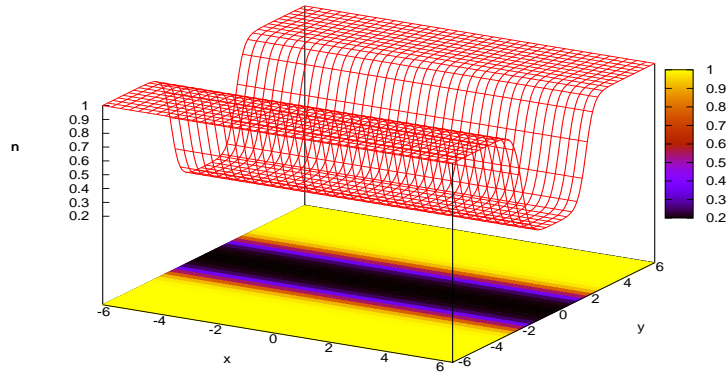


Figure 4.4: **STC** density profile ( $h_1 = 0.6, h_2 = -0.4, w = 2.0, y_0 = 0.0, \sigma_y = 1.0, \sigma = 0.5$ )

**Profile : SGH & SGC**

$$n(x, y) = h_1 + h_2 \exp\left(-\frac{(y - y_0)^2}{\sigma^2}\right) \quad (4.5)$$

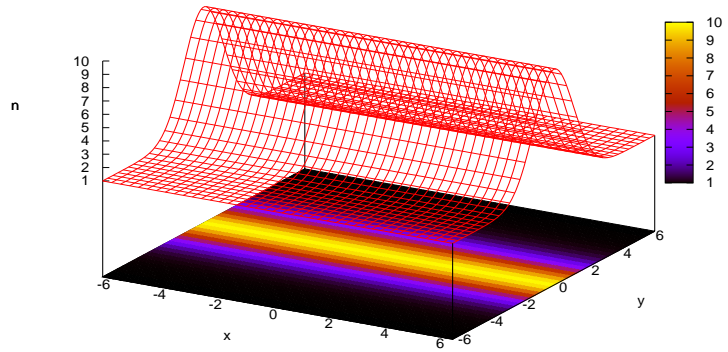


Figure 4.5: **SGH** density profile ( $h_1 = 1.0, h_2 = 9.0, y_0 = 0.0, \sigma^2 = 3.0$ )

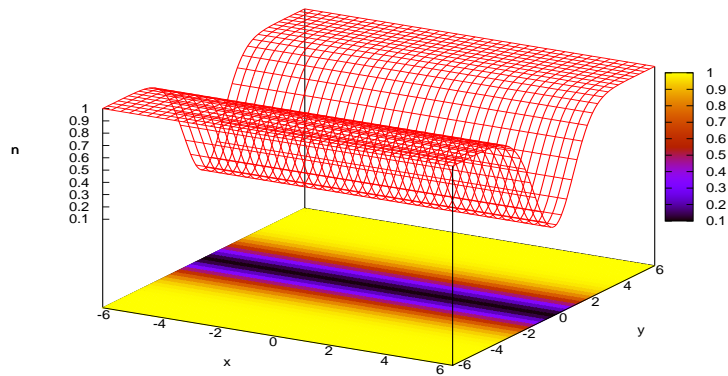


Figure 4.6: **SGC** density profile ( $h_1 = 1.0, h_2 = -0.9, y_0 = 0.0, \sigma^2 = 3.0$ )

**Profile : RTH & RTC**

$$n(x, y) = h_1 - h_2 \tanh \left\{ \frac{\sqrt{(x - x_0)^2 / \sigma_x^2 + (y - y_0)^2 / \sigma_y^2} - w}{\sigma} \right\} \quad (4.6)$$

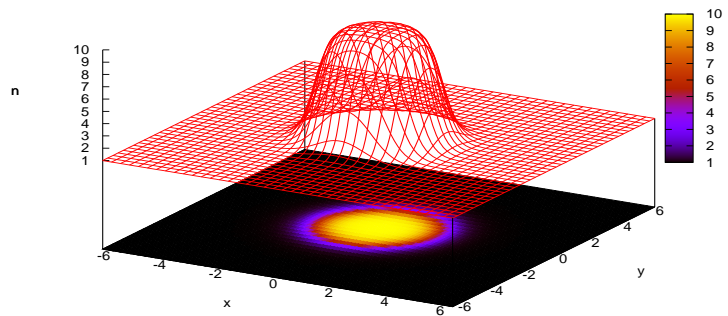


Figure 4.7: **RTH** density profile ( $h_1 = 5.5, h_2 = 4.5, w = 2.0, x_0 = 0.0, y_0 = 0.0, \sigma_x = 1.0, \sigma_y = 1.0, \sigma = 0.5$ )

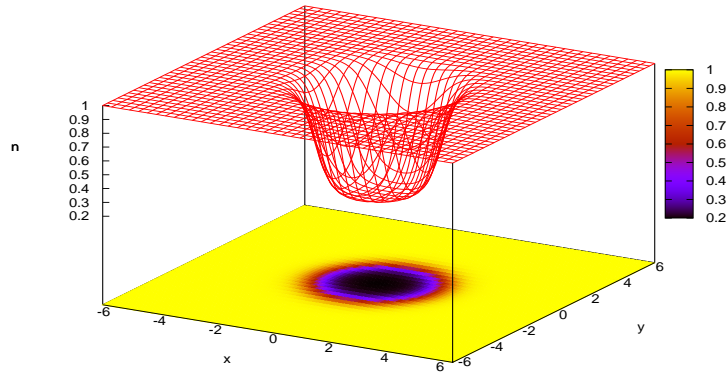


Figure 4.8: **RTC** density profile ( $h_1 = 0.6, h_2 = -0.4, w = 2.0, x_0 = 0.0, y_0 = 0.0, \sigma_x = 1.0, \sigma_y = 1.0, \sigma = 0.5$ )

**Profile : RGH & RGC**

$$n(x, y) = h_1 + h_2 \exp \left\{ - (x - x_0)^2 / \sigma_x^2 - (y - y_0)^2 / \sigma_y^2 \right\} \quad (4.7)$$

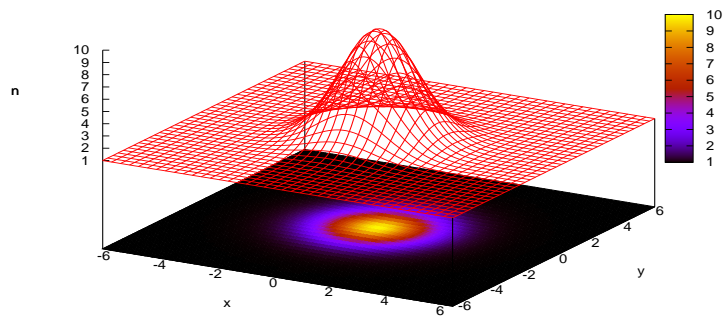


Figure 4.9: **RGH** density profile ( $h_1 = 1.0, h_2 = 9.0, x_0 = 0.0, y_0 = 0.0, \sigma_x = \sqrt{3.0}, \sigma_y = \sqrt{3.0}$ )

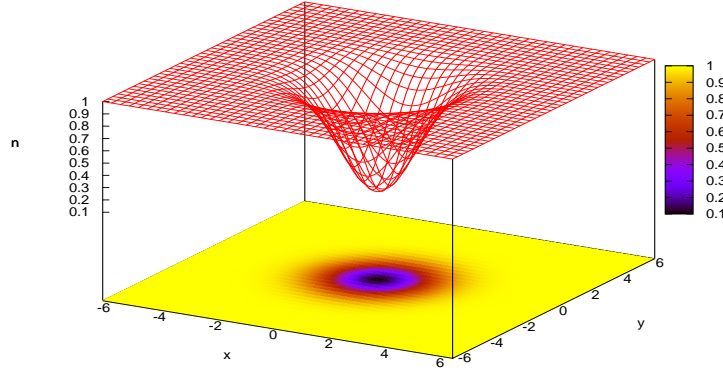


Figure 4.10: **RGC** density profile ( $h_1 = 1.0, h_2 = -0.9, x_0 = 0.0, y_0 = 0.0, \sigma_x = \sqrt{3.0}, \sigma_y = \sqrt{3.0}$ )

## 4.2 Inhomogeneity Induced Drift Velocity

We place the monopolar current pulse structure in the inhomogeneous region of the plasma for the various density profiles. We report the evolution here for the specific density profile **STH** defined in the previous section. We observe that the monopole which is otherwise stationary in a homogeneous plasma acquires a drift velocity in the presence of density inhomogeneity. This drift is transverse to the density gradient. The monopole is seen to be moving along the constant density contours. In Fig. (4.11) the propagation of the monopole in the density profile of **STH** has been shown at various times. For the case shown in Fig. (4.11) we have chosen the simulation box of size  $L_x = L_y = 10$  and  $x$  and  $y$  coordinates range from  $-5.0$  to  $5.0$ . For the plasma density we have chosen  $h_1 = 5.5, h_2 = 4.5, w = 2.5, y_0 = 0.0, \sigma_y = 1.0$  and  $\sigma = 1.0$  for the profile **STH**. The maximum and minimum value of density is therefore  $n_{max} = 10$  and  $n_{min} = 1$  respectively. The local electron skin depth therefore ranges from  $0.3 \leq d_e (= 1/\sqrt{n}) \leq 1.0$ . The high density plasma region here is confined within  $|y| \leq w$  for all  $x$ . The density falls sharply within a length  $\delta y = \sigma$  from 10 to unity beyond  $|y| \sim w$ .

The additional drift caused by the density inhomogeneity can be understood from the simplified form of the 2-D G-EMHD equation by ignoring electron inertia. Therefore, by replacing  $\Omega_b \rightarrow b$  in the Eq. (3.3) of the evolution of the generalized

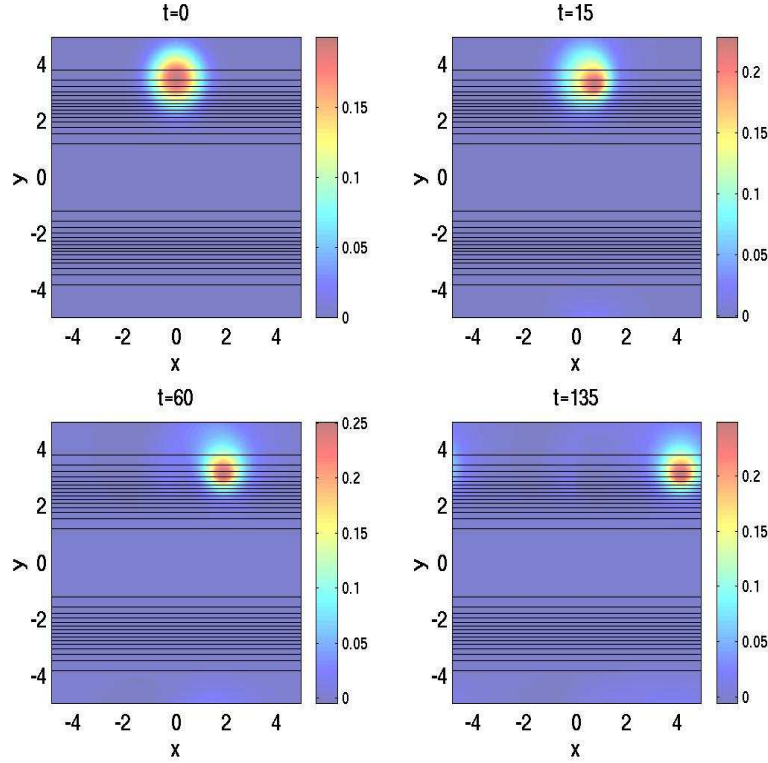


Figure 4.11: The propagation of the monopolar structure (color contours) in an inhomogeneous plasma density is depicted by showing the location of the structure at various times in the different subplots of the figure. The thick black lines represent the plasma density contour. In this case the plasma density is chosen to be a function of  $y$  only. The central  $y$  region of width  $w = \pm 2.0$  corresponds to a high density (10 times of the density at the edge region)

vorticity ( $\Omega_b$ ) along the symmetry direction we obtain the reduced equation as

$$\frac{\partial b}{\partial t} + \frac{b\hat{z} \times \nabla n}{n^2} \cdot \nabla b = 0 \quad (4.8)$$

The equation suggests the presence of an additional drift velocity which is of the form of

$$\vec{v}_d = \frac{b\hat{z} \times \nabla n}{n^2} \quad (4.9)$$

For the density profile of Eq. (4.4),  $n$  is a function of  $y$  alone and thus the monopole

drift along  $x$  direction, and the magnitude of the drift velocity is given by

$$v_{dx} = b \frac{\partial}{\partial y} \left( \frac{1}{n} \right) \quad (4.10)$$

From the subplots of the Fig. (4.11), the value of  $v_{dx}$  evaluated by observing the distance propagated by the structure along  $x$  is 0.0307. This is obtained by the expression

$$v_{dx} = \frac{x_{t=135} - x_{t=60}}{\Delta t} \quad (4.11)$$

where  $x_{t=135} \approx 1.9$  and  $x_{t=60} \approx 4.2$  are the position of monopole at the time  $t = 135$  and  $t = 60$  respectively, and is taken from the last two subplots of the Fig. (4.11). This observed drift velocity of the monopole is close to that estimated from the Eq. (4.10) for the electron drift velocity, as  $b$  typically ranges from 0.0233 to 0.1997 in the monopolar structure and  $\partial(1/n)/\partial y$  ranges from 0.1131 to 0.448 over the structure. This implies that the value of  $v_{dx}$  from the expression can be about 0.0026 to 0.089. The observed value lies within this range. In fact the average of  $v_{dx}$  evaluated over the  $y$  extent of the structure (through which the structure would translate) turns out to be very close 0.0369 to the observed velocity. This clearly indicates that the monopole is essentially propagating with the drift velocity of  $\langle v_{dx} \rangle$ . Thus the direction as well as the magnitude of the propagation velocity is observed to match with the expression given by Eq. (4.9).

It should be noted that the other density gradient dependent terms arising through the finite electron inertia related terms are typically smaller in magnitude and they generally contribute as a source causing modification of the spatial profile of the magnetic structure.

It should be noted that the dipole solutions translate even in a homogeneous plasma. Thus in the presence of inhomogeneity their propagation will depend on the superposition of their axial speed and the density gradient induced additional drift velocity discussed above. Clearly, this would then lead to richer class of phenomena. We have investigated this, and report it in the next section. One of the main conclusion is that the dipole can penetrate inside a density hump but avoids density cavities.

### 4.3 Dipole Penetration in High Density Region

Since the dipoles can propagate by themselves in a homogeneous plasma we can place it at any initial location, and observe as it propagates towards the region where plasma density is inhomogeneous. We first report our simulations here for the **STH** density profile. Initially the dipole is placed at a location away from the density gradient region, i.e. where the plasma density is low and uniform with  $n = 1$ . It is oriented in such a fashion that it propagates towards the higher density plasma region. An interesting aspect of the evolution is that the dipolar structure

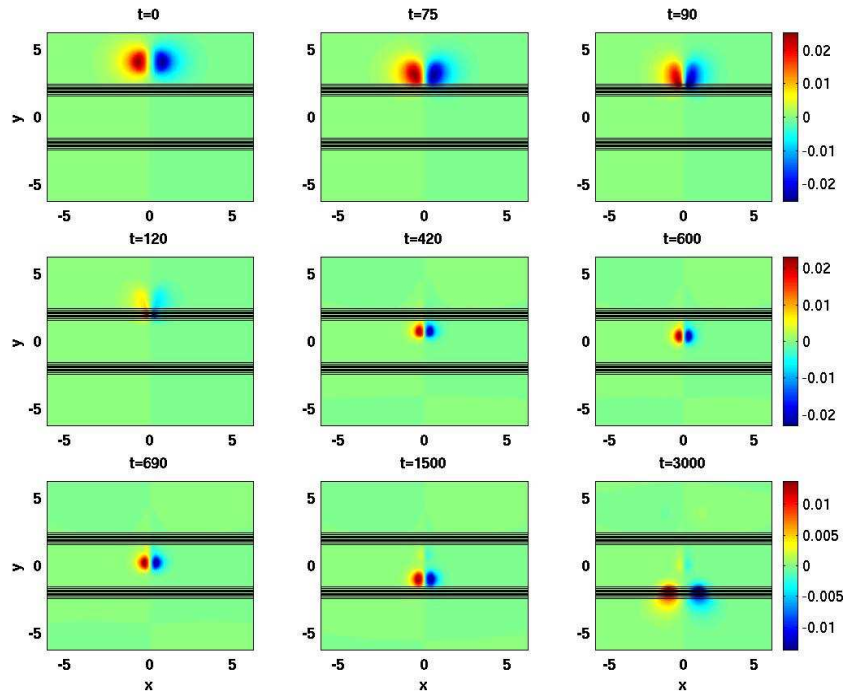


Figure 4.12: Various stages of the propagation of a dipolar structure through an inhomogeneous density plasma has been shown. The inhomogeneity in plasma density is similar to that of Fig. (4.11) in this case. The figure clearly shows the penetration of the dipole through the plasma density inhomogeneity to enter the high density region. The lobes of the dipole structure are squeezed towards each other as they pass through the inhomogeneous region. However, once inside the high density homogeneous region they again acquire a balanced form.

is observed to cross past the inhomogeneous density and enters the high plasma density region. The subplots of Fig. (4.12) clearly illustrate the penetration of the

dipolar structure in the high density plasma region. (For the plots of Fig. (4.12) the associated parameters of the density profile **STH** are  $h_1 = 5.5$ ,  $h_2 = 4.5$ ,  $w = 2.0$ ,  $\sigma_y = 1.0$ ,  $y_0 = 0.0$  and  $\sigma = 0.4$ . The box length in this case is  $L_x = L_y = 4\pi$ .) We observe that at the inhomogeneous density region the axial translational velocity of the dipole increases considerably. The two lobes get squeezed towards each other forming a shock like structure in the direction transverse to the density gradient. This behavior appears to be in stark contrast to the propagation characteristics of the monopolar structures, which merely show a movement transverse to the density gradient direction. This observation of dipole propagation can, however, be understood readily. For the dipole structure approaching the high density plasma region ( along decreasing  $y$ , in Fig. (4.12) ) the left lobe corresponds to positive values of  $b$  whereas the right lobe has negative  $b$  values. Clearly, when the two lobes of the dipole encounter the density inhomogeneity the left lobe has a drift velocity due to the density inhomogeneity towards right (positive  $x$  direction) whereas the right one drifts towards the negative  $x$  direction. This squeezes the two lobes of the dipoles closer in  $x$ . As a result the size of the lobes as well as their separation gets significantly reduced. This also causes an enhancement in the magnitude of  $|b|$  of the two lobes. The axial propagation velocity of dipole is known to increase with increasing  $|b|$  and reduced separation between its lobes. Thus, the reduced distance between the lobes as well as the enhanced amplitude of  $|b|$  results in an increased axial propagation velocity of the dipole. This accelerates the penetration of the dipolar structure in the high density plasma region.

Let us now study in detail the behavior of the dipole as it enters the high density plasma region. Though the shape of the dipole is considerably distorted while it traverses the inhomogeneous plasma region, but once it is inside the high density homogeneous plasma region it regains the familiar dipolar form. The scale length of the dipole, in the high density region changes by the same factor as the ratio of the skin depth of the high and low density regions. For instance , initially the size of the dipole was chosen to have  $r_0 = 1.0$  and at  $t = 690$  when it is completely inside the high density region, a reduction by a factor of approximately  $1/3$  in the size is observed. We thus observe that the dipolar structures are fairly robust. Even after encountering a strong density inhomogeneity, once in the region of homogeneous plasma they adjust smoothly to the new value of the skin depth that corresponds to the high density region. It should be noted that for the case

when this new dipole approaches the decreasing plasma density at the other end, the effect is entirely different. The sign of  $\nabla n$  being opposite, in this case the lobes separate due to the density gradient induced drift. Thus, the dipole separates and forms two monopoles at this end. These monopoles then drift along the constant density contours. Thus the structure does not come out of the high density plasma region.

Thus we see that the dipole penetrates the high density region but is unable to come out of the other end where the density again decreases. In the above case we had started from an exact solution of EMHD equations in a low density plasma. We have then let the structure evolve towards high density region. It is observed that once inside the high density region the structure does not come out from it. We have also simulated the case with **STC** density profile. Here, the dipole solution encounters a density cavity in its path. The evolution is shown in the plot of Fig. (4.13). The central region  $|y| \leq w$  of the box corresponds to a low density plasma region  $n = 0.2$  and  $h_1 = 0.6$ ,  $h_2 = -0.4$  and other parameters are same as that of Fig. (4.12). In this case as the structure encounters the density inhomogeneity region with decreasing plasma density the lobes show a separation due to the density gradient induced drift. The separation results in a reduced axial velocity of the dipole, which ultimately diminishes to zero as the separation distance between the two lobes exceeds the electron skin depth. The two lobes then separately move as two monopolar structures, transverse to the density gradient. Thus, this too illustrates that the dipole is unable to penetrate the region of lower plasma density.

The same features are exhibited even when the dipole encounters a density profile with a finite transverse extent. We demonstrate this here for the **RTH** and **RGC** density profiles. The various stages of the simulation have been presented in Figs. (4.14) and (4.15). The choice of parameters for simulation with the **RTH** density profile are  $h_1 = 5.5$ ;  $h_2 = 4.5$ ;  $w = 2.0$ ;  $x_0 = 0.0$ ;  $y_0 = 0.0$ ;  $\sigma_x = 1.0$ ;  $\sigma_y = 1.0$ ;  $\sigma = 0.4$ . For this particular density profile a dipole is placed with its center on the line  $x = 0$  at the positive value of  $y = 4.0$ . The axis of the dipole is parallel to the  $y$  axis as can be seen from the subplot at  $t = 0$  of Fig. (4.14). The dipole velocity is directed along the negative  $y$  axis so that it approaches the high density plasma region. It can be seen from the subsequent subplots that due to the density inhomogeneity related drift velocity of the individual lobes,

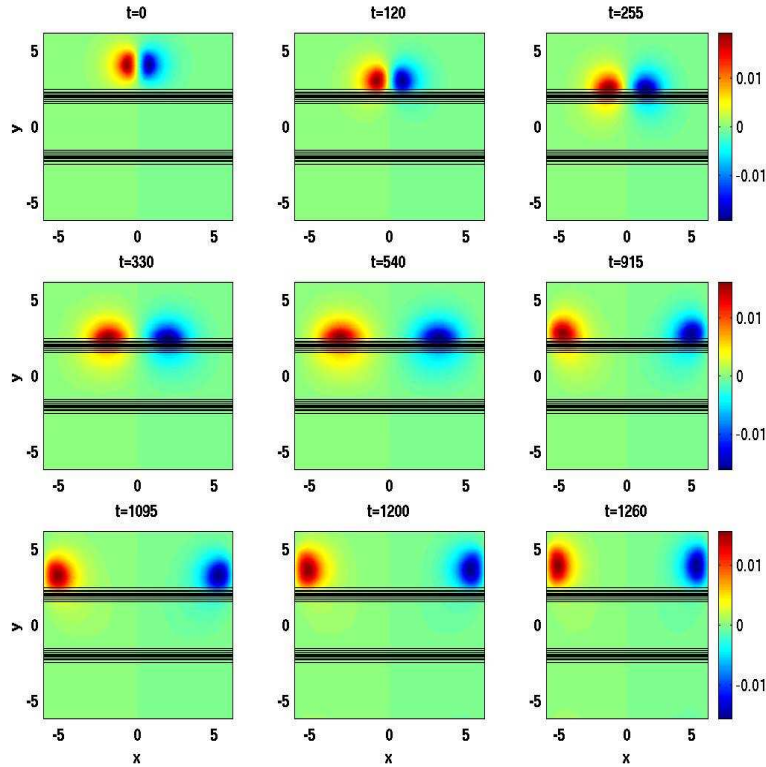


Figure 4.13: In this figure the dipole is shown to approach a density cavity (lower density plasma region). It can be observed that the dipole is unable to penetrate the lower density plasma. The two lobes of the dipole get separated transverse to the density gradient direction and subsequently they evolve as separate monopolar structures.

the two lobes of the dipole approach each other. This enhances the axial dipolar velocity and the dipole structure enters the high density region. Once inside the homogeneous high density region it translates along its axis which is along the diameter of the circular high density region. Upon reaching the other end the dipole again encounters the inhomogeneous plasma density region. However, the direction of the density gradient is now opposite to the one it encountered while entering the high density region. Thus, in this region the two lobes of the dipole separate from each other. As the separation between the lobes exceeds the skin depth distance the lobes act like individual monopolar structures and move along the constant density contours. In this case the density gradient being along the radial direction, the two structures move along the perimeter of the circle. They

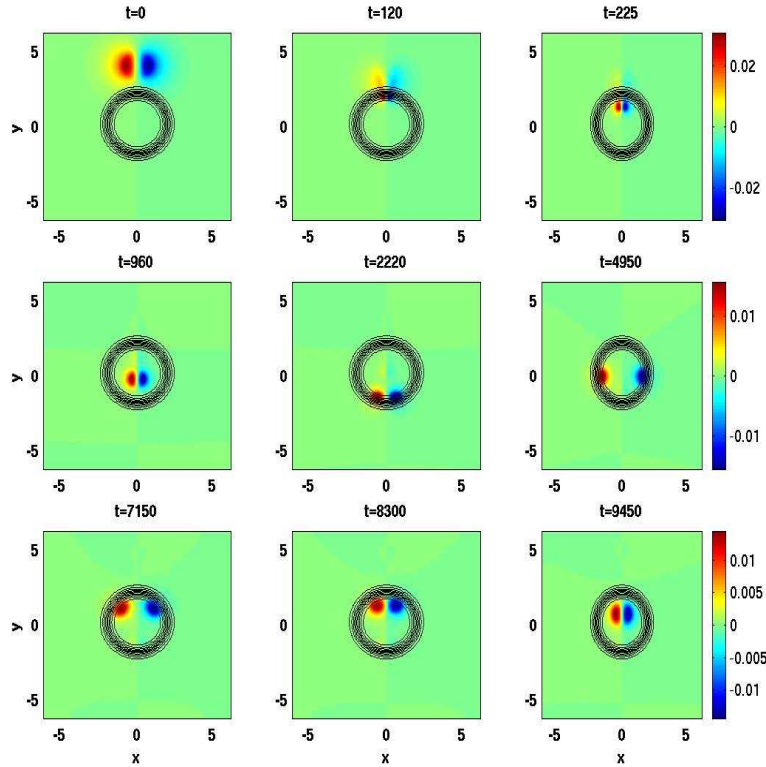


Figure 4.14: The trapping of the dipolar structure in a high density plasma has been illustrated in this figure. A high density plasma with a circular profile in the  $x - y$  plane represented by the thick black contour lines are depicted on the various subplots. A dipole structure can be seen to penetrate the high density region. However, once inside the high density region it continues to remain trapped in this region.

thus again come in close contact at the same point of the circle from where they had entered the high density region. At this place they again form a dipolar structure and translate along the diameter of the high density region. The simulations show that this cycle keeps repeating.

We have also studied the case of Gaussian radial cavity ( **RGC profile**) placed at the center of the simulation box. We show dipole propagation in the Fig. (4.15) for this **RGC** profile. The choice of parameters for simulation with this density profile are  $h_1 = 1.0; h_2 = -1.0; x_0 = 0.0; y_0 = 0.0; \sigma_x = 1.0; \sigma_y = 1.0$ . For this parameters the ratio of the maximum depth of density profile to the background amplitude of the density is around  $\approx 0.2$ . In this case the dipole is placed initially

at the position  $(0, 4.086)$  and the sign of the each lobe of the dipole is chosen in such a manner that it is propagating towards the cavity. When it passes through the density inhomogeneity, each lobe of the dipole starts separating until the axial velocity of the dipole becomes zero. After that each lobe behave like a monopole traversing around the outside periphery of the cavity as shown in the subplots at  $t = 360.0, 420, 495.0$  of Fig. (4.15). At later time it is observed that both lobes meet at other end of the cavity where they again form structure of the dipole and propagate towards negative  $y$  axis. These studies have thus clearly demonstrated that a dipole current pulse can penetrate and remain trapped inside a high density plasma region.

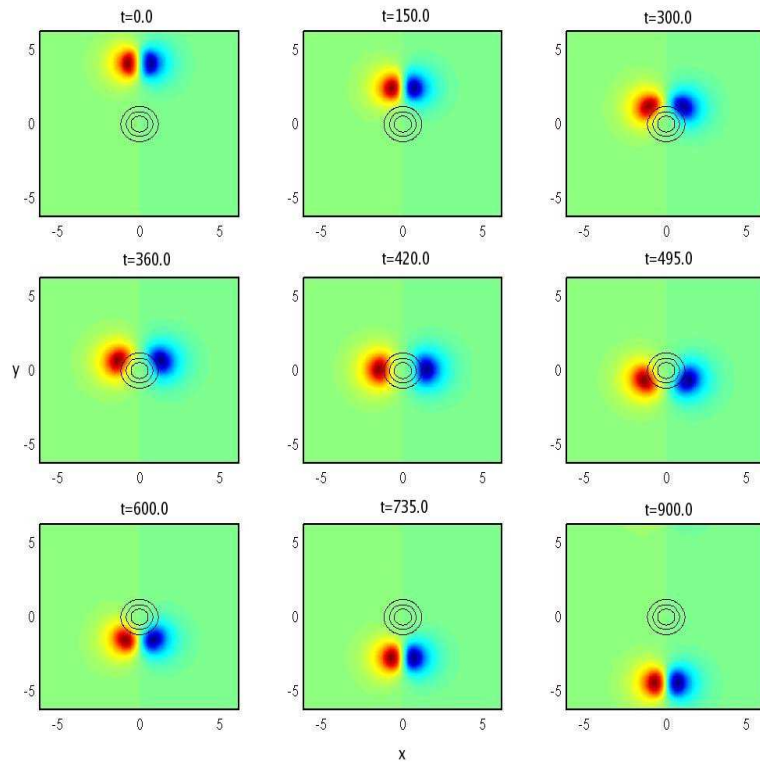


Figure 4.15: The propagation of the dipole through an inhomogeneous density profile when it form a cavity within the finite region of the space as is shown in the each subplot of the figure with the black thick contours. In this case the dipole structure do not get to penetrate inside the cavity.

We now provide a conclusive evidence of the fact that the penetrated structure in the high density exhibits the usual traits of the known dipole solutions of the

EMHD equation. For instance, the dipoles upon head-on collisions are known to exchange partners and propagate in a direction orthogonal to their initial propagation [36]. We show this happens also for the dipolar structures which enter the high density hump and collide within the high density region with the other dipole. Choosing the **RTH** profile for density we place two dipoles initially at the location of  $(0, 4.08)$  and  $(0, -4.08)$  as shown in the subplot at  $t = 0$  of the Fig. (4.16). Both these dipoles enter the high density plasma region and after collision are seen to exchange their partners forming the new dipolar configuration and propagate away from each other in a direction perpendicular to the original direction of propagation. This is evident in subplots at  $t = 675.0, 990.0, 1290.0$ . Once

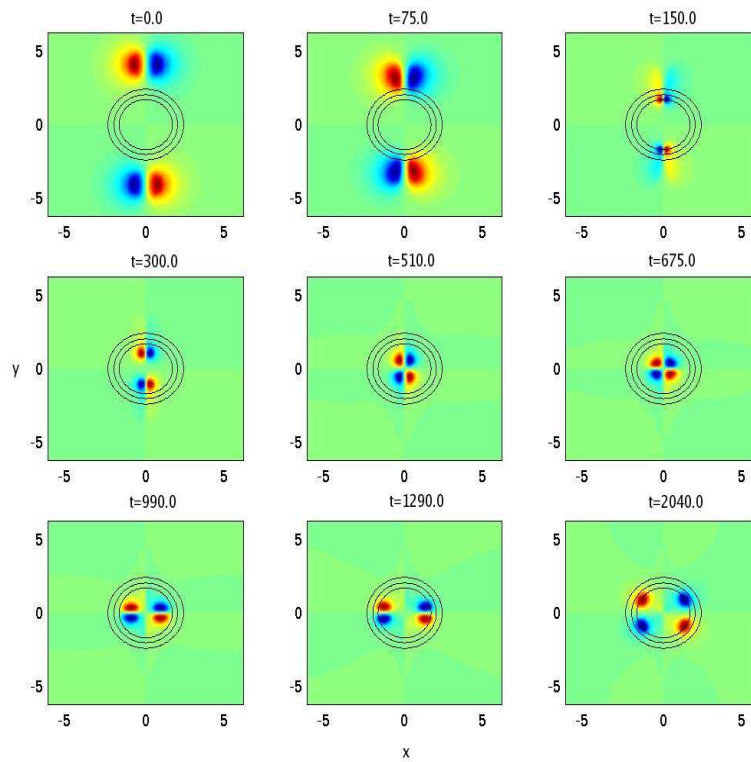


Figure 4.16: This figure represents the collisional behavior of two dipoles in the presence of density inhomogeneity when the **RTH** density profile is considered in the simulation.

they reach the high density edge the lobes of these newly formed dipole get separated and they move along the constant density contours as monopoles (subplot at  $t = 2040.0$ ). The monopolar lobes again meet (subplot at  $t = 300.0$ ) forming

dipoles and propagate radially inward. This cycle also keeps getting repeated.

## 4.4 Trapping vs. Transmission through High Density Region

The propagation characteristics of the dipolar structure studied in various contexts in the preceding section clearly demonstrates that EMHD magnetic structures of dipolar form can enter a high density plasma region. However, once inside a high density plasma region it remains trapped there. One would, however, expect that a weaker inhomogeneity and/or a smaller density reduction may transmit the current pulse. In this section we seek features which provide a quantitative criteria for trapping vs. transmission. We carry out studies with the two profiles **STH** and **SGH** by choosing various values of their parameters. These parameters essentially decide the inhomogeneity scale, the total density change and the width of the inhomogeneity region.

Our studies show that while the form of inhomogeneity does indeed determine whether the structure is transmitted or remains trapped, the strength of current pulse pattern has no role in this. In Fig. (4.17) we show the snapshots at various times from some of our case studies for the profile **SGH**. We show the propagation of a dipole with axial speed  $u = 0.01$  (this velocity is the propagation speed of the structure in a homogeneous plasma where the density  $n_0 = 1.0$ ) for the subplots of first, second and third column. The fourth column correspond to a dipole which propagates at a faster speed of  $u = 0.1$ . The thick black line in the subplots show the location where the density gradient is the maximum. The parameters concerning the density profile **SGH** for the four different cases corresponding to the four columns of Fig. (4.17) are (a)  $h_1 = 1.0, h_2 = 1.0, y_0 = 0.0, \sigma = 0.7071$ , (b)  $h_1 = 1.0, h_2 = 1.0, y_0 = 0.0, \sigma = 1.0$ , (c)  $h_1 = 1.0, h_2 = 1.0, y_0 = 0.0, \sigma = 1.414$  and (d)  $h_1 = 1.0, h_2 = 1.0, y_0 = 0.0, \sigma = 0.7071$  respectively. It is observed that the dipole is trapped for both the cases (a) and (d). This can be discerned from the fact that for these two cases the two lobes get separated by a distance more than the typical value of the electron skin depth as they try to come out from the other end. The separation of the lobes with distances larger than the typical value of skin depth essentially reduces the dipolar structure to a set of monopoles. On the

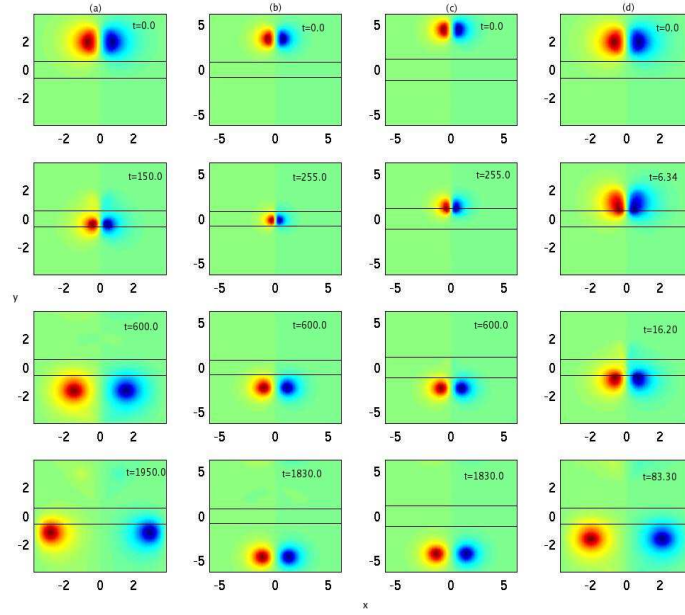


Figure 4.17: The four columns of the subplots represent four different cases of propagation of current pulse structure past the plasma density inhomogeneity. The detailed configuration of the density profile and the current pulse structure for each of the four cases has been mentioned in the text. The thick dark straight lines in the plot show the constant density contour at the location of maximum gradient. The cases corresponding to the (a) and (d) columns show trapping (lobes get separated upon reaching the other end) and those for (c) and (d) columns show transmission. In each subplots, the red and blue lobe of the structure implies positive and negative amplitude of the magnetic field directed along the symmetry direction  $\hat{z}$ , respectively.

other hand for cases (b) and (c) the dipole is transmitted past the inhomogeneity. It should be noted that for case (a) and case (d) the inhomogeneity profile is similar, however, the chosen current pulse structure for (d) was moving 10 times more rapidly and hence had a higher magnitude of the magnetic field associated with itself. Even then we observe that for both cases the dipole gets trapped within the high density region. Several detailed studies have been carried out with different speeds of the incoming dipole and all of them reveal that the dipole structure gets trapped irrespective of its speed and/or the maximum amplitude of the magnetic field that it has. We also studied the prospect of trapping in cases (b) and (c) by choosing different dipolar pulse structures. Here too no matter

what the dipolar parameters were the structure always got transmitted past the inhomogeneity. Such kind of studies have been carried out with profile **STH** also. The studies, therefore, clearly illustrate that the trapping and/or transmission is solely dependent on the density profile and is not dependent on the current pulse pattern.

Table 4.1: Profile **SGH**

$h_1$	$h_2$	$\sigma^2$	$\hat{L}_n/\sigma$	$\langle L_n \rangle / \sigma$	Status
1.0	1.0	0.9	1.8568	2.31	<i>Untrap</i>
1.0	1.0	1.0	1.8944	2.22	<i>Untrap</i>
1.0	1.0	1.5	1.8766	2.28	<i>Untrap</i>
1.0	1.0	2.0	1.8951	2.29	<i>Untrap</i>
1.0	1.1	3.0	1.7616	2.16	<i>Trap</i>
1.0	1.2	3.0	1.6733	2.02	<i>Trap</i>

To study the dependence of trapping and/or transmission characteristics on the density profile we carried out a large number of studies with various choices of the parameters associated with the inhomogeneity. Both kinds of density profiles represented by Eqs. (4.4) and (4.5) are considered. The results for Profile **SGH** and Profile **STH** have been summarized in Table (4.1) and Table (4.2) respectively.

Table 4.2: Profile **STH**

$h_1$	$h_2$	$w$	$\sigma$	$\hat{L}_n/\sigma$	$\langle L_n \rangle / \sigma$	Status
2.5	1.5	2.0	0.4	1.666	2.13	<i>Trap</i>
2.5	1.5	1.0	0.4	1.666	2.19	<i>Trap</i>
1.5	0.5	2.0	0.4	3.0	4.02	<i>Untrap</i>
1.5	0.5	1.0	0.4	3.0	3.81	<i>Untrap</i>
2.5	1.5	1.0	0.6	1.666	2.19	<i>Trap</i>
2.5	1.5	1.0	0.8	1.666	2.18	<i>Trap</i>
3.5	2.5	2.0	0.4	1.40	1.81	<i>Trap</i>
5.5	4.5	2.0	0.4	1.20	1.63	<i>Trap</i>

For simulations shown in Table (4.2) we have chosen  $y_0 = 0.0$  and  $\sigma_y = 1.0$ . The value of other parameters for these studies have been mentioned in the table itself. We introduce here a parameter  $L_n = n/\nabla n$  as the scale length for the density variation. It should be noted that for a linear density profile of the form  $n_0(y) = n_{00}(1 + \alpha y)$ ,  $L_n = 1/\alpha$  and is a constant. For our choice of density given by profile **SGH** and **STH**,  $L_n$  would vary. The fastest rise in density would occur at a location where the value of  $L_n$  is minimum.

The minimum value of density gradient scale length has been denoted by  $\hat{L}_n$  in our Tables (4.1) and (4.2). The typical measure for density scale length can also be obtained by evaluating the average  $L_n$  around its minimum value over a distance of  $\sigma$  (As mentioned earlier the parameter  $\sigma$ , typically represents the total extent of the region where the density is inhomogeneous). We denote the average scale length of density variation by  $\langle L_n \rangle$  in our tables. The outcome of the studies in terms of whether the current pulse structure gets transmitted or remains trapped has also been listed in these tables. The form of the current pulse used for carrying out the simulations listed in the two tables were all identical. The interesting aspect worth noting is that in all these studies, cases where trapping occurs the ratio  $r = \hat{L}_n/\sigma$  (or  $r_1 = \langle L_n \rangle / \sigma$ ), is smaller in comparison to those for which transmission takes place. Thus whether a structure will be trapped and/or transmitted is decided by the ratio of  $L_n/\sigma$ , higher this ratio more are the chances of transmission.

From considerations of time reversal invariance of the collision less G-EMHD equations, the current pulse structure which enters a local high density region, should invariably come out of the region from the other end. However, this does not happen and we observe that the structure in some cases gets trapped within the high density region. The breaking of the time reversal invariance indicates the presence of an underlying process of energy dissipation. We will see in the next Chapter that this is associated with the current shock layer [80] that forms as the dipole enters the high density region.

## 4.5 Summary

In this Chapter the G-EMHD equations in 2-D were used to study numerically the evolution and propagation of nonlinear coherent solutions of the EMHD equations

(which depict electron current pulses) in the presence of density inhomogeneity. The two varieties of coherent solutions (viz., the stationary monopolar solutions and the traveling dipolar solutions) were chosen for the study. Interesting novel aspects of their propagation were observed and analyzed. Our studies clearly show that density inhomogeneity leads to an additional drift of the current pulse solutions. This drift is along the constant density contours. The monopoles which are stationary structures in a homogeneous plasma thus move along the constant density contours of plasma. The dipoles which already have a translational speed along their axis in a homogeneous plasma show interesting behavior in the presence of inhomogeneity. Their propagation is now governed by the combination of their axial drift and the drift due to the density inhomogeneity. The interplay between these two drifts for dipole generates variety of possibilities. The dipole current pulses can move across the density inhomogeneity to penetrate a high density region. However, once inside a high density region we observe that they remain trapped there. The criteria for trapping vs. transmission was determined by us and was shown to be dependent on a parameter which measures the ratio between the typical density inhomogeneity scale length and the total distance traversed by the structure in the inhomogeneity.

An important point to ponder here is that this particular observation of trapping violates the time reversal invariance of the dynamical equation. This suggests that there is some dissipative process at work. In fact while the structure enters the high density plasma region it forms current shock structures at the inhomogeneity layer [ see Fig. (4.12)]. The process of energy dissipation through shock formation and its relevance to the fast ignition scheme will be discussed in the Chapter 5.

## Chapter 5

# Collision - less Energy Dissipation of Electron Current Pulse: Application to Fast Ignition

In the previous Chapter 4 it is shown that an electron current pulse with dipolar magnetic field can penetrate a high density plasma region but often it is unable to come out in the low density plasma region. It thus gets trapped inside a high density plasma region. This indicates a violation of time reversal invariance and is suggestive of the presence of a dissipative mechanism at work. In the present Chapter we show that indeed a strong energy dissipation occurs as a result of sharp current layer magnetic shock formation while the pulse crosses the plasma density inhomogeneity layer to enter the high density region. This mechanism of energy dissipation from the electron current pulse is shown to be independent of the magnitude and the character of the dissipative processes present in the system. Thus energy gets dissipated even from a collision - less electron current pulse via this mechanism.

Electrons prove to be a good accessible source of energy, they can be easily accelerated to high energies because of their low mass. However, since the Rutherford collision cross section of electrons diminishes rapidly with increasing energy of electrons, they can not be efficiently employed for the task of energy deposition in a plasma. With this novel collision - less mechanism at work, however, they can now be suitably used for efficient heating of the plasma medium. Furthermore as the

mechanism is dependent on the inhomogeneity of the plasma density, it provides a method by which a localized heating of the plasma at a desirable location can be maneuvered. The other advantage is that the electrons can be used to heat an overdense region of plasma as well, where lasers can not penetrate and hence can not be employed. This is precisely the situation in the context of hot spot creation in Fast Ignition (FI) [5] laser fusion scheme for ignition. The relevance of the proposed collision - less mechanism of energy dissipation to the frontline FI concept of laser fusion is shown in detail. The existing PIC simulations [29, 30, 32, 33] as well as a recent experiment [84] conducted at ILE Osaka provides strong support for the proposed collision - less heating scheme.

## 5.1 Introduction

The propagation of a short duration electron current pulse is perceived by plasma as a propagating high frequency electromagnetic disturbance. The plasma tries to shield itself from this disturbance by inducing return currents. This configuration of currents in the plasma helps, as it ensures that electron currents exceeding the Alfvén limit [51] can also easily penetrate inside a plasma medium. Some simulations have clearly shown that the combination of forward current (due to incoming current pulse) and return shielding current of plasma, is unstable to fast electromagnetic instabilities known as Weibel instability [29]. This instability separates the forward and return currents spatially. This leads to the formation of cylindrical current channel. The center of cylindrical channel carries forward current which is surrounded by a cylindrical shell of return plasma current. The flow configuration, thus varies along axial and radial direction of the cylinder and can be taken as independent of  $\hat{\theta}$ , the poloidal angle of the cylinder. Thus this is essentially a 2-D current configuration. Such a current configuration produces only poloidal  $\hat{\theta}$  magnetic fields.

There are typically two kinds of electron current pulses which are exact solutions of the 2-D nonlinear EMHD system for homogeneous plasma as discussed in Chapter 4. These two varieties of solutions have been shown in the plot of Fig. (5.1). The top three subplots (a), (b) and (c) show the contour plot of the associated magnetic field, the profile of magnetic field and the electron flow at the mid

$y = 0$  section of the structure respectively for the monopolar electron current pulse. These are radially symmetric rotating electron current flow patterns which are non-propagating in a homogeneous plasma. The subplots (d), (e) and (f) corresponds

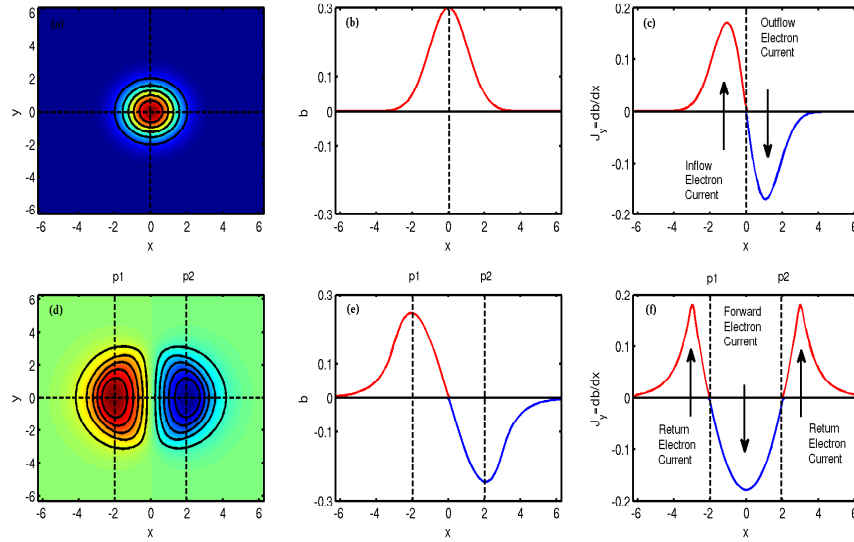


Figure 5.1: This is the schematic diagram for current pulse associated with the 2-D nonlinear solutions of Electron Magnetohydrodynamics (EMHD) model equations. Subplots (a), (b) and (c) show the contour plot of the associated magnetic field, the profile of magnetic field and the electron flow at the mid  $y = 0$  section of the structure respectively for the monopolar. Subplots (d), (e) and (f) corresponds to the same features for the dipolar structure.

to the same features for the dipolar solutions which move with uniform axial speed  $u$  in a homogeneous plasma. The speed  $u$  typically increases with the maximum amplitude of  $|b|$  shown by the peak value in subplot (e) and it also increases with the increasing proximity of the two lobes. This dipolar solution can thus be considered as a model for the finite propagating electron current pulse in the plasma for our studies. For these dipolar structures the central region (subplot(f)) shows a forward (along the propagation direction) current flow which bifurcates and returns along both sides as a return current. The poloidal symmetry axis ( $\hat{\theta}$ ) of the cylindrical current channel corresponds to the symmetry axis ( $\hat{z}$ ) of slab geometry of the 2-D EMHD system ( as considered for this thesis). The propagating direction ( $\hat{y}$ ) of dipole corresponds to the axis of cylindrical current channel.

We would study here the evolution of dipole current pattern and its total energy content as it moves through inhomogeneous plasma density. For this purpose we have employed the simplified form of G-EMHD model equation [78].

## 5.2 Shock Formation: Current Pulse Propagation through Inhomogeneity

The Generalized Electron Magnetohydrodynamic (G-EMHD) model has been discussed in detail in Chapter 2. We employ the 2-D evolution equations assuming  $\hat{z}$  being the symmetry axis. The electron current flow is confined in 2-D  $x - y$  plane for dipole as shown in subplot (f) of Fig. (5.1). Incorporating the effect of collisional dissipation through resistivity  $\eta$  and viscosity in electron flow  $\mu$  (this can be either classical and/or anomalous arising through turbulence) in the G-EMHD model we have:

$$\begin{aligned} \frac{\partial \Omega_b}{\partial t} + \frac{1}{n} \hat{z} \times \nabla b \cdot \nabla \Omega_b &= \Omega_b \frac{\partial b}{\partial x} \frac{\partial}{\partial y} \left( \frac{1}{n} \right) + \eta \nabla^2 b - \mu \nabla^2 \nabla^2 b \\ \Omega_b &= b - \frac{1}{n} \nabla^2 b + \frac{1}{n^2} \frac{\partial n}{\partial y} \frac{\partial b}{\partial x} \end{aligned} \quad (5.1)$$

Here plasma density ( $n$ ) has been chosen to vary along  $\hat{y}$ , the direction of current pulse propagation. The density has the **STH** profile described in Chapter 4 given by.

$$n(x, y) = h1 - h2 \tanh \left\{ \frac{\sqrt{(y - y_0)^2 / \sigma_y^2} - w}{\sigma} \right\} \quad (5.2)$$

Where  $h1, h2, y_0, \sigma_y, w$  and  $\sigma$  are parameters which define this profile and have been chosen as 5.5, 4.5, -3.0, 1.0, 2.2 and 0.6 respectively. The profile thus has homogeneous regions of both low ( $n = 1$ ) as well as high densities ( $n = 10$ ) in the simulation domain separated by a spatial region in which the density varies sharply. As mentioned the direction  $\hat{y}$  is also the propagation direction of dipole and it is placed in a fashion such that it moves towards increasing plasma density. Fig. (5.2) shows the evolution of an initial 2-D dipolar configuration of current pulse as it moves past an increasing plasma density. The simulations show that as dipole encounters an increasing plasma density, a transverse drift velocity (dis-

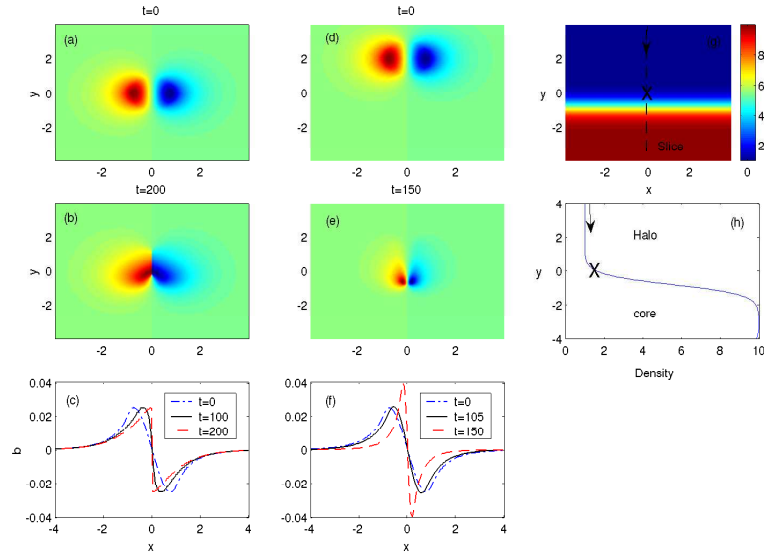


Figure 5.2: The contour plots of the magnetic field  $b$  in the  $x - y$  plane is shown in subplots [a,b] (inertialess case) [d,e] (full G-EMHD) at two different times. The numbers  $(-2,0,2)$  on the axis of these plots show length in units of electron skin depth (corresponding to the low density plasma). The magnetic field  $b$  profile in  $x$  at the mid plane of the structure in  $y$  has been depicted at various times in subplot (c) and (f) for inertialess and the full G-EMHD simulations respectively. The subplot (g) and (h) show the inhomogeneous plasma density profile through which the dipolar structure evolves. The cross  $\times$  and the arrow  $\rightarrow$  mark on these subplots show the initial location of the dipole for inertialess (dipole has no axial velocity in this case) and full G-EMHD simulations.

cussed in Chapter 4) given by  $\vec{v}_d = -b\partial(1/n)/\partial y$  is experienced by structure. The sign of magnetic field ( $b$ ) being opposite in both lobes, the lobes drift towards each other while approaching a high density plasma region (see Fig. (5.3) for schematic illustration ). This results in a collision between two lobes resulting into a current shock formation. The shock formation can be clearly seen from the constant contour plots of  $b$  in Fig. (5.2). The shock forms even when electron inertia is neglected. To show this we have simulated the inertialess limit of Eq. (5.1). In the inertialess case the shock structure is more prominent. The dipole has no axial velocity for inertialess case. Thus for this case the structure has been placed initially itself at a location where plasma density gradient is finite (the location is high-

lighted by  $\times$  symbol in the density profile as shown in subplots (g,h) of Fig. (5.2)). For simulation with full G-EMHD equations including electron inertial terms the dipole has an axial translational speed. In this case the lobes of dipole are pushed closer to each other, their size diminishes and the associated maximum magnetic field increases, as a result of which dipole translates faster through inhomogeneous region. The structure, therefore, keeps penetrating towards higher density region and it also keeps getting sharper. However, once it reaches the plateau of high density side it again re-adjusts its shape to a dipolar form corresponding to local skin depth.

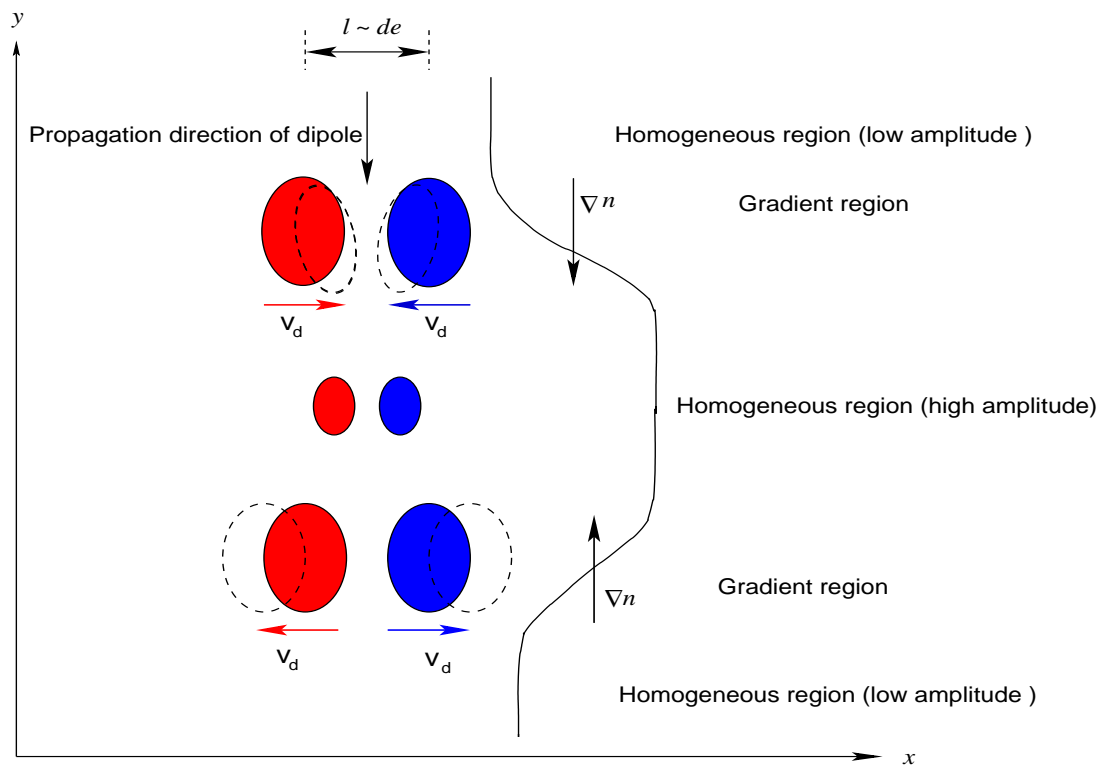


Figure 5.3: Schematic diagram of the dynamics of the dipole when it encounters the density inhomogeneity (shown by a thick curved black line that is varying along the  $y$ - direction having different region of inhomogeneity).

### 5.3 Evolution of Total Energy Associated with Current Pulse

We now look at the evolution of total energy associated with current pulse as it moves past inhomogeneity forming current shock structure. The energy associated with dipole structure is sum of magnetic and electron kinetic energy and is given by the expression  $E = \int \int (b^2 + (\nabla b)^2/n) dx dy$ , which is conserved in the absence of any dissipation. The choice of  $\eta = \mu = 0$  ensures that there is no energy dissipation while structure (resolved well by spatial grid) moves through homogeneous region. Our simulations indeed show that there is no change in  $E$  while dipolar structure is in the plateau region of low as well as high densities. The constancy of energy

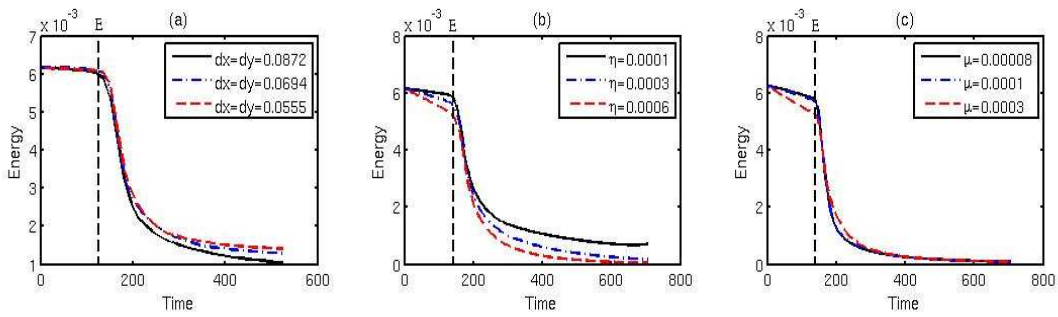


Figure 5.4: Evolution of the total energy of the structure for full G-EMHD simulations, as it propagates through the inhomogeneous plasma density (a) for various grid resolutions (b) for simulations with finite resistivity parameter  $\eta$  and (c) with finite viscosity parameter  $\mu$  in G-EMHD equations. A thick dashed vertical line shows the time when the dipole enters the inhomogeneous plasma density region.

has also been tested in inhomogeneous region for those magnetic configurations which do not produce shock structures (e.g. monopoles). We, however, observe that in this particular case when there is shock formation, as the dipolar magnetic structures translate through inhomogeneous density region, the energy  $E$  exhibits a sharp fall ( $\Delta E$ ) as shown in subplot (a) of Fig. (5.4). The timing of this drop in energy content of dipole is observed to coincide with interval when dipolar structure translates past inhomogeneous plasma density region. This sharp fall in energy is due to the shock formation, which cannot be resolved adequately no matter how fine one chooses the spatial resolution to be. The value of  $\Delta E$  is typically same

for different choices of grid resolution  $\Delta x$ , as can be seen from subplot (a) of Fig. (5.4) . The shock width essentially adjusts itself according to grid resolution for the runs with  $\eta = \mu = 0$ . Since  $\Delta E$  is not sensitive to any change in the value of  $\Delta x$  it shows that total energy dissipation is independent of the value of grid dissipation.

We have also carried out simulations with finite and various values of  $\eta$  and  $\mu$ . The energy dissipation for these cases have been shown in subplots (b) and (c) of Fig. (5.4). It can be seen that in these cases the energy also dissipates while structure passes through homogeneous region of low as well as high plasma densities. However, the drop in energy while the structure moves through the inhomogeneous density region remains approximately same for different values of  $\eta$  and  $\mu$ . Also this  $\Delta E$  compares well with the case of  $\eta = \mu = 0$  of subplot (a) of the same figure, where only grid dissipation was operative. We thus find that the energy dissipation is independent of the value as well as the form of dissipation. This, as argued below is due to a suitable adjustment of shock width  $l_x$  with dissipation coefficient. So, even when the dissipation coefficient tends towards zero the total energy dissipation is finite and of a constant value.

## 5.4 Energy Dissipation through Shock Formation

We now analyze the process of shock formation and magnitude of energy dissipation associated with it. As the two lobes of the dipole approach each other it leads to the steepening of the electron current gradients. We have shown that the shocks form even when one carries out the inertialess G-EMHD simulation. Thus, we choose to analyze the simplified inertialess limit of the evolution equations for which  $\Omega_b = b$  and Eq. (5.1) gets simplified to  $\partial b/\partial t - b(\partial b/\partial x)\partial(1/n)/\partial y = \eta\nabla^2 b$ . For a simple density variation of the form  $\partial/\partial y(1/n) = -K$ , (here  $K$ , the inverse of the normalized density scale length, is assumed to be a positive constant with the negative sign signifying an increasing plasma density with  $y$ ) one obtains Burger's equation. The Burger's equation is known to produce shock structures. Since shock is along  $x$ , for small  $\eta$ , we have  $\eta\nabla^2 b \sim \eta\partial^2 b/\partial x^2$ . The analytical form of the shock structure can be obtained by seeking stationarity in a frame moving with a speed  $u$  ( detailed derivation of shock structure has been given in Appendix

C). Thus, upon replacing  $\partial/\partial t$  by  $-u\partial/\partial x$  and integrating with respect to  $x$  we get in the inertialess limit

$$b(x) = \frac{u}{K} + \frac{b_0K - u}{K} \tanh \left\{ \frac{b_0K - u}{2} \left( \frac{x}{\eta} + K_2 \right) \right\} \quad (5.3)$$

We have used the condition  $b = b_0$ , and  $db/dx = 0$  at the boundaries. The parameter  $K_2$  is the second constant of integration to be determined from the condition  $x = -\infty$ ,  $b = b_0$ . It is clear from the expression of  $b$  that the layer width  $l_x = 2\eta/(b_0K - u)$  scales linearly with  $\eta$ . The rate of heat dissipation in this sharp layer would be given by

$$Q = \int^a \int^L \int^{l_x} \eta \left( \frac{\partial b}{\partial x} \right)^2 dx dy dz \quad (5.4)$$

The range of  $y = L$  (the shock length) and  $z$  (the third dimension) is the system length along this dimension  $= a$ . The  $x$  coordinate, however, has to be integrated over the layer thickness  $l_x \sim \eta$ . Retaining only  $b_0K$  in comparison to  $u$  we obtain the rate of energy dissipation in the shock structure as

$$Q = \eta \frac{b_0^2 a L}{l_x} = \frac{b_0^3 K L a}{2} = \frac{b_0^2 a^2}{2} K L v_e \quad (5.5)$$

Here we have replaced one of the  $b_0$  by  $av_e$  to obtain the last equality. Here  $v_e$  is the incoming electron velocity. The independence of energy dissipation  $Q$  from the magnitude of classical resistivity parameter  $\eta$  in the presence of sharp density gradients is known as the EMHD resistance and has been considered in literature earlier [1]. Here we have demonstrated it explicitly by numerical simulations.

We next evaluate the fraction of the incoming energy which gets dissipated in the shock structure by this mechanism. The incoming rate of magnetic energy influx is  $E_{Mag} = (b_0^2/2)v_e a^2$ , provided one assumes that the typical incoming current configuration has identical extent in the two transverse dimensions (typically, for a structure of the size of electron skin depth, both kinetic and magnetic energies are of similar order). From Eq. (5.5) we see that a fraction  $(KL)$  of the incoming magnetic energy associated with the current pulse gets dissipated in the shock structure of length  $L$ . Thus, if the shock length is of the order of the inhomogeneity scale length  $K^{-1}$  then the entire incoming magnetic energy would get dissipated.

The electron inertia related terms may play an interesting role of providing anomalous viscosity for a collision-less case. As the density gradient induced drift velocity brings the two lobes of the dipoles towards each other it generates a sharp electron velocity shear layer in the central region. This sharp velocity shear region is known to be susceptible to the Kelvin - Helmholtz (KH) like instability [54, 56] in the presence of electron inertia related terms. This instability essentially manifests through electron inertia dependent non-linearity  $\hat{z} \times \nabla b \cdot \nabla \nabla^2 b$  in the evolution Eq. (5.1) for  $G$ . The instability converts the electron flow energy into fine scale vortices. In 3-D the vortex flows cascade the energy towards finer scales which would eventually dissipate into heat through electron Landau damping in the direction parallel to the magnetic field. This effect can be modeled by an anomalous electron viscosity coefficient  $\mu$ . In an earlier 3-D EMHD simulations [53] it has been shown that the nonlinear stage of the velocity shear driven instability exhibits electromagnetic turbulence and produces an effective viscosity  $\mu$ . In the collisionless  $\eta = 0$  case, this anomalous viscosity  $\mu$ , would play a crucial role and define the shock width. Thus mocking up the electron inertia related effects by an effective viscous dissipation  $\sim \mu \nabla^2 \nabla^2 b$  we can write an approximate equation in the collisionless limit as  $\partial b / \partial t + Kb \partial b / \partial x = -\mu \partial^4 b / \partial x^4$ . The balance between nonlinear and the dissipation term defines the shock width, which now scales as  $l_x \sim (\mu / Kb)^{1/3}$ . A net energy dissipation rate  $Q$  over a length  $L$  in this case is  $\sim \int [\mu (d^2 b / dx^2)^2 dx] 2\pi a L \sim \mu 2\pi a L b^2 / l_x^3 \sim 2\pi a K L b^3$ . Using, Ampere's law we have  $b \sim a v_e$ , which gives

$$Q \sim K L b^2 a^2 v_e$$

This leads to a similar conclusion as before about the effectiveness of the shock dissipation mechanism and the independence of the magnitude of energy dissipation in the shock region to the anomalous viscosity coefficient  $\mu$ .

It is interesting to note that the total dissipated energy  $Q$  depends on the same ratio, viz.,  $KL = L/L_n$  which defines the criteria for transmission vs. trapping in Chapter 4. It thus clearly shows that whenever the energy dissipation is higher than some threshold the structure remains trapped and is unable to get transmitted from the other end.

## 5.5 Oblique Incidence of Current Pulse on Plasma Density Inhomogeneity

In our previous studies on the interaction of dipolar current pulse structure with plasma density inhomogeneity we have considered the dipole axis (which is also the propagation direction of the current pulse) to be oriented along the direction of background plasma inhomogeneity gradient. In a realistic case it would not be possible to orient the propagation exactly along the inhomogeneity gradient. Here, we study the effect of oblique incidence, ( i.e. when the axis of the incident dipole is chosen to be oriented at various angles with respect to the direction of the inhomogeneity gradient) on the evolution.

The inhomogeneous density profile has the form of **STH** described by Eq. (5.2). For these studies we have chosen the parameter values of  $h_1 = 5.5, h_2 = 4.5, y_0 = -2.5, \sigma_y = 0.0, w = 2.0, \sigma = 0.4$ . The dipolar current pulse structures are placed initially at the low density homogeneous region of the plasma as can be seen from the subplots of the topmost row in Fig. (5.5). The axis of the dipole in these subplots have been chosen to be inclined at various angles  $\theta$  with respect to the  $\hat{y}$  (the direction of plasma density gradient). Due to the inclination of the dipole axis with respect to the density inhomogeneity, one of its lobes experiences the plasma inhomogeneity earlier compared to the other lobe. Also the drift  $\vec{v}_d$  directed along  $\hat{x}$  is no longer normal to the dipolar axis. This breaks the symmetry of earlier simulations presented in Chapter 4. As a resultant of this the axis of the dipole turns, which is evident from the subplots corresponding to subsequent times in Fig. (5.5). The lobes ultimately even switch their location. The one in the left side ends up on the right side. This would in principle even reverse the axial drift, causing the dipole to reflect from the inhomogeneity. We, however, observe (in most of the simulations that we have carried out so far ) that once the lobes switch their sides, they also drift apart due to inhomogeneity ( $\vec{v}_d$  being directed so as to separate the switched lobes further apart ). Although not explicitly shown in Fig. (5.5), a longer duration evolution explicitly demonstrates this. The separation of the lobes due to  $\vec{v}_d$  once they switch sides automatically reduces the axial drift. The dipole, therefore, never reflects off the inhomogeneity but separates forming two monopoles.

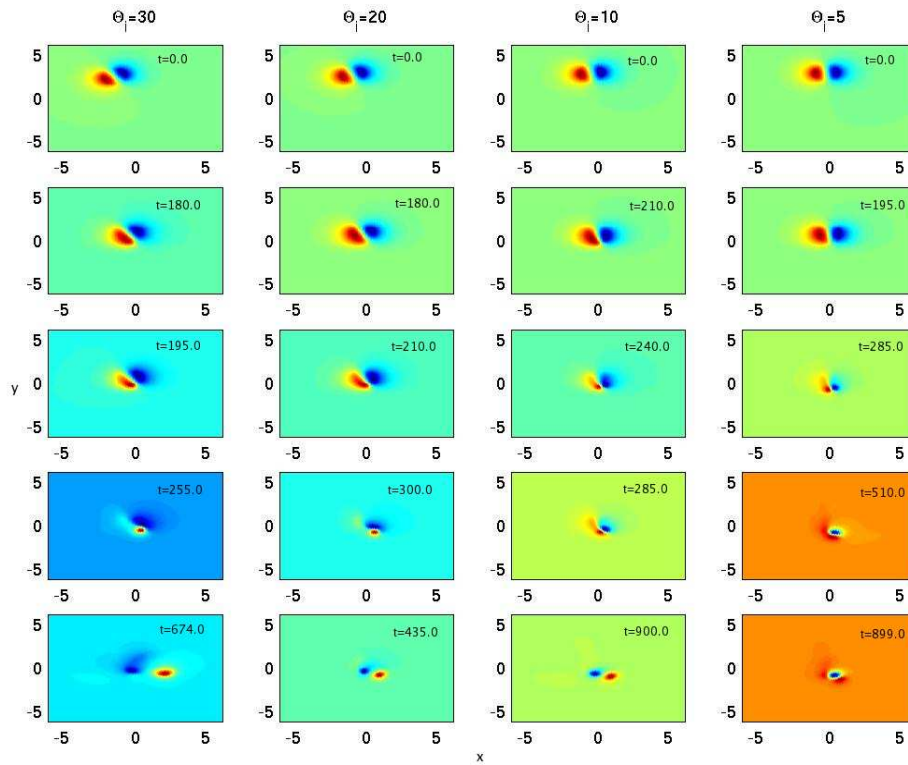


Figure 5.5: The propagation of current pulse structure incident at angles of 30, 20, 10 and 5 degrees with respect to the density gradient direction have been shown in the plots of first, second, third and fourth columns respectively.

It is clear that the evolution for the case of oblique incidence of the structure shows stark differences from the case of parallel incidence. It is therefore pertinent to investigate whether this has any impact on the mechanism of energy dissipation. In Fig. (5.6) we show the evolution of energy for these simulations. The various curves in the figure show the evolution of energy for cases with different incidence angles of the dipole. For these simulations one observes again a rapid fall of energy during the period that the two lobes are entangled in intense interaction when they experience the plasma density inhomogeneity. This essentially occurs when the lobes cross over each other to switch their locations. At later time when the lobes have already switched their locations and start drifting apart the energy remains constant. It is interesting to note, however, that the magnitude of energy dissipation that takes place in these cases of oblique incidence is typically of the same order as that observed when  $\theta$ , the angle of incidence is zero. The energy

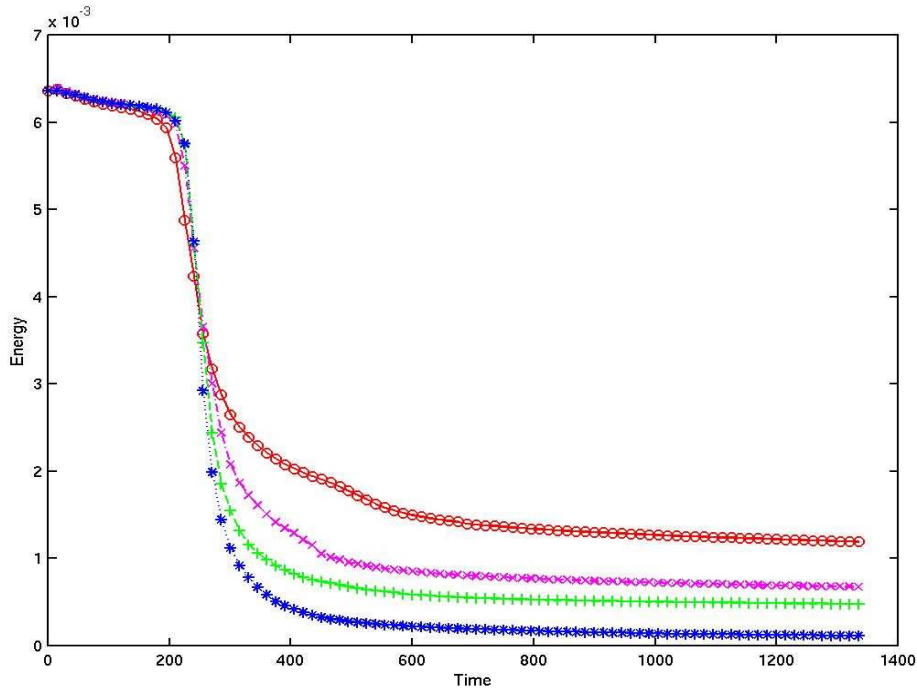


Figure 5.6: The evolution of the total energy has been shown when the current pulse is incident at (i)  $5^\circ$  ( curve with blue stars), (ii)  $10^\circ$  (curve with green + sign, (iii)  $20^\circ$  (curve with magenta crosses) and (iv)  $30^\circ$  (curve with red circles).

dissipation does decrease with increasing inclination  $|\theta|$ . However, even for as large an angle as  $\theta = 30$  degrees there is only around 20% difference in the total energy dissipation when compared to the  $\theta = 0$  case.

We thus see that although a slight change in incidence angle alters drastically the entire propagation course of the dipole current layer, it has little influence on the magnitude of energy dissipation while passing through the inhomogeneous region.

## 5.6 Application : Fast Ignition

The process of collision - less energy dissipation from energetic electrons holds a lot of promise and can have far reaching consequences in terms of applications. We discuss the case of Fast Ignition here to illustrate our point. The FI scheme [5] is essentially a variant of the Inertial confinement scheme for which the tasks

of target compression and ignition are carried out separately. This has several advantages. First of all it is easier to compress a cold target. Also the presence of hydrodynamic instabilities such as Rayleigh Taylor etc., during the accelerating and decelerating phases of compression become inconsequential. The target being cool there is no mixing of hot and cold regions which seriously deteriorates the efficiency of the process in conventional Inertial Confinement Fusion (ICF) [57, 58]. In FI after compression one needs to create a hot spot in plasma for ignition. For that purpose a second fast femtosecond laser pulse is employed. However, the target being overdense the laser cannot propagate inside the overdense region to create a hot spot. One instead relies on the energetic electrons generated at the critical density layer of the target for the creation of hot spot. The scaled down experiments have shown pretty impressive results for this scheme, where tenfold increase in fusion neutron yield has been observed [60]. However, there is skepticism currently on the account that the one would require higher energy electrons, e.g. 10 *MeV* or higher for the hot spot creation in full fledged ignition experiments. Since the Rutherford's collision cross section of electrons diminishes with energy, the greatest concern is that the higher energy electrons would simply pass through the target. After incorporating corrections due to dense targets and effects of correlated collisions the typical stopping distance estimate for a 1 *MeV* electron is considerably longer than the target size of 50 micron. Thus, if the target is transparent for the high energy electrons, the creation of hot spot in FI remains an outstanding issue. The proposed collision - less dissipation mechanism, however, provides a means to overcome this difficulty as has been shown below.

Let us now estimate the typical energy of the electrons that can be stopped through our proposed mechanism. We use the non dimensional expression for the energy dissipation here. The current  $I$  in the channel is related to the magnitude of the magnetic field  $B$  through Ampere's law as  $B = 2I/ac$ , where  $a$  is the dimension of the channel. The rate of energy dissipation  $Q$  can then be expressed in dimensional variables as  $Q = (B^2/4\pi)\pi a^2 v_e = I^2 v_e / c^2$ ,  $v_e$  being the electron velocity. Since the rate of energy dissipation is essentially  $I^2 R$  ( $R$  the resistance) heating of the system, for this case the resistance would be  $R = v_e / c^2$  in CGS units. The effective voltage drop can then be estimated from  $V = IR$ . The typical magnitude of the electron currents in FI experiments are in the range of several hundreds of *kAmps*, and the electrons typically have relativistic energy,

their velocity  $v_e \sim c$ , the speed of light. Thus the resistance  $R \sim 1/c \sim 30\Omega$ . (We assume here that the expression for energy dissipation obtained in the previous section can be used even for the relativistic electrons. This, however, needs to be ensured and further studies on this are necessary). This helps in estimating the energy of those electrons which can get stopped by this mechanism for a given value of current in the channel. Thus for a  $300KAmps$  of current, electrons with energy as high as  $10MeV$  can be stopped by this process. This estimate is certainly very promising as it supports the possibility of heating through electron current pulses for ignition.

We would now like to see whether the energy dissipation observed in our simulations provides an estimate of  $R$  which is consistent with the derivation above. The current pulse structure propagates with a normalized velocity  $v_N = 0.01$ . From Fig. (5.3) it is clear that within a time interval of  $\Delta t_N = 100$ , the total dissipated energy is  $\Delta E_N = 5 \times 10^{-3}$ . The suffix  $N$  is used to indicate the normalized values here. This provides us with the value of normalized resistivity as  $R_N = 5 \times 10^{-3}/0.01 = 0.5$ . For the current pulse structures of the typical dimension of electron skin depth a relationship  $\omega_c \sim \omega_p v_e/c$  can be obtained between the typical values of the magnetic fields and the electron velocity  $v_e$ . The value of  $R_N$  provided above then translates to a resistance of  $R \sim 0.5/(c\omega_c/\omega_p) \sim 0.5/v_e$ . In the case of fast ignition scenario  $v_e \sim c$  which implies that  $R \sim 0.5/c = 0.5 \times 30\Omega = 15\Omega$ , which is in close agreement with the analytical estimate made above.

## 5.7 Summary

We have presented a new mechanism of rapid energy dissipation through shock formation for a current pulse moving past an inhomogeneous plasma medium. The mechanism was illustrated through G-EMHD fluid simulations and an analytical understanding was also provided. It is interesting to note that our proposed mechanism is consistent with some recent PIC simulations [29, 30, 32, 33] carried out in the context of propagation of energetic electron current towards the dense target core for the fast ignition plasma. These PIC results show a predominance of heating in the region where density gradient is high (the region where we observe

shock formation). A recent experiment carried out at ILE Osaka [84] also clearly illustrates that electrons with as high as about 15 *MeV* energy passing through the inhomogeneous region of the target get stopped, showing the relevance of our proposed scheme. The role of additional effects arising due to dense plasma, uncompensated charge, relativistic electrons for true fast ignition parameters on this particular mechanism needs to be studied. Thus, a detailed investigation on comparison of PIC simulations, G-EMHD fluid simulations and the proposed heating mechanism, promises to be quite rewarding.

We have also shown in this chapter that even when the the current pulse propagates at an angle oblique to the density gradient, the associated energy dissipation gets effected only weakly with respect to the orientation angle. Though the subsequent evolution of the pulse is strongly altered.

## Chapter 6

# Kelvin Helmholtz Destabilization of Short Current Pulse in an Inhomogeneous Plasma

Kelvin Helmholtz (KH) [59, 85] is an important fluid instability that develops when the fluid flow is sheared. It has been shown in some recent studies [54, 56, 72] that for a sheared electron flow configuration, this particular instability has a somewhat different manifestation than the hydrodynamic fluid case. This is due to the presence of self consistent magnetic fields associated with the electron flow. The previous studies on sheared electron flow have been carried out for spatially infinite extent of the flow and for a homogeneous plasma. In this Chapter we present our study showing the KH destabilization of a short current pulse when the background plasma density is inhomogeneous. These studies have been carried out in 2-D where the evolution is constrained due to the presence of an additional non dissipative square integral invariant other than energy. For the case of 2-D simulations, therefore, the nonlinear regime of the instability produces a coherent state. In this particular case of short current pulse in an inhomogeneous density plasma, we observe an emergence of a novel coherent state as an aftermath of KH destabilization. This is in the form of a collection of vortices aligned as beads along the direction where the higher density region of the plasma has an elongated extent.

In Chapter 5 the presence of anomalous viscosity due to turbulence induced

by the KH destabilization of sharp current layers was conjectured for the collision - less electron fluid case. The demonstration of KH destabilization for short electron pulses in an inhomogeneous plasma here, shows that such a conjecture is well founded. The turbulence generation can only be seen by carrying out the simulation in 3-D, which is a topic of future study.

### 6.1 Introduction

The Kelvin Helmholtz (KH) instability [59, 85] is a classic fluid instability arising due to a sheared fluid flow configuration. This instability has been studied extensively in the context of hydrodynamic fluid in the past 100 years or so. It has also been studied for conducting fluid such as plasmas, but primarily when the shear is in the flow of heavier ion species [86]. Lately, the case of sheared electron flow against a background neutralizing ions has been investigated. The flow of electron produces current and an associated self consistent magnetic field. As a result of which the KH mode in this context has a distinct character for sheared electron current flows. This has been discussed in several recent publications [54, 56, 72].

The nonlinear studies of the instability has also been conducted. These studies have shown that in 2-D the nonlinear phase of instability produces a coherent state [54], but in 3-D it leads to turbulence [53]. The anomalous viscosity of the electron fluid in the presence of turbulence has also been evaluated in those studies. This is due to KH destabilized excitations cascading directly, towards short scales in 3-D and causing anomalous viscous damping of the electron flow. These studies on sheared electron current flow , however, has been conducted for infinite flow configuration and for chosen sheared flow profiles in space for a homogeneous density plasma.

Chernkov *et al.* [12] were the first to investigate the electron velocity shear in the context of the low density pinches. In their study they ignored the electron inertia and found that this mode is stable. Jain *et al.* [54] have shown that in the presence of the inertia this particular mode is unstable. The growth rate for the instability for these sheared electron flows is strongly dependent on the sharpness of the shear layer in comparison to the local electron skin depth. Jain *et al.* [53, 54] have simulated the EMHD model equation for studying the linear

and nonlinear aspects of the velocity shear modes in electron current channels in the 2-D as well as 3-D geometry. Gaur *et al.* [72] studied extensively the role of the skin depth and the existence of the whistler waves on the velocity shear driven instability in the context of the 2-D EMHD model. They also investigated the effect of the whistler waves on the KH instability. The presence of whistler wave had a stabilizing influence on KH mode. J. F. Drake *et al.* [87] have shown that the instability broadens the current layer. As the current shear layer width becomes comparable to the ion skin depth the instability weakens.

Our studies on the propagation of current pulse structure through plasma density inhomogeneity in the previous Chapters have clearly shown that very sharp elongated shear layers get formed as the structure propagates through the inhomogeneous density region. Here we investigate the possibility of KH destabilization of such sharp current layers in the presence of density inhomogeneity.

## 6.2 Destabilization of Current Layers

In the context of our G-EMHD simulations [78, 80] (where the shear flow gets self consistently generated at the location of density gradient region) we have so far not observed the appearance of the unstable KH mode. The reason for this can be readily understood by realizing that in the G-EMHD simulations presented so far the time spent by the structures in the inhomogeneous density region (where it forms sharp layers), is not sufficient to observe the development of the unstable KH mode from numerical noise. Once the structure moves past the inhomogeneous region the flow no longer remains sharply sheared to get destabilized. The length of the inhomogeneous region could not be increased to fit in several growth periods due to numerical constraints.

We hereby devise a novel scheme to sustain the sharp shear layer for a significant duration without increasing the length of the inhomogeneous region. We choose an elongated (many electron skin depths along  $\hat{y}$ ) region of high plasma density having **RTH** profile (described in Chapter 4) which has the form of

$$n(x, y) = h_1 - h_2 \tanh \left[ \frac{\sqrt{(x - x_0)^2/\sigma_x^2 + (y - y_0)^2/\sigma_y^2} - w}{\sigma} \right] \quad (6.1)$$

The values of the various parameters were chosen as,  $h_1 = 5.5, h_2 = 4.5, \sigma_x^2 = 0.2, \sigma_y^2 = 2.0, w = 2.0, x_0 = 0.0, y_0 = -2.0, \sigma = 0.4$ . The width of the high density region along  $\hat{x}$  has been chosen to be smaller than the typical value of electron skin depth. This has been deliberately done so as to have a sharper shear width (smaller than the electron skin depth for the KH instability) along  $\hat{x}$  in the current flow when trapped inside this density structure. The length of the structure along  $\hat{y}$  is typically  $\sqrt{10}$  times longer than the width. This particular density profile has been chosen here solely for illustrating the destabilization of sharper current shear layers when they persist for a sufficiently long times. However, this particular choice may also have practical relevance. With the advent of wires having dimension of the order of nano meters, an elongated plasma can be created by ionizing them. Such a plasma can easily have a width sharper than the electron skin depth, corresponding to the density profile that we have chosen here for our study.

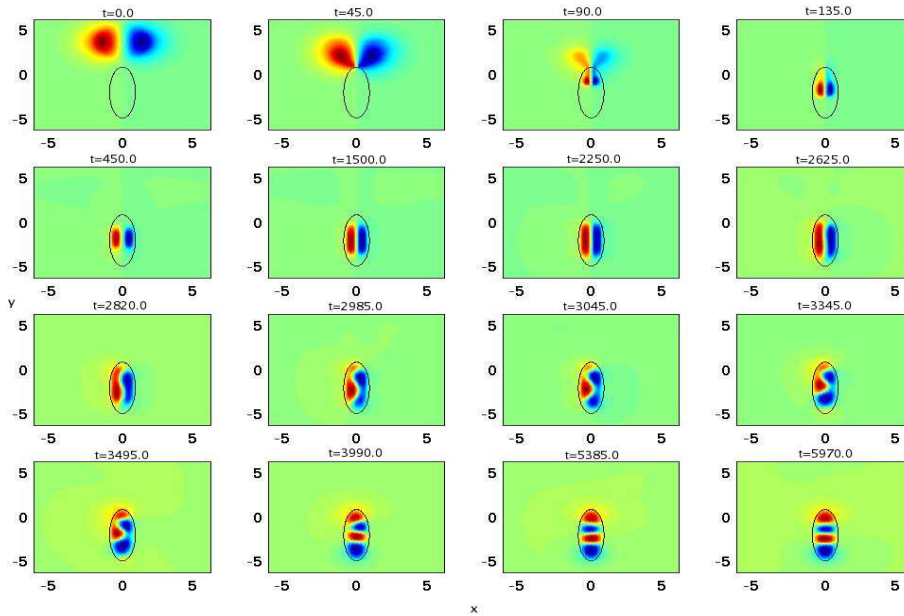


Figure 6.1: The various stages of evolution as the current pulse propagates towards an elongated sharp density profile. The thick black curve represents the outline of the density profile. The collimation of the current pulse structure as it enters the high density plasma region can be clearly seen. The KH destabilization is clearly evident from the plots at  $t = 2820$ .

In Fig. (6.1) we show the evolution of a dipolar current pulse structure as

it encounters the inhomogeneity profile. The thick black line drawn in the figure shows a constant density to illustrate the form of the density profile with respect to the current pulse location. The density profile has  $\nabla n$  directed inwards everywhere. The dipole axis has been placed in such a fashion that it enters this elongated high density plasma region of the shape of a wire through its top sharp edge. At the entry location the drift velocity ( $\vec{v}_d$ ) associated with density gradient (discussed in Chapter 4) brings the lobes closer and the axial speed increases. Once the dipole reaches the central location of the wire (see subplot for  $t = 450$ ) the  $\nabla n$  experienced by left/right (corresponding to positive/negative  $b$ ) lobe is in positive/negative  $\hat{x}$  direction respectively. This results in a drift velocity ( $\vec{v}_d$ ) [78] which is directed along positive  $\hat{y}$  for both lobes. The axial drift of the dipole (the lobes are separated by a distance less than electron skin depth and hence they still behave as dipoles) is along negative  $\hat{y}$ . The two drifts cancel and the dipole is able to propagate no more. This is the basis of extending the residence time of the dipole in an inhomogeneous region. Since the dipole is squeezed by the density profile in the transverse direction, it extends axially and acquires the shape of the elongated density profile at around  $t = 1500$ . This elongated structure with rotating electron currents in two lobes forming a sharp shear flow at the axis, persists for a very long time (from  $t = 1500$  to even at  $t = 2250$ ). It is only around  $t = 2625$  that a certain distortion in the structure becomes apparent. These, we believe, are the initial disturbances in the flow arising from KH instability.

The KH destabilization [54, 72] can occur provided the system permits modes having wavelength longer than the shear width along the flow direction. The exact dipolar solution of the homogeneous plasma typically has identical extent in the two directions. The shear scales associated with flow in both the directions are, therefore, also identical. The structure size of a typical EMHD dipole does not permit longer scales along any of the directions. Thus the dipolar structure propagates in a homogeneous plasma as a very robust stable pattern, even though the current flow in it is significantly sheared. In fact when EMHD simulations are carried out for an arbitrary dipolar form (not exact solutions derived by Kingsep *et al.* [1]) with magnetic field contours deliberately chosen to be considerably elongated along one of the directions, the structure adjusts itself to a circular form during the initial phase of evolution, and then it propagates as a stable pattern. This can be seen in the subplots of Fig. (6.2) where we show the plots of one such

simulation.

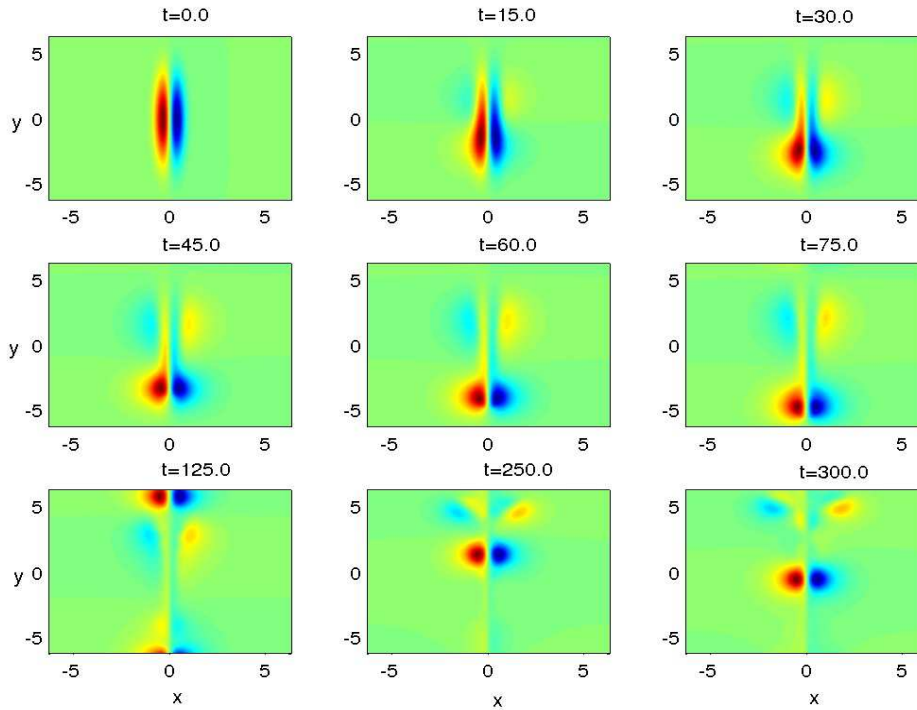


Figure 6.2: In this figure the robustness of the dipole solution is shown. Initially the dipole structure is taken elongated along the  $y$ -axis. During the evolution it is observed that dipole ,finally ,form the Isichenko *et al.* solution [65] propagating along the negative  $\hat{y}$  direction with some constant axial velocity.

However, when we constrained the dipole to remain forcefully elongated while residing in the elongated high density region in our G-EMHD simulation, the KH destabilization was observed clearly [see Fig. (6.1)]. Let us now quantitatively assess the condition for KH destabilization for various studies conducted in the past (Sharad *et al.* [78, 80]) where KH was not observed and the simulations reported here. The destabilization can occur provided the residence time of the structure in the inhomogeneous region (the location where the flow shear remains sharper than the skin depth) is longer than the growth periods for the perturbations to amplify from the numerical noise level.

In the studies reported earlier (Sharad *et al.* [78, 80]) the shear width of the dipolar structure at the location of the inhomogeneity was around  $\epsilon = 0.2$ .

The maximum growth rate will occur for a wavenumber  $k \sim 0.5/\epsilon \approx 2.5$ . (The growth rate for KH mode vanishes for  $k\epsilon \approx 1$  and is maximum for  $k\epsilon \approx 0.5$ ) Thus the maximum growth rate of the KH mode would be less than, i.e.  $\gamma \leq kV_0\sqrt{(1+4k^2)/(3+4k^2)} = 2.4091V_0$  (the growth rate of a step velocity shear profile) [56]. On the other hand the residence time of the structure in the inhomogeneous region is merely  $t_r = L_{in}/V_0 = 1.414/V_0$ . Thus the number of e-foldings during the time the structure moves past the inhomogeneous region is  $\gamma t_r = 2.4091 \times 1.414 = 3.4065$ , which is quite low for the instability to manifest from the numerical noise of typical order of magnitude  $\mathcal{O}(10^{-6})$  in single precision and  $\mathcal{O}(10^{-12})$  in double precision in the simulations reported in our papers [78, 80]. Let us now analyze the simulations shown in Fig. (6.1) with this perspective. Here, the shear width can be taken to be around half the width of the density inhomogeneity i.e.  $\approx w/2 = 1.0$ . The typical distance between the extreme  $b$  values measured from the subplot at  $t = 1500$  of Fig. (6.1) yields a better estimate of  $\epsilon = 0.8$ . The perturbation scale length that shows up in the instability can be again estimated from appearance of the mode observed at  $t = 2625$  and subsequent times. The confining high density region typically supports two wavelengths. Thus  $\lambda \approx 8/2 = 4$  from the figure. This gives a value of  $k = 2\pi/\lambda = 1.57$ . The residence time can be taken either anything between  $t_{r1} = 2625 - 1500 = 1125$  or  $t_{r2} = 2625 - 450 = 2175$ . The axial drift of the dipole can provide a crude second estimate of the electron flow velocity in the central region as  $V_{01} = 0.01$ . A better and correct estimate can be obtained by directly measuring  $\partial b/\partial x$  at the central region at  $t = 1500$ . This gives the typical estimate for the electron velocity as  $V_{02} = \partial b/\partial x = \Delta b/\epsilon = 0.08/0.8 = 0.1$ . This is about 10 times higher than the original axial drift of the dipole. The growth rate obtained from  $kV_0\sqrt{(1+4k^2)/(3+4k^2)}$  ranges from  $\gamma = 0.0133$  to  $0.133$  for  $V_0 = 0.1$  and  $V_0 = 0.01$  respectively. By taking the conservative estimate of the growth rate of  $0.0133$  the number of e-foldings  $\gamma t_r$  is around  $14.9625$  and  $28.9275$  for  $t_{r1}$  and  $t_{r2}$  respectively. While the former is sufficient to increase the amplitude from a noise at single precision level to a value of the order unity the latter can raise it even from a double precision level. This explains the observation of the KH destabilization in the present case and its absence in the previous simulations [78, 80].

### 6.3 Formation of Stationary Vortex Beads

The simulation plots at later times show the nonlinear development of the mode. The  $b$  field structure is subsequently seen to break up and form smaller vortices having identical scale in both the directions. The instability thus saturates in the nonlinear regime by forming a novel coherent stable structure of the collection of these vortices. For the simulation shown in Fig. (6.1) this constitutes a collection of four alternating sign vortices arranged along the elongated high density region of the plasma which looks like beads tied to a string. This is an extremely stable pattern and persists for the entire duration of our simulations.

It is interesting to note that in this case also the plasma system maneuvers through the process of KH destabilization to acquire a structure having an aspect ratio of unity for each individual vortices. An elongated structure in a homogeneous plasma medium has been observed to adjust itself to a symmetric shape by merely extending/shrinking in appropriate directions. This was not possible here, as the structure was squeezed inside an inhomogeneity with an elongated shape. In this case of constrained simulations the system uses a novel approach of breaking into smaller vortices through KH destabilization process to achieve its final goal, where each of the vortices again has a symmetric shape. It, therefore, appears that the system always prefers a symmetric form for individual vortices.

### 6.4 Summary

In this Chapter we have shown that the sharp current layer structure formed at the inhomogeneity layer is indeed unstable to the Kelvin - Helmholtz like velocity shear driven mode. In our present 2-D simulations it forms a coherent pattern of a collection of vortices aligned along the elongated direction of the density inhomogeneity. This is so because the G-EMHD system also preserves two non - dissipative square integral invariant in 2-D as has been shown in Chapter 2. In 3-D the KH destabilization in the context of infinite flows has been seen to generate turbulence and leads to anomalous viscosity effects [53]. We expect the same would happen for the finite current shear flow structures in an inhomogeneous plasma medium in 3-D. This would then appear as the relevant dissipative mechanism for

the energetic collision-less electrons as has been conjectured in Chapter 5.

We also observe that the system typically tries to achieve an isotropic flow configuration. The exact dipole solutions of EMHD [65] also have a sheared electron flow configuration, but still the structure is stable. A distorted dipole which, however, is not an exact solution adjusts itself suitably to a form for which the typical scale lengths in the two dimensions are identical. We observe that the elongated shear flow purposely constrained in the high density region destabilizes through KH instability and finally forms vortices having equal scale length in the 2-D space.

# Chapter 7

## Guiding and Collimation of Fast Electron Current Pulse in a Plasma

In this Chapter we discuss another application of electron flow through an inhomogeneous plasma. One often wishes to collimate and guide the electron current inside a plasma. There have been proposals to use specially structured targets prepared of different materials for this purpose [62, 63]. Such targets would neither be easy to prepare nor can they be employed with ease in each and every experiment. Here we offer a mechanism whereby a proper tailoring of the plasma density offers an easier accessible scheme. We illustrate this by placing arbitrary shaped wire like high density plasma along the path of the electron current pulse structure. It is observed that the current flows along the path defined by the high plasma density region. In an experiment [64] at ILE Osaka the energetic electrons generated at the critical density layer were guided with the help of solid wire. The experiment showed that the electrons moved along the wire, as the wire was tilted the path of the electrons changed accordingly. We feel that the high plasma density spontaneously created by the ionization of the wire by the electrons is responsible for this.

### 7.1 Introduction

We provide here a mechanism whereby the electron current pulse structures can be guided in a plasma. We have shown with the help of G-EMHD simulations that

a tailored plasma density inhomogeneity can guide an electron current pulse at will. A physical understanding of the guiding process has also been provided. The proposed mechanism finds support in recent experiments reported by Kodama *et al.* [64], where it is clearly shown that the current path in the plasma can be altered at will by placing an appropriately oriented wire. In the experiment the electron current was seen to propagate along the direction of the solid wire. The wire gets ionized by the front of the energetic electron current pulse, thereby creating an appropriate high density plasma along the path of the wire through which later portion of the pulse gets guided. An alternative mechanism has also been proposed recently by Robinson *et al.* [62] for artificially guiding the current pulse. They use structured target whose resistivity varies transverse to the propagation direction. The strong magnetic field generated at the interface of materials having different resistivity was important for the guiding of current pulse. Later this mechanism was experimentally verified in the work by Kar *et al.* [63]. However, the preparation of such specially tailored targets for use in experiments may not often be practical. The mechanism that we propose here offers a simpler solution, whereby a path defined by higher plasma density created by a simple scheme of ionizing an oriented wire provides for current pulse guiding. The experimental work of Kodama *et al.* [64] demonstrates this clearly. The PIC simulations have also been carried out which support the experimental observations of the guiding experiment conducted by Kodama *et al.* [64]. However, since the PIC simulations contain all the details, the essence of underlying physical mechanism of guiding is not apparent from these simulation. Here, we reproduce the observations of electron current pulse guiding by the fluid simulation of G-EMHD model [78]. We also provide a physical interpretation of the phenomena.

We use the simplified 2-D G-EMHD equations with magnetic field along the symmetry direction to illustrate the phenomena of guiding. The study has been conducted for both current pulses with monopolar and dipolar magnetic structures.

## 7.2 Guiding of Monopoles

Monopoles are the stationary solutions of the EMHD equations [65] which are like electron current vortices having single signed magnetic fields as shown in the

first row of Fig. (5.1). We choose these solutions as initial configurations for our simulations. In the presence of a density inhomogeneity the magnetic field patterns associated with these current pulses acquire an additional drift velocity  $\vec{v}_d = \vec{B} \times \nabla n/n^2$  discussed in Chapter 4, which is clearly transverse to the density gradient as well as the direction of magnetic field  $\vec{B}$ . Thus a proper choice of density profile, e.g., with constant density along the desired guiding path and a steep variation of density everywhere in the orthogonal direction, monopolar structures can then move due to  $\vec{v}_d$  along the contours of constant plasma density.

The maneuverability for guiding these monopolar solutions are, however, quite restrictive as they cannot penetrate across the plasma density gradient. We will show in the next section that the dipolar current pulse structures which moves across the plasma density gradient shows a greater maneuverability in this regard. We would show that the inhomogeneous density can be used to collimate, guide and even bifurcate the current pulse in subsequent Sections of this Chapter.

### 7.3 Collimation of the Current Pulse

In this section we show that the drift velocity associated with the density gradient in conjunction with the axial velocity of the dipoles allows a far superior maneuverability. The axial velocity helps dipole propagate across the constant density contours, thereby making regions of differing plasma density accessible for the electron path.

We show here that a broad current pulse can be suitably collimated by choosing a narrow high plasma density region. In Fig. (7.1) a dipole is shown to encounter a narrow high density plasma region. The form of the narrow high density region has been depicted by black solid lines in the figure. This is formed using the **RTH** density profile described by the expression

$$n(x, y) = h_1 - h_2 \tanh \left[ \frac{\sqrt{(x - x_0)^2/\sigma_x^2 + (y - y_0)^2/\sigma_y^2} - w}{\sigma} \right] \quad (7.1)$$

with the following values of the parameters  $h_1 = 5.5, h_2 = 4.5, \sigma_x^2 = 0.2, \sigma_y^2 = 3.5, w = 2.0, x_0 = 0.0, y_0 = -2.0, \sigma = 0.4$ .

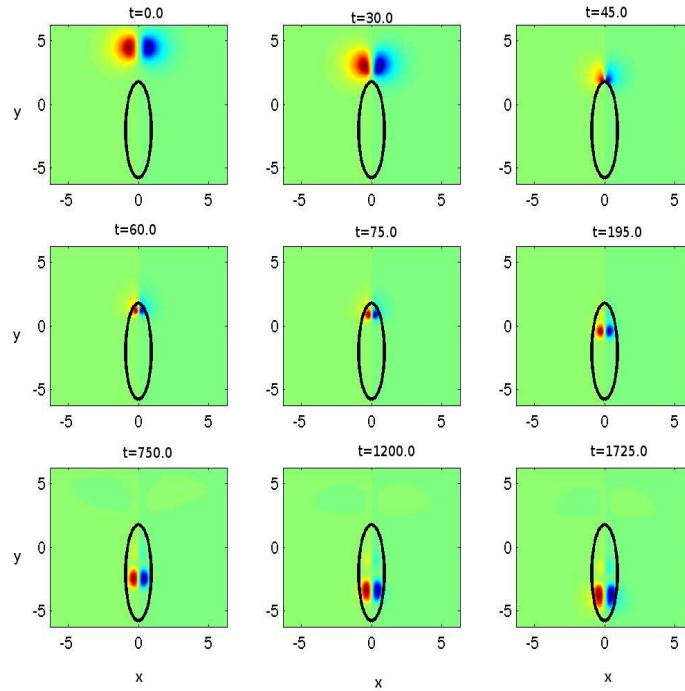


Figure 7.1: In this figure the collimating behavior of the dipole has been demonstrated. The current pulse passes through a high density profile that has an elongated profile (shown in the figure by the closed black thick line) along the  $y$ -direction.

As the dipole approaches the high density region it can be seen that it gets collimated, enters the higher density side and propagates along it, reaching the target destination at the other end. The broad initial pulse remains collimated as can be seen from the Fig. (7.1) This is a very attractive proposition as a simple choice of plasma inhomogeneity can suitably focus a divergent flow of electrons, an attribute often desirable for various applications. The observed features can be easily interpreted in terms of an interplay of the two velocity associated with the dipolar current pulse. The drift associated with the density gradient brings the two lobes with opposite polarity of the magnetic field together as the dipole approaches the high density region. This results in the collimation of the current pulse structure. The collimated structure moves with greater axial speed and penetrates the high density region of the plasma. Once inside the high density region the current pulse propagates along it to reach the other end through the axial dipolar velocity which overwhelms the  $\vec{v}_d$  drift acting in the opposite direction

(at the central region of the elongated high density plasma).

## 7.4 Guiding Behavior of the Current Pulse

We now show that one can even reverse the propagation direction of the dipole current pulse by a suitably tailored plasma density inhomogeneity. A curved high density profile shown by the thick lines in Fig. (7.2) is chosen. The current pulse trajectory has been shown in the snapshots of Fig. (7.2). We have seen that by

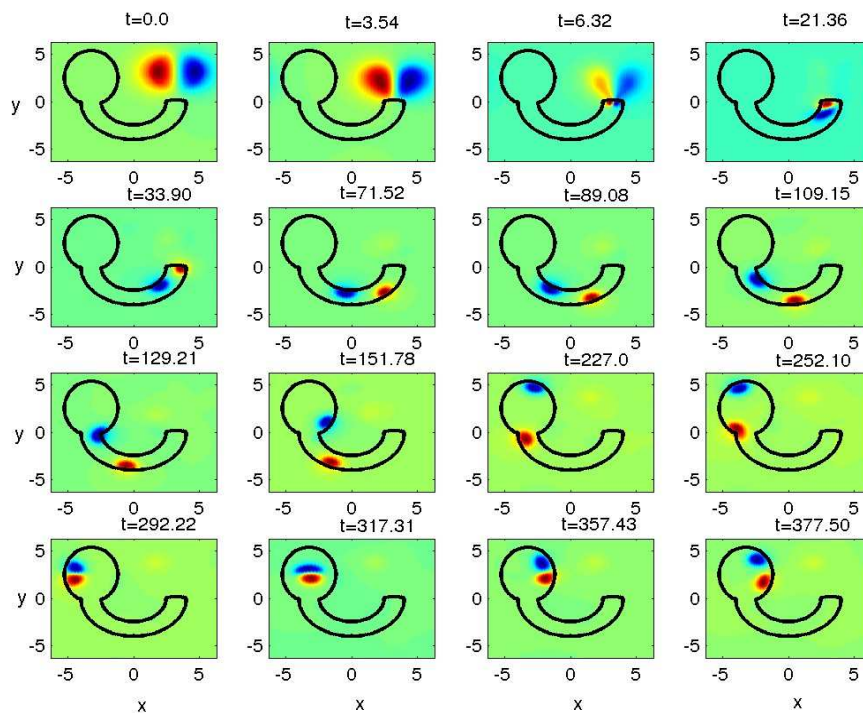


Figure 7.2: This figure shows that a dipolar current pulse can be guided. The single black contour in each subplot represents the curved high density profile chosen in the simulation. The inside region of the closed black line is of the high density amplitude. The circular region attached at the left end of the half circular region is of high amplitude in comparison to the half circular region.

choosing appropriate different forms of the high density plasma region the dipole current pulse can be guided and sent to any particular destination where it can get absorbed. It can be seen from Fig. (7.2) that it is even possible to reverse the

propagation direction. The current pulse follows the contours of the high density narrow region of plasma.

This happens because if the dipole structure separates into monopoles as shown in subplots  $t = 21.36, 33.9$  of Fig. (7.2) upon entering the high density region the structure can move only along the constant contours of the plasma density profile. If, however, it remains intact as dipole as in Fig. (7.1), it can in any case cannot come out in a lower density plasma region. The observed propagation of current pulse through G-EMHD simulations along the direction defined by the contours of the high density narrow plasma region finds support in certain experimental observations. In a recent experiment Kodama *et al.* [64] have generated fast electrons by impinging ultra intense laser pulse on a target in the shape of a gold cone. By attaching a solid wire on the cone tip was shown by Kodama *et. al.* [64] that the electrons followed the path defined by the solid wire. When the wire was tilted with respect to the cone axis the electrons hit the target at an off axis location defined by the tilted wire. The experiment can be understood on the basis of our mechanism. The wire gets ionized by the front of the energetic electron pulse, creating a narrow high density plasma region of the shape of the wire. The subsequent part of the electron pulse then gets guided along this inhomogeneous plasma as proposed by us.

## 7.5 Bifurcation of the Current Pulse Structure

We now provide another example of maneuvering the current pulse. We show that one can also bifurcate a current pulse arising from the same source and let the two parts propagate and reach altogether different destinations. In the simulation again we have chosen a curved form of high density profile as shown by the thick lines in the subplots. The bifurcation of the current pulse can be seen from the snapshots of Fig. (7.3). As the pulse enters the high density region, it can be seen to get separated in two parts which then propagate along different directions.

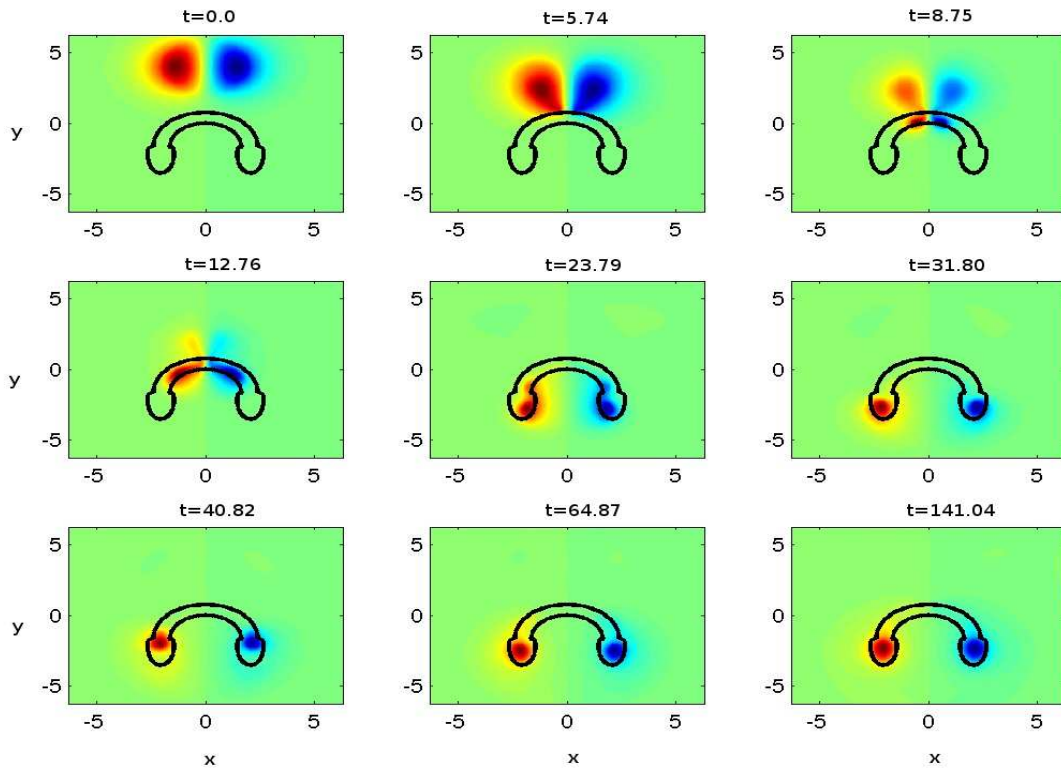


Figure 7.3: This figure show the bifurcation of the current pulse. The thick black lines show the plasma density profile that has been chosen for these simulation.

## 7.6 Summary

We have proposed a novel scheme based on a suitably tailored plasma density inhomogeneity to control the propagation of electron current pulses in plasma medium. Our studies have shown the possibility of collimating the current pulses, guiding them along a desired path and towards a desired destination. We have also shown that electron current pulses arising from the same source can be suitably bifurcated and made to propagate along distinct trajectories towards different destinations.

# Chapter 8

## Conclusion and Scope for Further Research

In this Chapter we summarize the main results obtained in the thesis. We also outline the directions for further research here.

### 8.1 Summary and Conclusions

The main focus of this thesis has been on the study of electron transport through inhomogeneous plasma medium. We present here a brief overview of work carried out and the significant novel results obtained in this area by us which have been presented in the various Chapters of this thesis.

- **Development of a fluid model for electron propagation in an inhomogeneous plasma**

The Electron - Magnetohydrodynamics (EMHD) [1, 2, 3, 4] provides a description of fast electron dynamics against the background neutralizing ions. The Electron - Magnetohydrodynamic (EMHD) fluid model was generalized by us for the case when the plasma has an inhomogeneous density. The new model is termed as the Generalized EMHD (G-EMHD) [78]. A detailed derivation of the G-EMHD model has been given in Chapter 2 of this thesis. Various limits of G-EMHD equations in reduced spatial dimension and simplified electron flow configuration have been obtained and have been

presented in Chapter 2. In 2-D the model takes a simplified form in which the equations can be cast in terms of a coupled set of equations between two scalar fields corresponding to the magnetic field and the vector potential component respectively along the symmetry axis.

The model was shown to preserve the total energy integral in the non-dissipative limit. In the simplified 2-D case and when the electron current was also confined in 2-D an additional square integral invariant is also supported by the model.

- **Development of a finite difference numerical code for studying electron propagation through G-EMHD equations in 2-D**

A finite difference code was developed to study the electron dynamics using G-EMHD equations. Chapter 3 contains the detailed description of the numerical algorithm adopted for simulating the G-EMHD equations. The G-EMHD equations has been cast in the form of convective equations with appropriate source terms. A flux corrected scheme [79] was employed for the evolution of G-EMHD equations. Unlike EMHD equations where one needs to solve Helmholtz equations in conjunction with the evolution equation at each time step for the evaluation of magnetic field, (and by taking its curl, the convective velocity) in the case of G-EMHD we have a Helmholtz like operator whose coefficients are functions of space (as they depend on the plasma density). This poses some challenge. At the moment we have represented the operator in the form of a matrix whose inversion provides us with the requisite magnetic field. The memory requirements are huge for the description of such a matrix and increases as a square of the total spatial grid points, i.e. as  $(Nx \times Ny)^2$  where  $Nx$  and  $Ny$  are the number of grid points chosen along the  $x$  and  $y$  directions respectively. It is therefore imperative that an alternative scheme be developed which reduces the RAM requirements.

The code was validated against the known EMHD results for the homogeneous plasma [36]. Furthermore, the preservation of the square integral invariants supported by the G-EMHD equations in the non-dissipative limit was also verified numerically. The rate of their decay in the presence of

dissipative coefficients was compared by the theoretical expression.

- **Fundamental Observations on current pulse propagation through inhomogeneity**

An electron current pulse shows a wide variety of novel behavior in the presence of plasma inhomogeneity. This was studied by us using the numerical simulations of G-EMHD equations with the code developed by us. The objective was to specifically understand the role of plasma density inhomogeneity on the electron current pulse propagation. For this purpose we chose exact current pulse solutions of the homogeneous EMHD as our initial conditions [65]. This ensured that the changes observed were entirely due to the density inhomogeneity. Both varieties of nonlinear solutions were used, namely one having monopolar magnetic field configuration and representing rotating electron currents, which is a stationary solution of EMHD equations. The EMHD equations also permits traveling solutions with dipolar magnetic fields. These dipoles move with constant axial speed and have a current configuration which mocks up a spatially separated forward electron current along the central axis and return shielding current at the edges.

A variety of inhomogeneous plasma density profiles were chosen for studying the propagation of these current pulses. The numerical studies [78, 81] show (i) that the current pulse structures acquire an additional drift in the presence of density inhomogeneity which is transverse to the magnetic field and the density gradient. (ii) The stationary monopolar solutions of EMHD equations therefore drift along the constant plasma density contours and they cannot move in regions with differing plasma density. (iii) The dipole is seen to penetrate inside a high density plasma region but it has difficulty coming out from there towards a lower density region of the plasma. It thus typically gets trapped within a high plasma density region. (iv) A detailed characterization of the trapping vs. transmission from a high density plasma region of the dipole has been carried out which clearly identifies the trapping condition in terms of a threshold criteria. (v) As the dipole structure passes through the density inhomogeneity to penetrate the high density region, it forms magnetic shocks and/or sharp current layers. These observations have been elucidated in Chapter 4.

- **Collisionless electron energy dissipation**

The trapping of the dipole current pulse structure in high density region indicates the violation of time reversal invariance and is suggestive of a dissipative mechanism at work [80, 81]. Indeed it is shown in Chapter 5 that a strong energy dissipation is associated with the magnetic shock which form at the inhomogeneity layer when the dipole structure enters the high density region. It is shown that the energy dissipation is independent of the magnitude and the character of the dissipation present in the system. The physics of current shock formation and the associated energy dissipation has been understood theoretically. The analysis shows that the total dissipated energy depends on the ratio of typical distance traversed by the current pulse in an inhomogeneous plasma and the density inhomogeneity scale length.

The energy dissipation via current shock formation at the density inhomogeneity layer offers an excellent mechanism of collision - less energy dissipation from electrons. Electrons are a good source of energy as they can be easily accelerated to high energies. Furthermore, the electrons can be used to heat overdense plasma region where lasers are unable to penetrate. Only difficulty in using them as a source for heating so far has been that their was that classical Rutherford collision cross section gets considerably weakened with increasing energy. Thus, the efficiency of the classical collisional mechanism for heat deposition by energetic electrons in a plasma has not been impressive. However, the use of the proposed collision -less scheme in conjunction with a tailored plasma density inhomogeneity promises to efficiently heat a particular localized spot in the plasma by highly energetic electrons.

The success of a frontline concept of inertial confinement fusion scheme, viz., the Fast Ignition (FI) concept [5] relies on electron energy deposition for the creation of hot spot in a precompressed target. Though the scaled down FI experiments [60, 61] have shown impressive results, it is still being viewed with skepticism mainly because the full scale experiments would require very high energy electrons which are essentially collision - less within the target size. We feel that in this context the proposed density inhomogeneity based electron stopping mechanism would be of great relevance. A recent experiment [84] at ILE Osaka in fact has provided sufficient evidence in favor of

our proposed mechanism. Furthermore, the existing data from various PIC codes [29, 30, 32, 33] studies conducted by various groups, on electron transport through inhomogeneous plasma targets, invariably show heating at the location of density inhomogeneity. This provides another evidence in favor of our proposed mechanism at work.

- **KH destabilization of finite electron current pulses and formation of novel coherent nonlinear structure in an inhomogeneous plasma**

The energy dissipation in the shock layer is independent of the magnitude and the type of the underlying dissipation in the system [80]. While the low energy electrons stop due to the usual electron - ion collisions, the energetic electrons would stop due to anomalous viscosity arising from the turbulence generated by the KH destabilization of the sharp current layer. The KH destabilization of sharp electron current flows have been shown in a series of publications [54, 72] where unbounded electron flows have been considered. The KH destabilization of these unbounded flows has led to coherent nonlinear state in 2-D [54] and turbulence with associated anomalous viscosity in 3-D [53]. This is because the 2-D system supports an additional second integral square invariant, which constrains the evolution.

We present in Chapter 6 the KH destabilization of a finite extent sharply sheared electron current pulse which forms at the inhomogeneous plasma density layer. Since for our 2-D G-EMHD system also conserve two integral square invariants in the non-dissipative limit, our simulations show that the nonlinear stage of KH destabilization produces a coherent pattern of rotating circular vortices confined within the high density plasma region. The collection of vortices are seen to align along the contours of the density profile to form a novel coherent state with alternating sign vortices arranged like beads in a wire [81]. These studies have been represented in Chapter 6.

- **Electron current pulse guiding through density inhomogeneity**

In Chapter 7 we discuss another application where the density inhomogeneity has an important role. Often one wants to collimate and guide the electron currents. There have been proposals to use specially structured targets prepared of different materials [62, 63]. Such targets would neither be easy to

prepare nor can they be employed with ease in each and every experiment. Again a proper tailoring of the plasma density offers an scheme which can be implemented easily. We illustrate this by placing arbitrary shaped elongated high density plasma structure of the shape of a wire along the path of the electron current pulse structure. It is observed that the current flows along the path defined by the high density plasma. In an experiment [64] at ILE Osaka the energetic electrons generated at the critical density layer by an ultraintense laser pulse were guided with the help of solid wire. The experiment showed that the electrons moved along the wire, as the wire was tilted the path of the electrons changed accordingly. We feel that inhomogeneous plasma density spontaneously created by the ionization of the wire by the electrons is responsible for this. We have also shown that a divergent electron flow can be suitably collimated by a proper choice of plasma density inhomogeneity. Furthermore, our studies also demonstrate that electron current from an identical source can be suitably bifurcated and sent to distinct locations. These studies have been presented in Chapter 7.

## 8.2 Future Directions for Research

We now list specific issues which needs to be studied further in this area:

- [1] One of the issue that has put severe constraint on the studies conducted in this thesis pertains to the use of direct inversion of a matrix for solving the Helmholtz like equation with space dependent coefficients. This has restricted the resolution severely and we could only resolve electron skin depth for a maximum to minimum density ratio of the order of 10. The experiments on Fast Ignition (FI) [5] would require at least three orders of density variations to be depicted properly. (The variation from the critical density surface where  $n = 10^{22}/cc$  to the target core where  $n = 10^{25}/cc$  ). To be able to study this one needs to employ a recursive relaxation scheme using standard Helmholtz solvers [83] for the solution of Helmholtz like equation with space dependent coefficients, that we have to deal with for studying electron transport through inhomogeneous plasma medium.

## Chapter 8: Conclusion and Scope for Further Research

- [2] The 3-D G-EMHD studies are another important area for investigation. These studies can clearly demonstrate that the KH destabilization of the sharp current layer formed at the plasma inhomogeneity layer can ultimately degenerate into turbulence, giving rise to anomalous viscosity in the electron fluid system. The 3-D G-EMHD system also provides a simple realistic system to study turbulence in an inhomogeneous media.
- [3] The propagation of the current pulse structures in a cylindrical geometry poses a more realistic scenario for the FI experiments [60, 61]. From fundamental point of view also, the cylindrical case would be interesting. In the slab case the magnetic field lines for both monopoles as well as dipoles were extending to infinity along the symmetry direction. In the case of cylindrical geometry the magnetic fields are closed along the  $\theta$  direction. This may have novel consequences.
- [4] A further generalization of the G-EMHD model to incorporate relativistic effects is necessary. This will provide a better description for energetic electron dynamics in the context of FI experiments.
- [5] A two fluid description for electrons constituting the forward energetic current and the reverse background shielding current in the model would be closer to reality and needs to be pursued.

# Appendix A

## Derivation of the G-EMHD Model Equations

We start with the normalized 3-D G-EMHD model equation.

$$\frac{\partial \vec{g}}{\partial t} = \nabla \times (\vec{V} \times \vec{g}) - \eta \nabla \times \vec{V} \quad (\text{A.1})$$

where  $\vec{V}$ ,  $\nabla \times \vec{V}$  and  $\vec{g}$  are defined as:

$$\vec{V} = -\frac{\nabla \times \vec{B}}{n}$$

$$\nabla \times \vec{V} = \frac{\nabla^2 \vec{B}}{n} + \frac{\nabla n \times \nabla \times \vec{B}}{n^2}$$

and

$$\vec{g} = \frac{\nabla^2 \vec{B}}{n} + \frac{\nabla n \times \nabla \times \vec{B}}{n^2} - \vec{B}$$

Eq. (A.1) can be expanded as:

$$\frac{\partial \vec{g}}{\partial t} = \vec{V} \underbrace{(\nabla \cdot \vec{g})}_0 - \vec{g}(\nabla \cdot \vec{V}) + (\vec{g} \cdot \nabla) \vec{V} - (\vec{V} \cdot \nabla) \vec{g} - \eta \nabla \times \vec{V} \quad (\text{A.2})$$

or,

$$\frac{\partial \vec{g}}{\partial t} = \vec{g} \left( \frac{\vec{V} \cdot \nabla n}{n} \right) + (\vec{g} \cdot \nabla) \vec{V} - (\vec{V} \cdot \nabla) \vec{g} - \eta \nabla \times \vec{V} \quad (\text{A.3})$$

## Appendix A: Derivation of the G-EMHD Model Equations

This represents the simplified form of the 3-D G-EMHD model equation.

### Two Dimensional G-EMHD model

For the reduction of the G-EMHD model in two dimension we assume the general coordinate system like  $\hat{e}_p, \hat{e}_q$  and  $\hat{e}_s$  as the right handed triad of unit vectors. We take the symmetry axis to be along  $\hat{e}_s$ . The magnetic field being divergenceless it can be expressed in terms of two scalar fields in 2-D as  $\vec{B} = b\hat{e}_s + \hat{e}_s \times \nabla\psi$ . The electron velocity ( $\vec{V}$ ) and the generalized vorticity ( $\vec{g}$ ) can be written as:

$$\begin{aligned}\vec{V} &= -\frac{\nabla \times \vec{B}}{n} \\ &= \hat{e}_s \times \frac{\nabla b}{n} - \hat{e}_s \frac{\nabla^2 \psi}{n}\end{aligned}$$

$$\nabla \times \vec{V} = \hat{e}_s \left( \nabla \cdot \left( \frac{\nabla b}{n} \right) \right) - \hat{e}_s \times \nabla \left( \frac{\nabla^2 \psi}{n} \right)$$

and

$$\begin{aligned}\vec{g} &= \left( \frac{\nabla^2 \vec{B}}{n} - \vec{B} - \frac{\nabla n \times \nabla \times \vec{B}}{n^2} \right) \\ &= \hat{e}_s \times \nabla \left( \frac{\nabla^2 \psi}{n} - \psi \right) + \left( \nabla \cdot \left( \frac{\nabla b}{n} \right) - b \right) \hat{e}_s\end{aligned}$$

Substituting the expression for  $\vec{V}$ ,  $\nabla \times \vec{V}$  and  $\vec{g}$  in Eq. (A.3), and on separating the components along  $\hat{e}_s$  (symmetry direction) as well as in the perpendicular plane of the  $\hat{e}_s$  direction (poloidal plane) we get the following two equations.

$$\begin{aligned}\frac{\partial}{\partial t} \left\{ b - \nabla \cdot \left( \frac{\nabla b}{n} \right) \right\} + \hat{e}_s \times \nabla b \cdot \nabla \left[ \frac{1}{n} \left\{ b - \nabla \cdot \left( \frac{\nabla b}{n} \right) \right\} \right] + \hat{e}_s \times \nabla \psi \cdot \nabla \left( \frac{\nabla^2 \psi}{n} \right) \\ = \eta \nabla \cdot \left( \frac{\nabla b}{n} \right)\end{aligned}\quad (\text{A.4})$$

and

$$\frac{\partial}{\partial t} \left\{ \psi - \frac{\nabla^2 \psi}{n} \right\} + \frac{\hat{e}_s \times \nabla b}{n} \cdot \nabla \left\{ \psi - \frac{\nabla^2 \psi}{n} \right\} = \eta \frac{\nabla^2 \psi}{n}\quad (\text{A.5})$$

### Integral invariants of the G-EMHD:

## Appendix A: Derivation of the G-EMHD Model Equations

In order to get the integral invariants of 2-D G-EMHD we are using the Eq. (A.4) & (A.5) in the limit of inviscid fluid,  $\eta \rightarrow 0$ . Here the derivation of integral invariant is carried out when current associated with magnetic field ( $\vec{B}$ ) is along both symmetry direction ( $\hat{e}_s$ ) as well as in the perpendicular plane of  $\hat{e}_s$ . It means both scalar quantities  $b$  and  $\psi$  are finite.

On multiplying Eq. (A.4) by  $b$  and integrating over 2-D volume  $d^2X$  Eq. (A.4) can be written as:

$$\int b \frac{\partial b}{\partial t} d^2X - \int b \frac{\partial}{\partial t} \left( \nabla \cdot \left( \frac{\nabla b}{n} \right) \right) d^2X + \int b \hat{e}_s \times \nabla b \cdot \nabla \left\{ \frac{1}{n} \left( b - \nabla \cdot \left( \frac{\nabla b}{n} \right) \right) \right\} d^2X + \int b \hat{e}_s \times \nabla \left( \psi - \frac{\nabla^2 \psi}{n} \right) \cdot \nabla \left( \frac{\nabla^2 \psi}{n} \right) d^2X = 0 \quad (\text{A.6})$$

The first and second term can be combined in the form of  $(1/2) \int \frac{\partial}{\partial t} \{b^2 + (\nabla b)^2/n\} d^2X$  using by part integration and the condition that the field vanishes on the boundary. The third term can be written as  $(1/2) \int \nabla \cdot (\hat{e}_s \times \nabla b^2/n) (b - \nabla \cdot (\nabla b/n)) d^2X$  and it vanishes over whole space. Thus, we get

$$\frac{1}{2} \int \frac{\partial}{\partial t} \left\{ b^2 + \frac{(\nabla b)^2}{n} \right\} d^2X + \int b \hat{e}_s \times \nabla \left( \psi - \frac{\nabla^2 \psi}{n} \right) \cdot \nabla \left( \frac{\nabla^2 \psi}{n} \right) d^2X = 0 \quad (\text{A.7})$$

Again on multiplying Eq. (A.5) by  $\nabla^2 \psi$  and integrating over the 2-D space,

$$\int \nabla^2 \psi \frac{\partial \psi}{\partial t} d^2X - \int \nabla^2 \psi \frac{\partial}{\partial t} \left( \frac{\nabla^2 \psi}{n} \right) d^2X + \int \nabla^2 \psi \frac{\hat{e}_s \times \nabla b}{n} \cdot \nabla \left( \psi - \frac{\nabla^2 \psi}{n} \right) d^2X = 0 \quad (\text{A.8})$$

The first and second term can be merged into  $(1/2) \int \frac{\partial}{\partial t} \{(\nabla \psi)^2 + (\nabla^2 \psi)^2/n\} d^2X$  by applying by part integration over the first term followed by the condition that fields vanishes on the boundary.

$$\frac{1}{2} \int \frac{\partial}{\partial t} \left\{ (\nabla \psi)^2 + \frac{(\nabla^2 \psi)^2}{n} \right\} d^2X - \int \nabla^2 \psi \frac{\hat{e}_s \times \nabla b}{n} \cdot \nabla \left( \psi - \frac{\nabla^2 \psi}{n} \right) d^2X = 0 \quad (\text{A.9})$$

## Appendix A: Derivation of the G-EMHD Model Equations

Now on adding Eq. (A.7) and Eq. (A.9), then

$$\frac{1}{2} \int \frac{\partial}{\partial t} \left\{ b^2 + \frac{(\nabla b)^2}{n} + (\nabla \psi)^2 + \frac{\nabla^2 \psi}{n} \right\} d^2 X + \int \left\{ b \hat{e}_s \times \nabla \left( \psi - \frac{\nabla^2 \psi}{n} \right) \cdot \nabla \left( \frac{\nabla^2 \psi}{n} \right) - \nabla^2 \psi \frac{\hat{e}_s \times \nabla b}{n} \cdot \nabla \left( \psi - \frac{\nabla^2 \psi}{n} \right) \right\} d^2 X = 0$$

or,

$$\frac{1}{2} \int \frac{\partial}{\partial t} \left\{ b^2 + \frac{(\nabla b)^2}{n} + (\nabla \psi)^2 + \frac{\nabla^2 \psi}{n} \right\} d^2 X + \underbrace{\int \nabla \cdot \hat{e}_s \times \nabla \left( \psi - \frac{\nabla^2 \psi}{n} \right) b \frac{\nabla^2 \psi}{n} d^2 X}_0 = 0$$

or

$$\frac{1}{2} \frac{d}{dt} \int \left\{ b^2 + \frac{(\nabla b)^2}{n} + (\nabla \psi)^2 + \frac{\nabla^2 \psi}{n} \right\} d^2 X = 0$$

or,

$$\frac{dE}{dt} = 0 \quad (\text{A.10})$$

This equation implies that the quantity  $E$  is constant where  $E$  is the total energy, i.e. summation of the magnetic energy  $(b^2 + (\nabla \psi)^2)$  and kinetic energy  $(1/n)((\nabla b)^2 + \nabla^2 \psi)$ . At this stage energy is the only invariant for this case.

Now, let us derive invariants for the case when current associated with the magnetic field is confined only in perpendicular plane of  $\hat{e}_s$ , i.e.  $\psi = 0$ . Thus, in this case 2-D G-EMHD model reduces to the following equation.

$$\frac{\partial}{\partial t} \left\{ b - \nabla \cdot \left( \frac{\nabla b}{n} \right) \right\} + \hat{e}_s \times \nabla b \cdot \nabla \left[ \frac{1}{n} \left\{ b - \nabla \cdot \left( \frac{\nabla b}{n} \right) \right\} \right] = 0 \quad (\text{A.11})$$

Here, apart from the energy  $(b^2 + (\nabla b)^2/n)$  one more invariant is associated with this equation. That can be obtained by multiplying Eq. (A.11) with

## Appendix A: Derivation of the G-EMHD Model Equations

$(1/n)(b - \nabla \cdot (\nabla b/n))$  and integrating over 2-D volume space  $d^2X$ . Therefore,

$$\int \frac{1}{n} \left( b - \nabla \cdot \left( \frac{\nabla b}{n} \right) \right) \frac{\partial}{\partial t} \left( b - \nabla \cdot \left( \frac{\nabla b}{n} \right) \right) d^2X + \int \frac{1}{n} \left( b - \nabla \cdot \left( \frac{\nabla b}{n} \right) \right) \hat{e}_s \times \nabla b \cdot \nabla \left( \frac{1}{n} \left( b - \nabla \cdot \left( \frac{\nabla b}{n} \right) \right) \right) d^2X = 0$$

or,

$$\frac{1}{2} \int \frac{1}{n} \frac{\partial}{\partial t} \left( b - \nabla \cdot \left( \frac{\nabla b}{n} \right) \right)^2 d^2X + \frac{1}{2} \int \hat{e}_s \times \nabla b \cdot \nabla \left( \frac{1}{n} \left( b - \nabla \cdot \left( \frac{\nabla b}{n} \right) \right) \right)^2 d^2X = 0$$

or,

$$\frac{1}{2} \int \frac{1}{n} \frac{\partial}{\partial t} \left( b - \nabla \cdot \left( \frac{\nabla b}{n} \right) \right)^2 d^2X + \underbrace{\frac{1}{2} \int \nabla \cdot \left\{ \hat{e}_s \times \nabla b \left( \frac{1}{n} \left( b - \nabla \cdot \left( \frac{\nabla b}{n} \right) \right) \right)^2 \right\}}_0 d^2X = 0$$

Thus,

$$\frac{1}{2} \frac{d}{dt} \int \frac{1}{n} \left( b - \nabla \cdot \left( \frac{\nabla b}{n} \right) \right)^2 d^2X = 0$$

or

$$\frac{dH}{dt} = 0 \tag{A.12}$$

where  $H (= \int (1/n)(b - \nabla \cdot (\nabla b/n))^2 d^2X)$  is the additional invariant apart from energy for this case when  $\psi = 0$ .

# Appendix B

## Solution of the Nonlinear EMHD Equation

Let us start with the simplified form of the 2-D EMHD equation with the assumption that only the symmetry component ( $b$ ) of the total magnetic field ( $\vec{B} = b\hat{z} + \hat{z} \times \nabla\psi$ ) exist, i.e.  $\psi = 0$ . So,

$$\frac{\partial\Omega_b}{\partial t} + [b, \Omega_b] = 0 \quad (\text{B.1})$$

Here, the symbols  $[ , ]$  and  $\Omega_b$  used in the above equation corresponds to Poisson bracket and  $(b - \nabla^2 b)$  respectively. The solution of this equation can be obtained by going to the moving frame with the coordinate transformation  $\xi = y - ut$  assuming that the translational velocity ( $u$ ) of the solution is along  $\hat{y}$  direction. Therefore, Eq. (B.1) can be reduced as,

$$[\Omega_b, b - ux] = 0 \quad (\text{B.2})$$

This suggests that  $\Omega_b = f_b(b - ux)$ , where  $f_b$  is function of  $(b - ux)$ . Thus, a traveling solution can be obtained by seeking solution of the following equation:

$$b - \nabla^2 b = f_b(b - ux) \quad (\text{B.3})$$

## Appendix B: Solution of the Nonlinear EMHD Equation

or,

$$\nabla^2 b - b = -f_b(b - ux) \quad (\text{B.4})$$

The general solution would correspond to any choice of the function  $f_b$ . Isichneko *et al.* [65] has obtained the analytical form of the solution that is localized within the finite spatial extent of  $r_0$ . Here the solution is obtained by the transformation of this equation in the cylindrical co-ordinate system with the assumption that  $\partial/\partial z = 0$  and  $x = r \cos(\theta)$ . Thus,

$$\frac{1}{r} \frac{\partial}{\partial r} \left( r \frac{\partial b}{\partial r} \right) + \frac{1}{r^2} \frac{\partial^2 b}{\partial \theta^2} - b = -f_b(b - ur \cos(\theta)) \quad (\text{B.5})$$

In order to get the solution of Eq. (B.5), Isichenko *et al.* [65] considered the linear variation of vorticity functions  $f_b(= \alpha(b - ur \cos(\theta)))$  inside of  $r_o$ , and zero outside of  $r_o$  (it means  $\alpha$  should be zero). Hence,

**Governing equation inside of  $r_o$  ( $r < r_o$ )**

$$\frac{1}{r} \frac{\partial}{\partial r} \left( r \frac{\partial b}{\partial r} \right) + \frac{1}{r^2} \frac{\partial^2 b}{\partial \theta^2} - b = -\alpha(b - ur \cos \theta) \quad (\text{B.6})$$

**Governing equation outside of  $r_o$  ( $r \geq r_o$ )**

$$\frac{1}{r} \frac{\partial}{\partial r} \left( r \frac{\partial b}{\partial r} \right) + \frac{1}{r^2} \frac{\partial^2 b}{\partial \theta^2} - b = 0 \quad (\text{B.7})$$

The governing Eq. (B.6) gives the solution of the scalar field,  $b$ , in the form of the first kind of Bessel function. Here, let me write the form of the solution for field  $b$  inside of  $r_0$  :  $b = [d_1 J_1(k_1 r) + d_2 r] \cos \theta$ . Eq. (B.7) forms the simple Poisson equation and allows the solution for the quantity  $b$  in the form of the second kind of Bessel function,  $b = d_3 K_1(r) \cos \theta$ . The constants  $d_1, d_2$  and  $d_3$  can be obtained by using the boundary conditions that the fields and its derivative are continuous at the boundary of  $r_0$ . Thus the continuity of the field at the boundary will give the relation

$$d_1 J_1(k_1 r_0) + d_2 r_0 = d_3 K_1(r_0) \quad (\text{B.8})$$

## Appendix B: Solution of the Nonlinear EMHD Equation

and the other condition on its derivative ( $b'_i(r = r_0) = b'_o(r = r_0)$ ) will give the relation

$$d_1 J'_1(k_1 r_0) + d_2 = d_3 K'_1(r_0) \quad (\text{B.9})$$

Using these equations we get the relations

$$\frac{d_1}{d_2} = \frac{K_1(r_0) - r_0 K'_1(r_0)}{J_1(k_1 r_0) K'_1 - J'_1(k_1 r_0) K_1(r_0)} \quad (\text{B.10})$$

and,

$$\frac{d_3}{d_2} = \frac{J_1(k_1 r_0) - J'_1(k_1 r_0) r_0}{J_1(k_1 r_0) K'_1 - J'_1(k_1 r_0) K_1(r_0)} \quad (\text{B.11})$$

Thus, the value of the constants  $d_1$  and  $d_3$  can be calculated by knowing the constant  $d_2$ . So, on substituting the inside solution for  $b$  in Eq. (B.6) we get the equation:

$$d_1 \left[ r^2 \frac{d^2 J_1(k_1 r)}{dr^2} + r \frac{dJ_1(k_1 r)}{dr} + (k_1^2 r^2 - 1) J_1(k_1 r) \right] = (d_2 - \alpha d_2 + \alpha u) r^3 \quad (\text{B.12})$$

where  $k_1^2 = \alpha - 1$ . From this equation it is clear that the inside solution will only be satisfied when

$$d_2 - \alpha d_2 + \alpha u = 0$$

or,

$$d_2 = -\frac{\alpha u}{1 - \alpha} \quad (\text{B.13})$$

Now we can obtain the constants  $d_1$  and  $d_3$  using this form of  $d_2$ . Here we are writing the solution of the field  $b$  explicitly.

$$\begin{aligned} b_i(r, \theta) &= (d_1 J_1(k_1 r) + d_2) \cos(\theta), & r < r_0 \\ b_o(r, \theta) &= d_3 K_1(r) \cos(\theta), & r > r_0 \end{aligned}$$

This solution of  $b$  form the dipolar structure for a set of free parameters ( $u, \alpha, r_0$ ) [see Fig. (4.2) of the Chapter 4].

# Appendix C

## Solution of the Inertialess G-EMHD Model

We begin with the Eq. (2.2) of the Chapter 2.

$$\frac{\partial (\nabla \times \vec{P})}{\partial t} = \nabla \times (\vec{V}_e \times \nabla \times \vec{P}) - \nu \nabla \times \vec{V}_e \quad (\text{C.1})$$

where  $\vec{P} = \vec{V}_e - (e\vec{A})/(m_e c)$  is the generalized momentum containing both electron flow velocity ( $\vec{V}_e$ ) as well as vector field ( $\vec{A}$ ). The electron flow velocity is defined as  $\vec{V}_e = -(c/4\pi n_e e) \nabla \times \vec{B}$  (obtained by neglecting the displacement current in the Ampere's law). Expansion of the generalized vorticity  $\nabla \times \vec{P}$ :

$$\nabla \times \vec{P} = \nabla \times \vec{V}_e - \frac{e}{m_e c} \nabla \times \vec{A} \quad (\text{C.2})$$

## Appendix C: Solution of the Inertialess G-EMHD Model

Upon substituting the expression for velocity  $\vec{V}_e = -(c/4\pi en_e)\nabla \times \vec{B}$  and the relation  $\vec{B} = \nabla \times \vec{A}$  in Eq. (C.2) we get.

$$\begin{aligned}
 \nabla \times \vec{P} &= -\frac{c}{4\pi e} \nabla \times \left( \frac{\nabla \times \vec{B}}{n_e} \right) - \frac{e\vec{B}}{m_e c} \quad (C.3) \\
 &= -\frac{c}{4\pi e} \left[ \frac{1}{n_e} \nabla \times \nabla \times \vec{B} + \nabla \left( \frac{1}{n_e} \right) \times \nabla \times \vec{B} \right] - \frac{e\vec{B}}{m_e c} \\
 &= -\frac{c}{4\pi e} \left[ \frac{1}{n_e} \nabla (\nabla \cdot \vec{B}) - \frac{\nabla^2 \vec{B}}{n_e} - \frac{\nabla n_e \times \nabla \times \vec{B}}{n_e^2} \right] - \frac{e\vec{B}}{m_e c} \\
 &= \frac{c}{4\pi en_e} \left[ \nabla^2 \vec{B} + \frac{\nabla n_e \times \nabla \times \vec{B}}{n_e} \right] - \frac{e\vec{B}}{m_e c}
 \end{aligned}$$

Comparing the magnitude of the first and second term of RHS in Eq. (C.3).

$$\begin{aligned}
 \frac{|\frac{c}{4\pi e} \nabla \times (\nabla \times \vec{B}/n_e)|}{|e\vec{B}/m_e c|} &= \frac{ck^2 B/4\pi en_e}{eB/m_e c} \\
 &= \frac{c^2}{\omega_{pe}^2} k^2 \\
 &= d_e^2 k^2
 \end{aligned}$$

where  $d_e = c/\omega_{pe}$ , in which  $\omega_{pe} = 4\pi n_e e^2/m_e$  is the plasma frequency. The first term of RHS in the Eq. (C.3) is neglected if  $d_e^2 k^2 \ll 1$ . This is the inertialess condition. Under this condition the form of the generalized vorticity would be.

$$\nabla \times \vec{P} = -\frac{e\vec{B}}{m_e c} \quad (C.4)$$

Now on substituting this new form of  $\nabla \times \vec{P}$  in Eq. (C.1) we obtain.

$$\frac{\partial \vec{B}}{\partial t} = \nabla \times (\vec{V}_e \times \vec{B}) + \frac{\nu}{m_e c} \nabla \times V_e \quad (C.5)$$

## Appendix C: Solution of the Inertialess G-EMHD Model

or,

$$\frac{\partial \vec{B}}{\partial t} = -\frac{1}{e} \nabla \times \left( \frac{\vec{J} \times \vec{B}}{n_e} \right) - c \nabla \times (\vec{J}/\sigma) \quad (\text{C.6})$$

where  $\sigma = n_e e^2 / m_e \nu$  is a constant quantity and is defined as conductivity. Again Eq. (C.6) is simplified using the relation for current  $\vec{J} = (c/4\pi) \nabla \times \vec{B}$ . Thus we obtain.

$$\frac{\partial \vec{B}}{\partial t} = -\frac{c}{8\pi e} \nabla \left( \frac{1}{n_e} \right) \times \nabla (B^2) + \frac{c^2}{4\pi\sigma} \nabla^2 \vec{B}$$

or,

$$\frac{\partial \vec{B}}{\partial t} + \frac{c}{4\pi e n_e} \frac{\nabla n_e}{n_e} \times \nabla (B^2/2) - \frac{c^2}{4\pi\sigma} \nabla^2 \vec{B} = 0 \quad (\text{C.7})$$

Let the density gradient is along  $\hat{y}$  direction (i.e.  $\nabla n_e = (\partial n_e / \partial y) \hat{y}$ ) and perpendicular to the magnetic field ( $\vec{B} = b(x, y) \hat{z}$ ). Then,

$$\frac{\partial b}{\partial t} + \underbrace{\frac{c}{4\pi e} \frac{b \hat{z} \times \nabla n_e}{n_e^2}}_{\text{Drift Velocity}} \cdot \nabla b = \frac{c^2}{4\pi\sigma} \left( \frac{\partial^2 b}{\partial x^2} + \frac{\partial^2 b}{\partial y^2} \right) \quad (\text{C.8})$$

or,

$$\frac{\partial b}{\partial t} + \underbrace{\left( -\frac{c}{4\pi e} \frac{1}{n_e^2} \frac{\partial n_e}{\partial y} \right)}_K b \frac{\partial b}{\partial x} = \underbrace{\frac{c^2}{4\pi\sigma}}_\eta \left( \frac{\partial^2 b}{\partial x^2} + \frac{\partial^2 b}{\partial y^2} \right) \quad (\text{C.9})$$

or,

$$\frac{\partial b}{\partial t} + K \frac{\partial}{\partial x} (b^2/2) = \eta \left( \frac{\partial^2 b}{\partial x^2} + \frac{\partial^2 b}{\partial y^2} \right) \quad (\text{C.10})$$

where  $K = -c/4\pi n_e e L_n$ , in which  $L_n = (1/n_e) \partial n_e / \partial y$  is interpreted as the inverse of density scale length. The solution of this equation can be obtained by going to the moving frame with the coordinate transformation;  $\xi = x + \beta y - ut$ , where  $\beta$  is a constant parameter and  $u$  represents the velocity of moving frame. Thus, in this new coordinate system the operators associated with the Eq. (C.10) are defined

## Appendix C: Solution of the Inertialess G-EMHD Model

as:

$$\frac{\partial}{\partial y} = \beta \frac{\partial}{\partial \xi}; \frac{\partial}{\partial x} = \frac{\partial}{\partial \xi}; \frac{\partial}{\partial t} = -u \frac{\partial}{\partial \xi}$$

Therefore, Eq. (C.10) becomes,

$$-u \frac{\partial b}{\partial \xi} + K \frac{\partial b^2/2}{\partial \xi} = \eta(1 + \beta^2) \frac{\partial^2 b}{\partial \xi^2}$$

or,

$$\frac{\partial(Kb^2/2 - bu)}{\partial \xi} = \eta(1 + \beta^2) \frac{\partial^2 b}{\partial \xi^2}$$

On integration,

$$\int \frac{\partial(Kb^2/2 - bu)}{\partial \xi} d\xi = \int \eta(1 + \beta^2) \frac{\partial}{\partial \xi} \left( \frac{\partial b}{\partial \xi} \right) d\xi + K_1$$

or,

$$\frac{Kb^2}{2} - bu = \eta(1 + \beta^2) \frac{\partial b}{\partial \xi} + K_1$$

where  $K_1$  is the integration constant and can be obtained by applying the boundary condition that  $b = b_0$  and  $\partial b/\partial \xi = 0$ . Thus  $K_1 = b_0(b_0K/2 - u)$ ,

$$\eta(1 + \beta^2) \frac{\partial b}{\partial \xi} = b(bK/2 - u) - b_0(b_0K/2 - u)$$

Integrating again,

$$\int \frac{db}{b(bK/2 - u) - b_0(b_0K/2 - u)} = \int \frac{d\xi}{\eta(1 + \beta^2)} + K_2$$

$$\frac{2 \tan^{-1} \left[ (bK - u) / \sqrt{(-2KK_1 - u^2)} \right]}{\sqrt{(-2KK_1 - u^2)}} = \frac{\xi}{\eta(1 + \beta^2)} + k_2$$

Using the identity  $\tan(ix) = i \tanh(x)$  the above relation can be written in the simplified manner.

$$b = \frac{u}{K} + \frac{(b_0K - u)}{K} \tanh \left[ \frac{(b_0K - u)}{2} \left( \frac{\xi}{\eta(1 + \beta^2)} + K_2 \right) \right] \quad (\text{C.11})$$

## Appendix C: Solution of the Inertialess G-EMHD Model

where  $K_2$  is the integration constant.

# Bibliography

- [1] A. S. Kingsep, K. V. Chukbar and V. V. Yankov, *Reviews of Plasma Physics*, (Consultant Bureau, New York), vol. 16 (1990).
- [2] F. Califano, R. Prandi, F. Pegoraro and S. V. Bulanov, *Phys. Plasmas* **6**, 2332 (1999).
- [3] A. Das and P. H. Diamond, *Phys. Plasmas* **7**, 170 (2000).
- [4] A. Das, *Phys. Plasmas* **15**, 022308 (2008).
- [5] M. Tabak, J. Hammer, M. E. Glinsky, W. L. Kruer, S. C. Wilks, J. Woodworth, E. M. Campbell, M. D. Perry and R. J. Mason, *Phys. Plasmas* **1**, 1626 (1994).
- [6] N. Attico, F. Califano and F. Pegoraro, *Phys. Plasmas* **7**, 2381 (2000).
- [7] N. Attico, F. Califano and F. Pegoraro, *Phys. Plasmas* **9**, 458 (2002).
- [8] S. V. Bulanov, F. Pegoraro and A. S. Sakharov, *Phys. Fluids B* **4**, 2499 (1992).
- [9] F. Califano, N. Attico, F. Pegoraro, G. Bertin and S. V. Bulanov, *Phys. Rev. Lett.* **86**, 5293 (2001).
- [10] L. Chacon, A. N. Simakov and A. Zocco, *Phys. Rev. Lett.* **99**, 235001 (2007).
- [11] J. C. Dorelli and J. Brin, *Phys. Plasmas* **8**, 4010 (2001).
- [12] A. A. Chernkov and V. V. Yankov, *Sov. J. Plasma Phys.* **8**, 522 (1982).
- [13] D. D. Ryutov, M. S. Derzon and M. K. Matzen, *Rev. Mod. Phys.* **72**, 000167 (2000).

## Bibliography

- [14] M. Sarfaty, R. Shpitalnik, R. Arad, A. Weingarten, Ya. E. Karasik, A. Fruchtman and Y. Maron, *Phys. Plasmas* **2**, 2583 (1995).
- [15] R. Shpitalnik, A. Weingarten, K. Gomberoff, Ya. Krasik and Y. Maron, *Phys. Plasmas* **5**, 792 (1998).
- [16] A. V. Gordeev, A. V. Grechikha, A. V. Gulin and O. M. Drozdova, *Sov. J. Plasma Phys.* **17**, 381 (1991).
- [17] C. W. Mendel, Jr. and S. A. Goldstein, *J. Appl. Phys.* **48**, 1004 (1977).
- [18] P. F. Ottinger, S. A. Goldstein and R. A. Meger, *J. Appl. Phys.* **56**, 774 (1984).
- [19] B. V. Weber, R. J. Commisso, R. A. Merger, J. M. Neri, W. F. Oliphant and P. F. Ottinger, *Appl. Phys. Lett.* **45**, 1043 (1984).
- [20] A. S. Kingsep, Yu. V. Mokhov and K. V. Chukbar, *Sov. J. Plasma Phys.* **10**, 495 (1984).
- [21] A. S. Sandhu, A. K. Dharmadhikari, P. P. Rajeev, G. R. Kumar, S. Sengupta, A. Das and P. K. Kaw, *Phys. Rev. Lett.* **89**, 225002 (2002).
- [22] A. S. Sandhu, G. R. Kumar, S. Sengupta, A. Das and P. K. Kaw, *Phys. Rev. E* **73**, 036409 (2006).
- [23] S. Kahaly, S. Mondal and G. R. Kumar, *Journal of Physics: Conference Series* **112**, 022103 (2008).
- [24] J. Sinha, S. Mohan, S. S. Banerjee, S. Kahaly and G. R. Kumar, *Phys. Rev. E* **77**, 046118 (2008).
- [25] S. Poornakala, A. Das, A. Sen and P. K. Kaw, *Phys. Plasmas* **9**, 1820 (2002).
- [26] V. Saxena, A. Das, A. Sen and P. K. Kaw, *Phys. Plasmas* **13**, 032309 (2006).
- [27] M. Honda, J. Meyer-ter-Vehn and A. Pukhov, *Phys. Plasmas* **7**, 1302 (2000).
- [28] M. Honda, J. Meyer-ter-Vehn and A. Pukhov, *Phys. Rev. Lett.* **85**, 2128 (2000).

## Bibliography

- [29] Y. Sentoku, K. Mima, Z. M. Sheng, P. Kaw, K. Nishihara and K. Nishikawa, *Phys. Rev. E* **65**, 046408 (2002).
- [30] Y. Sentoku, K. Mima, P. Kaw, and K. Nishikawa, *Phys. Rev. Lett.* **90**, 155001 (2003).
- [31] J. J. Honrubia and J. Meyer-ter-Vehn, *Nucl. Fusion* **46**, L25 (2006).
- [32] R. B. Campbell, R. Kodama, T. A. Melhorn, K. A. Tanaka and D. R. Welch, *Phys. Rev. Lett.* **94**, 055001 (2005).
- [33] R. J. Mason, *Phys. Rev. Lett.* **96**, 035001 (2006).
- [34] A. Fruchtman, A. A. Ivanov and A. S. Kingsep, *Phys. Plasmas* **5**, 1133 (1998).
- [35] A. Fruchtman and L. I. Rudakov, *Phys. Rev. Lett.* **69**, 2070 (1992).
- [36] A. Das, *Plasma Phys. Control. Fusion* **41**, A531 (1999).
- [37] D. Biskamp, E. Schwarz, A. Zeiler, A. Celani and J. F. Drake, *Phys. Plasmas* **6**, 751 (1999).
- [38] D. Biskamp, E. Schwarz and J. F. Drake, *Phys. Rev. Lett.* **76**, 1264 (1996).
- [39] D. Biskamp, E. Schwarz and A. Celani, *Phys. Rev. Lett.* **81**, 4855 (1998).
- [40] W. L. Kruer, *The Physics of Laser-Plasma Interactions*, (Addison-Wesley, New York, 1988).
- [41] F. Brunel, *Phys. Rev. Lett.* **59**, 52 (1987).
- [42] A. S. Sandhu, G. R. Kumar, S. Sengupta, A. Das and P. K. Kaw, *Phys. Rev. Lett.* **95**, 025005 (2005).
- [43] C. Gahn, G. Pretzler, A. Saemann, G. D. Tsakiris, K. J. Witte, D. Gaussmann, T. Schatz, U. Schramm, P. Thiroff and D. Habs, *Appl. Phys. Lett.* **73**, 3662 (1998).
- [44] P. P. Rajeev, P. Taneja, P. Ayyub, A. S. Sandhu and G. R. Kumar, *Phys. Rev. Lett.* **90**, 115002 (2003).

## Bibliography

- [45] G. Kulcsar, D. Alkawlawi, F. W. Budnik, P. R. Herman, M. Moskovits, L. Zhao and R. S. Marjoribanks, *Phys. Rev. Lett.* **84**, 5149 (2000).
- [46] S. P. Gordon, T. Donnelly, A. Sullivan, H. Hamster and R. W. Falcone, *Opt. Lett.* **19**, 484 (1994).
- [47] M. M. Murnane, H. C. Kapteyn, S. P. Gordon, J. Bokor, E. N. Glytsis and R. W. Falcone, *Appl. Phys. Lett.* **62**, 1068 (1993).
- [48] A. L. Lei, K. A. Tanaka, K. Mima, G. R. Kumar, K. Nagai, T. Norimatsu, T. Yabuuchi and K. Mima, *Phys. Rev. Lett.* **96**, 255006 (2006).
- [49] J. C. Gauthier *et al.*, *Proc. SPIE Int. Soc. Opt. Eng.* **2523**, 242 (1995).
- [50] S. Kahaly, S. K. Yadav, W. M. Wang, S. Sengupta, Z. M. Sheng, A. Das, P. K. Kaw and G. R. Kumar, *Phys. Rev. Lett.* **101**, 145001 (2008).
- [51] H. Alfven, *Phys. Rev.* **55**, 425 (1939).
- [52] E. S. Weibel, *Phys. Rev. Lett.* **2**, 83 (1959).
- [53] N. Jain, A. Das, P. Kaw and S. Sengupta, *Physics Letters A* **363**, 125 (2007).
- [54] N. Jain, A. Das, P. Kaw and S. Sengupta, *Phys. Plasmas* **10**, 29 (2003).
- [55] N. Jain, A. Das and P. Kaw, *Phys. Plasmas* **11** 4390 (2004).
- [56] A. Das and P. Kaw, *Phys. Plasmas* **8**, 4518 (2001).
- [57] J. D. Lindl, *Inertial Confinement Fusion: The Quest for Ignition and Energy Gain using Indirect Drive*, Springer-Verlag, New York (1998).
- [58] J. D. Lindl *et al.*, *Phys. Plasmas* **11**, 339 (2004).
- [59] P. G. Drazin and W. H. Reid, *Hydrodynamic Stability*, Cambridge University Press, Cambridge, London (1981).
- [60] R. Kodama, P. A. Norreys, K. Mima, A. E. Dangor, R. G. Evans, H. Fujita, Y. Kitagawa, K. Krushelnick, T. Miyakoshi, N. Miyanaga, T. Norimatsu, S. J. Rose, T. Shozaki, K. Shigemori, A. Sunahara, M. Tambo, K. A. Tanaka, Y. Toyama, T. Yamanaka and Nature M. Zepf, *Nature* **412**, 798 (2001).

## Bibliography

- [61] R. Kodama, H. Shiraga, K. Shigemori, Y. Toyama, S. Fujioka, H. Azechi, H. Fujita, H. Habarat, T. Hall, Y. Izawa, T. Jitsuno, Y. Kitagawa, K. M. Krushelnick, K. L. Lancaster, K. Mima, K. Nagai, M. Naki, H. Nishimura, T. Norimatsu, P. A. Norreys, S. Sakabe, K. A. Tanaka, A. Youssef, and M. Zepf and T. Yamanka, *Nature* **418**, 933 (2002).
- [62] A. P. L. Robinson and M. Sherlock, *Phys. Plasmas* **14**, 083105 (2007).
- [63] S. Kar, A. P. L. Robinson, D. C. Carroll, O. Lundh, K. Markey, P. McKenna, P. Norreys and M. Zepf, *Phys. Rev. Lett.* **102**, 055001 (2009).
- [64] R. Kodama, Y. Sentoku, Z. L. Chen, G. R. Kumar, S. P. Hatchett, Y. Toyama, T. E. Cowan, R. R. Freeman, J. Fuchs, Y. Izawa, M. H. Key, Y. Kitagawa, K. Kondo, T. Matsuoka, H. Nakamura, M. Nakatsutsumi, P. A. Norreys, T. Norimatsu, R. A. Snavely, R. B. Stephens, M. Tambo, K. A. Tanaka and T. Yabuuchi, *Nature* **432**, 1005 (2004).
- [65] M. B. Isichenko and A. M. Marnachev, *Sov. Phys. JETP* **66**, 702 (1987).
- [66] D. V. Flippov and V. V. Yan'kov, *Sov. J. Plasma Phys.* **12**, 548 (1986).
- [67] S. Dastgeer, A. Das, P. Kaw and P. H. Diamond, *Phys. Plasmas* **7**, 571 (2000).
- [68] S. Dastgeer and G. P. Zank, *The Astrophysical Journal* **599**, 715 (2003).
- [69] A. Celani, R. Pandit and G. Boffetta, *Physica Scripta* **T75**, 191-193 (1998).
- [70] J. Cho and A. Lazarian, *The Astrophysical Journal* **615**, L41-L44 (2004).
- [71] J. Cho and A. Lazarian, *The Astrophysical Journal* **701**, 236-252 (2009).
- [72] G. Gaur, S. Sundar, S. K. Yadav, A. Das, P. Kaw and S. Sharma, *Phys. Plasmas* **16**, 072310 (2009).
- [73] V. I. Petviashvili, *Pis'ma Zh. Eksp. Teor. Fiz.* **32**, 632 (1980).
- [74] V. I. Petviashvili and V. V. Yan'kov, *Dokl. Akad. Nauk SSSR* **267**, 825 (1982).
- [75] A. Fruchtman and K. Gomberoff, *Phys. Fluids B* **4**, 117 (1992).

## Bibliography

- [76] B. N. Kuvshinov, E. Westerhof, T. J. Schep and M. Berning, *Physics Letters A* **241**, 287 (1998).
- [77] B. N. Kuvshinov, J. Rem, T. J. Schep and E. Westerhof, *Phys. Plasmas* **8**, 3232 (2001).
- [78] S. K. Yadav, A. Das and P. Kaw, *Phys. Plasmas* **15**, 062308 (2008).
- [79] J. P. Boris, *Flux Corrected Transport Modules for Generalized Continuity Equations*, (NRL Memorandum Report 3237, Naval Research Laboratory, Washington DC ), 1976.
- [80] S. K. Yadav, A. Das, P. Kaw and S. Sengupta, *Phys. Plasmas* **16**, 040456 (2009).
- [81] S. K. Yadav and A. Das, *Phys. Plasmas* **17**, 052306 (2010).
- [82] A. Hasegawa and K. Mima, *Phys. Fluids* **21(1)**, 87 (1978).
- [83] P. Swarztrauber and R. Sweet, *Efficient Fortran Subprograms for the Solution of Elliptic Equations*, (NCAR TN/IA - 109, The National Center for Atmospheric Research, Colorado, USA ), 1975.
- [84] T. Yabuuchi, A. Das, G. R. Kumar, H. Habara, P. K. Kaw, R. Kodama, K. Mima, P. A. Norreys, S. Sengupta and K. A. Tanaka, *New Journal of Physics* **11**, 093031 (2009).
- [85] S. Chandrasekhar, *Hydrodynamic and Hydromagnetic Stability*, Dover Publications, Inc. Newyork (1981).
- [86] J. P. Freidberg, *Ideal Magnetohydrodynamics*, Plenum Press, New York (1987).
- [87] J. F. Drake, R. G. Kleva and M. E. Mandt, *Phys. Rev. Lett.* **73**, 1251 (1994).